

**Divalent cations stimulate DNA repair activities of bacterial
(6-4) photolyases**

Zur Erlangung des akademischen Grades eines
DOKTORS DER NATURWISSENSCHAFTEN

(Dr. rer. nat.)

von der KIT-Fakultät für Chemie und Biowissenschaften
des Karlsruher Instituts für Technologie (KIT)

genehmigte

DISSERTATION

von

Hongju Ma

aus

Sichuan, China

Dekan: Prof. Dr. Reinhard Fischer

Referent: Prof. Dr. Tilman Lamparter

Korreferent: Prof. Dr. Reinhard Fischer

Tag der mündlichen Prüfung: 17.07.2018

Die vorliegende Dissertation wurde am Botanischen Institut des Karlsruhe Instituts für Technologie (KIT), Lehrstuhl 1 für Molekulare Zellbiologie, im Zeitraum von Oktober 2014 bis Juli 2018 angefertigt.

Hiermit erkläre ich, dass ich die vorliegende Dissertation, abgesehen von der Benutzung der angegebenen Hilfsmittel, selbständig verfasst habe.

Alle Stellen, die gemäß Wortlaut oder Inhalt aus anderen Arbeiten entnommen sind, wurden durch Angabe der Quelle als Entlehnungen kenntlich gemacht.

Diese Dissertation liegt in gleicher oder ähnlicher Form keiner anderen Prüfungsbehörde vor.

Zudem erkläre ich, dass ich mich beim Anfertigen dieser Arbeit an die Regeln zur Sicherung guter wissenschaftlicher Praxis des KIT gehalten habe, einschließlich der Abgabe und Archivierung der Primärdaten, und dass die elektronische Version mit der schriftlichen übereinstimmt.

Karlsruhe, im Juli 2018

Hongju Ma

Publications

Aus dieser Arbeit sind folgende Publikationen entstanden:

Ma, H., Holub, D., Gillet, N., Kaeser, G., Thoullass, K., Elstner, M., Krauss, N., and Lamparter, T. (2018). Mechanism of magnesium stimulation of DNA repair in bacterial (6-4) photolyases. (Submitted).

Holub, D., Ma, H., Krauss, N., Lamparter, T., Elstner, M., and Gillet, N. (2018). Functional role of an unusual tyrosine residue in the electron transfer chain of a prokaryotic (6-4) photolyase. *Chemical Science* **9**, 1259-1272.

Ma, H., Zhang, F., Ignatz, E., Suehnel, M., Xue, P., Scheerer, P., Essen, L.O., Krauss, N., and Lamparter, T. (2017). Divalent cations increase DNA repair activities of bacterial (6-4) photolyases. *Photochem Photobiol* **93**, 323-330.

Zhang, F. *, Ma, H. *, Bowatte, K., Kwiatkowski, D., Mittmann, E., Qasem, H., Krauss, N., Zeng, X., Ren, Z., Scheerer, P., Yang, X., and Lamparter, T. (2017). Crystal structures of bacterial (6-4) photolyase mutants with impaired DNA repair activity. *Photochem Photobiol* **93**, 304-314.

Graf, D., Wesslowski, J., Ma, H., Scheerer, P., Krauss, N., Oberpichler, I., Zhang, F., and Lamparter, T. (2015). Key amino acids in the bacterial (6-4) photolyase PhrB from *Agrobacterium fabrum*. *PLoS One* **10**, e0140955.

Weitere Publikation, die nicht direkt mit dem Thema dieser Arbeit verknüpft sind:

Marizcurrena, J., López, W., Ma, H., Lamparter, T., and Sowinski, S. (2018). A highly efficient and cost-effective recombinant production of a bacterial photolyase from the Antarctic isolate *Hymenobacter sp.* UV11 (Submitted)

Zhao, H., Mauro, G., Mitea, S., Negrini, P., Guarino, M., Frigato, E., Braunbeck, T., Ma, H., Lamparter, T., Vallone, D., Bertolucci, C., and Foulkes, N. (2018)
Modulation of DNA repair systems in blind cavefish during evolution in constant darkness. (Submitted).

* Autoren haben in gleichem Maße zu der Arbeit beigetragen.

Abbreviations

BCP	bacterial cryptochrome/photolyase
CPD	cyclobutane pyrimidine dimers
Cry	cryptochrome
CPF	cryptochrome/photolyase family
Cry-DASH	(<i>Drosophila</i> , <i>Arabidopsis</i> , <i>Synechocystis</i> , Human)-type cryptochromes
ds DNA	double stranded DNA
DTT	dithiothreitol
DMRL	6,7-dimethyl-8-ribityllumazine
EDTA	Ethylenediaminetetraacetic acid
FAD	flavin adenine dinucleotide
Fe-S cluster	iron sulfur cluster
GST	glutathione S-transferase
HPLC	high performance liquid chromatography
IPTG	isopropyl- β -D-1-thiogalaktopyranosid
M ²⁺	divalent metal ion
MD	molecular dynamics
MTHF	5,10-methenyltetrahydrofolate
NER	nucleotide excision repair
OtCPF1	<i>Ostreococcus tauri</i> cryptochrome/photolyase family protein 1
PhrA	photolyase related protein A
PL	photolyase
PhrB	photolyase related protein B
Proma-PL	<i>Prochlorococcus marinus</i> photolyase
PEG	polyethylenglykol
PDB	protein data bank
RMSD	root mean square difference
ss DNA	single stranded DNA
TEAA	triethylamine acetate

TCEP	tris (2-carboxyethyl) phosphine
UV	ultraviolet
WT	wild type
(6-4) PPs	pyrimidine-pyrimidone-(6-4)-photoproducts
8-HDF	8-hydroxy-5-deazariboflavin

Contents

Publications..... I

Abbreviations..... III

Zusammenfassung..... 1

Summary..... 3

Introduction..... 5

1 UV light damages DNA..... 5

2 Repair of UV-damaged DNA 7

 2.1 Indirect repair: nucleotide excision repair 7

 2.2 Direct repair: photolyase..... 10

3 Photolyase/ cryptochrome family 10

 3.1 Photolyases 12

 3.2 Photoreduction 14

 3.3 Reaction mechanism of photolyases 17

4 PhrB from *Agrobacterium fabrum*..... 19

5 Aim of this project 21

Results..... 22

1 Different (6-4) DNA lesions affect the repair efficiency of PhrB 22

 1.1 Different length of (6-4) single stranded DNA lesions..... 22

 1.2 Single and double stranded (6-4) DNA lesions. 23

2 Divalent cations stimulate DNA repair activities of bacterial (6-4) photolyases 25

 2.1 Photorepair and photoreduction of PhrB 26

 2.2 Photorepair of CryB and Proma-PL..... 29

2.3 Photorepair and photoreduction of PhrA	31
2.4 Photorepair and photoreduction by OtCPF1	33
2.5 Summary of DNA repair.....	35
3 Key amino acids involved in DNA repair of PhrB	37
3.1 Key amino acids involved in metal ion-stimulated effect.	37
3.2 Mutants with impaired repair activity.....	38
4 Electron transfer pathway in photoreduction of PhrB	50
5 Crystal Structures of PhrB	55
5.1 Crystal structure of PhrB mutants with impaired DNA repair activity	55
5.2 Crystallization of PhrB under blue light	62
Discussion.....	65
1 Divalent metal ion effects on bacterial (6-4) photolyases	65
2. Model predicted for Mg ²⁺ effect on DNA repair	71
2.1 Crystal structure analysis of CPF proteins.....	71
2.2 Homology modeling and simulation prediction	74
2.3 Conclusion	79
3 Structure analysis of PhrB-I51W and PhrB-Y424F	80
4 Electron transfer chain of PhrB.....	82
Materials and methods	85
1 Protein preparation.....	85
1.1 Site-directed mutagenesis	85
1.2 Protein expression and purification	86
2 DNA repair assay.....	88

2.1 Preparation of CPD and (6-4) photoproducts	88
2.2 Repair assay	89
3 Photoreduction	90
4 Fluorimetry	90
5 Cofactor analysis.....	90
6. Crystallization.....	91
6.1 Crystallization assays.....	91
6.2 Crystal structure determination.....	92
References.....	93
Appendix.....	100
Acknowledgement	101

Zusammenfassung

Die (6-4) Photolyasen der bakteriellen Cryptochrom/Photolyase (BCP) -Gruppe gehören zu einer Familie von Flavoproteinen, die als Reparaturenzyme für UV-B-induzierte DNA-Läsionen (Photolyasen) oder als Blaulicht-Photorezeptoren (Cryptochrome) fungieren. Die (6-4) BCP-Proteine kommen ausschließlich in Prokaryoten vor.

In dieser Arbeit wurden 3 Mitglieder der (6-4) BCP-Gruppe, PhrB von *Agrobacterium fabrum*, CryB von *Rhodobacter sphaeroides* und Proma-PL von *Prochlorococcus marinus* mit einer eukaryotischen (6-4) Photolyase von *Ostreococcus tauri* OtCPF1 und einem Mitglied der Klasse III CPD Photolyasen PhrA von *Agrobacterium fabrum* verglichen. Es zeigte sich, dass die DNA-Reparatur-Effizienz von (6-4) BCP-Proteinen durch Mg^{2+} oder andere zweiwertige Kationen stimuliert wird, während bei OtCPF1 und PhrA keine Wirkung von zweiwertigen Kationen beobachtet wurde.

Der Einfluss zweiwertiger Kationen auf die Photoreduktion bei verschiedenen Photolyasen wurde ebenfalls untersucht. Die Photoreduktion von PhrB wurde durch Mg^{2+} negativ beeinflusst, während bei PhrA Mg^{2+} einen stimulierenden Effekt hatte. Es stellte sich klar heraus, dass die Abhängigkeit von Mg^{2+} bei der DNA-Reparatur der (6-4) BCP und nicht bei der Photoreduktion zu suchen ist. Dies veranlasste uns zu der Annahme, dass Mg^{2+} die DNA-Bindung und -Reparatur in (6-4) BCP-Proteinen beeinflusst. Zusammen mit den Strukturdaten und der Sequenzanalyse fanden wir eine vorgeschlagene Mg^{2+} Bindungsposition neben der DNA-Läsion und modifizierten die beiden betreffenden Aminosäuren durch ortsgerichtete Mutagenese. Der Effekt von Mg^{2+} ging für beide Mutanten verloren, während die Basisreparaturaktivität ohne Mg^{2+} von der Mutation nicht beeinflusst wurde. Vermutlich fördert Mg^{2+} die Bindung der (6-4) Läsion und erhöht die Elektronen-Affinität des Substrats. Außerdem wird die Barriere für Elektronentransfer verringert, wodurch und die Reaktion reibungsloser verläuft. Ich untersuchte auch die Reparatureffizienz für verschiedene Längen einzelsträngiger und doppelsträngiger DNA. Je länger die DNA war, desto schneller war die Reparatur. Bei

einer Länge der DNA von 12 nt oder mehr änderte sich allerdings mit Zunahme der Länge die Geschwindigkeit der Reparatur nicht mehr.

In dieser Arbeit werden auch die Mutanten PhrB-Y424F und PhrB-I51W vorgestellt. Tyr424 von PhrB ist Teil der DNA-Bindungsstelle und könnte eine Elektronenverbindung zum Fe-S-Cluster bilden. Die PhrB-Y424F-Mutante zeigte eine starke Verringerung der Bindung von Läsions-DNA und DNA-Reparatur. Die Mutante PhrB-I51W ist durch den Verlust des DMRL-Chromophors, reduzierte Photoreduktion und reduzierte DNA-Reparaturkapazität gekennzeichnet. Die Kristallstrukturen zeigen eine hohe Übereinstimmung mit der Wildtyp-Struktur, somit beeinflussen Mutationen nur lokale Proteinumgebungen.

Die Photoreduktion von PhrB unterscheidet sich von dem typischen Muster, da die dem FAD benachbarte Aminosäure der Elektronenkaskade ein Tyrosin (Tyr391) ist, während Photolyasen und Cryptochrome anderer Gruppen ein Tryptophan als direkten Elektronendonator von FAD besitzen. In einer Mutante, in der Tyr391 durch Tryptophan ersetzt wurde, ging der Cofaktor-FAD verloren und die PhrB-Struktur war instabil. Trp342 und Trp390 sind für den Ladungstransfer essentiell sind. Trp342 befindet sich an der Peripherie von PhrB. Die Rolle von Tyr391, die zwischen Trp390 und FAD liegt, war jedoch unklar, da der Ersatz durch Phenylalanin die Photoreduktion nicht blockierte. Bei der Substitution von Tyr391 durch Ala wurde die Photoreduktion blockiert, was darauf hindeutet, dass Tyr391 ein Teil der Elektronentransferkette ist und zeigt, dass der Ladungstransfer über die Triade 342-391-390 erfolgt. Diese Ergebnisse deuten auf ein *tunneling* (Elektronentransfer ohne Ladungsänderung) zwischen Trp390 und FAD hin.

Summary

The (6-4) photolyases of the bacterial cryptochrome/photolyase (BCP) group belong to a family of flavoproteins acting as repair enzymes for UV-B induced DNA lesions (photolyases) or as blue light photoreceptors (cryptochromes). The (6-4) BCP proteins are widely distributed in prokaryotes.

In this work 3 members of the (6-4) BCP group, PhrB of *Agrobacterium fabrum*, CryB of *Rhodobacter sphaeroides* and Proma-PL from *Prochlorococcus marinus*, were compared with a eukaryotic (6-4) photolyase from *Ostreococcus tauri* OtCPF1, and a member of the class III CPD photolyases PhrA from *Agrobacterium fabrum*. We found that the DNA repair efficiency of (6-4) BCP proteins is largely stimulated by Mg^{2+} and other divalent cations, whereas no effect of divalent cations was observed in OtCPF1 and PhrA.

The effect of divalent cations on photoreduction among those different types of photolyases was also studied. It was found that photoreduction is negatively affected by Mg^{2+} in PhrB, but stimulated by Mg^{2+} in PhrA. It turned out clearly that Mg^{2+} affects DNA repair of (6-4) BCP proteins rather than photoreduction. So we speculated that the Mg^{2+} should effect DNA binding and - repair in (6-4) BCP proteins. Together with the structural data and sequence analysis, we found a proposed Mg^{2+} binding position next to the DNA lesion and further modified the two related amino acids by site directed mutagenesis. The stimulated effect of Mg^{2+} was lost for both mutants, although the base repair activity without Mg^{2+} remained unaffected by the mutation. During the repair process Mg^{2+} seems to increase 6-4 lesion binding and the electron affinity of the substrate so decreasing the electron transfer barrier and make the reaction smoothly. I also investigated the repair efficiency for different lengths of single stranded and double stranded DNA and found that the longer the DNA is, the faster the repair will be, but when the length of DNA reach to 12 nt, the increase of length will not help the repaired speed anymore.

In this work the two PhrB mutants, PhrB-Y424F and PhrB-I51W, were also investigated. Tyr424 of PhrB is part of the DNA-binding site and could provide an electron link to the Fe-S cluster. The PhrB-Y424F mutant showed greatly reduced the binding of lesion DNA and DNA repair. The mutant PhrB-I51W is characterized by the loss of the DMRL chromophore, reduced photoreduction and reduced DNA repair capacity.

We found that photoreduction of PhrB differs from the typical pattern because the amino acid of the electron cascade next to FAD is a tyrosine (Tyr391), whereas photolyases and cryptochromes of other groups have a tryptophan as direct electron donor of FAD. I found that replacing Tyr391 by tryptophan will cause losing of cofactor FAD and further make PhrB structure fold unstable. Besides, through mutagenesis studies we identified Trp342 and Trp390 essential for charge transfer. Trp342 is located at the periphery of PhrB. The role of Tyr391, which lies between Trp390 and FAD, is however unclear as its replacement by phenylalanine did not block photoreduction. When Tyr391 was replaced by Ala, the photoreduction was blocked, indicating Tyr391 is a part of the electron transfer chain and revealing that charge transfer occurs via the triad 342-391-390. These results favor an electron-tunneling mechanism of electron transfer.

Introduction

1 UV light damages DNA

Sunlight contains three types of UV radiation: UV-A (315–400 nm), UV-B (280–315 nm) and UV-C (100–280 nm). UV-C has germicidal properties, so it was used in germicidal lamps. Due to the absorption by the atmosphere very small part of UV-C can reach to the Earth's surface; UV-B is also greatly absorbed by the Earth's atmosphere, and along with UV-C causes the photochemical reaction leading to the production of the ozone layer. It directly damages DNA and causes sunburn, but is also required for vitamin D synthesis in the skin and fur of mammals (Wacker and Holick, 2013); UV-A was once believed to be less damaging to DNA, and hence is used in cosmetic artificial sun tanning (tanning booths and tanning beds) and psoralen and ultraviolet A therapy for psoriasis. However, UV-A is later known to be able to cause significant damage to DNA via indirect routes (formation of free radicals and reactive oxygen species), and can cause cancer (Mouret *et al.*, 2006; Brem *et al.*, 2017).

UV irradiation of DNA causes formation of three different types of DNA lesions between two adjacent pyrimidine in the DNA chain on the same strand, termed CPD, (6-4), and Dewar lesions, described in Figure 1 (Kim *et al.*, 1994). CPDs are formed by a $[2\pi + 2\pi]$ cycloaddition reaction between the two C5=C6 bonds of the adjacent pyrimidines, which form from the excited triplet state of pyrimidines following singlet-triplet intersystem crossing. So, using acetophenone as a triplet sensitizer, which populates the thymine π, π^* triplet exclusively, and makes it possible to form CPD in DNA to exclusion of the (6-4) PPs (Meistrich and Lamola, 1972). CPDs appear *in vivo* between all pyrimidine pairs, but not in equal ratios. The formation trends are $5'-T(\text{CPD})T-3' > 5'-T(\text{CPD})C-3' > 5'-C(\text{CPD})T-3' > 5'-C(\text{CPD})C-3'$, where the yield of T(CPD)T is about three times higher than T(CPD)C (Mouret *et al.*, 2006) (Cadet *et al.*, 2005). The (6-4) PPs are formed more efficiently at TC rather than TT sites (Heil *et al.*, 2011).

The (6-4) photoproduct is thought to form in DNA as follows (Figure 1): a [2 + 2] cycloaddition of the C4 carbonyl (or amino) of the 3' thymine (cytosine) across the 5-6 double bond of the 5' thymine generates an oxetane (or azetidene) ring, which at temperatures above -80 °C undergoes ring opening by C4-O bond cleavage accompanied by a proton shift from N5 to generate the “open form” of the (6-4) photoproduct (O. and L., 1969). Irradiation of the (6-4) photoproduct by UV-A and UV-B converts the (6-4) photoproduct to the Dewar valence isomer, which can be reverted back to the open form by UV-C irradiation. (Sancar, 2003)

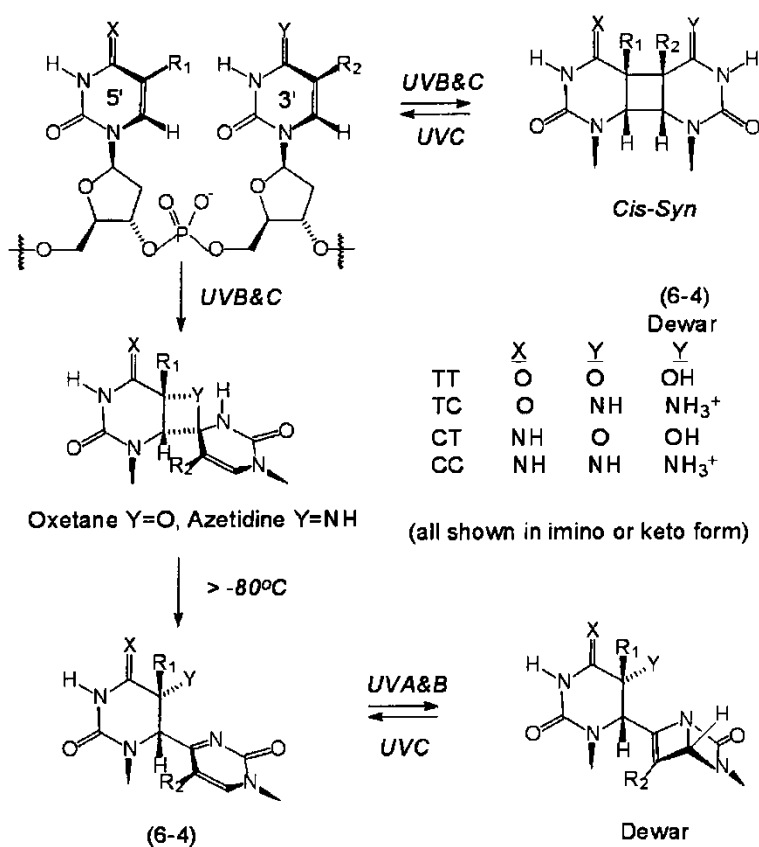


Figure 1. Formation of (6-4) photoproducts (Taylor, 1994; Sancar, 2003). The (6-4) photoproduct forms by a Paternó-Büchi reaction between two adjacent pyrimidines, which generates an oxetane or azetidene four-membered ring intermediate. This intermediate is not stable above -80 °C, and undergoes rearrangement to produce the open form of the photoproduct, the (6-4) photoproduct. Figure from (Taylor, 1994).

2 Repair of UV-damaged DNA

UV-induced DNA lesions are responsible for much of the destructive effect of UV light since they can act as a physical blockage for replication and transcription, thereby drastically impeding metabolic processes in DNA. UV damage may subsequently lead to mutagenesis or cell death (Sancar, 2016). These DNA photoproducts triggered mutations are predominately found as C to T or CC to TT transitions. Mutations on proteins involved in cell cycle control, apoptosis, or DNA repair could result in carcinogenesis, for example, the p53 mutation that caused skin cancer (Batista *et al.*, 2009) (Kanavy and Gerstenblith, 2011) (Pfeifer *et al.*, 2005).

Therefore, DNA repair mechanisms are essential for all organisms that are exposed to light. This UV light induced damage is repaired by photolyase in *E. coli* and by the nucleotide excision repair system in *E. coli* and in humans. The nucleotide excision repair, which is present in almost all organisms, is based on the coaction of multiple enzymes and requires an intact complementary DNA strand as template, *i.e.* cannot repair single stranded DNA. The so called photorepair is based on the action of a single protein, a photolyase. These enzymes can repair UV lesions in single and double stranded DNA.

2.1 Indirect repair: nucleotide excision repair

Nucleotide excision repair (NER) is an indirect method to repair DNA lesion, which is initiated by the DNA lesion recognition and binding (Figure 2). The DNA helix is subsequently unwound at the DNA lesion site, followed by the excision of a short oligonucleotides segment including the lesion site. The undamaged single-stranded DNA remains and DNA polymerase uses it as a template to synthesize a short complementary sequence. Final ligation to complete NER and form a double stranded DNA is carried out by DNA ligase (Fuss and Cooper, 2006).

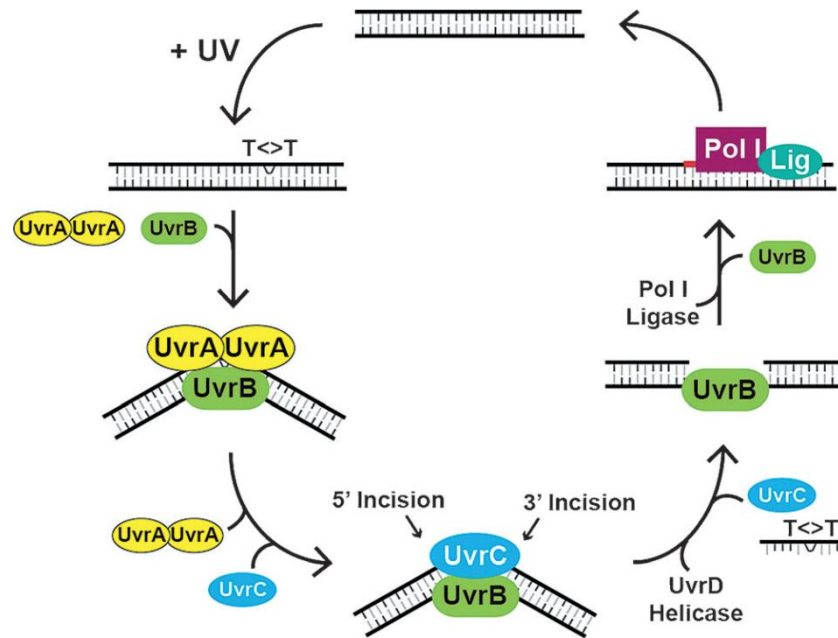


Figure 2. Reaction mechanism of excision repair in *E. coli*. The damage is recognized by the (UvrA)₂ homodimer which functions as a molecular matchmaker to recruit UvrB to the damage site. An ATP hydrolysis-dependent reaction then promotes the formation of a very stable UvrB–DNA complex. This complex recruits UvrC, which incises 5' and 3' to the damage due to active site nucleases within the N-terminal and C-terminal halves of the protein. UvrC and the excised dodecamer (12-mer) are then displaced by the UvrD helicase, and UvrB is displaced by DNA Polymerase I as it fills in the gap. The nick is then sealed by ligase (Lin and Sancar, 1992). Figure from Lin *et al.*, 1992.

NER is a versatile and flexible DNA repair mechanism which is conserved in prokaryotes and eukaryotes (Hoeijmakers, 2001; Morita *et al.*, 2010). This mechanism can repair a broad range of structurally unrelated DNA lesions. The most relevant lesions subject to NER are UV-induced CPDs and (6-4) PPs. In addition, numerous other helix-disrupting (or "bulky") lesions are eliminated by this process such as benzo[a]pyrene-guanine adducts caused by smoking and guanine-cisplatin adducts formed during cancer chemotherapy (Sancar, 1994). NER can be divided into two subpathways. The NER occurring in DNA that undergoes transcription is called transcription-coupled repair, while the NER in non-transcribed parts of the genome, including the non-transcribed

strand of transcribed genes, is called global genome repair. The two subpathways differ in how they recognize DNA damage but they share the same process for lesion incision, repair, and ligation. (Lehmann, 1995; Lindahl and Wood, 1999). Due to lacking of the photolyase-induced photoreactivation, NER plays a particular important role in the UV damaged DNA repair of placental mammals (Costa et al., 2003).

The Nucleotide excision repair process in *E. coli* and human are quite similar, but still have some different. For example, a more complete list of proteins involved in NER of human and the enzyme number involved in the whole repair process of human is about 4 times more than that in the *E. coli*. The DNA fragment that is excised is a oligomer of 12 nucleotides in *E. coli*, while in human is 30 nucleotides (Figure 3) (Sancar, 1994).

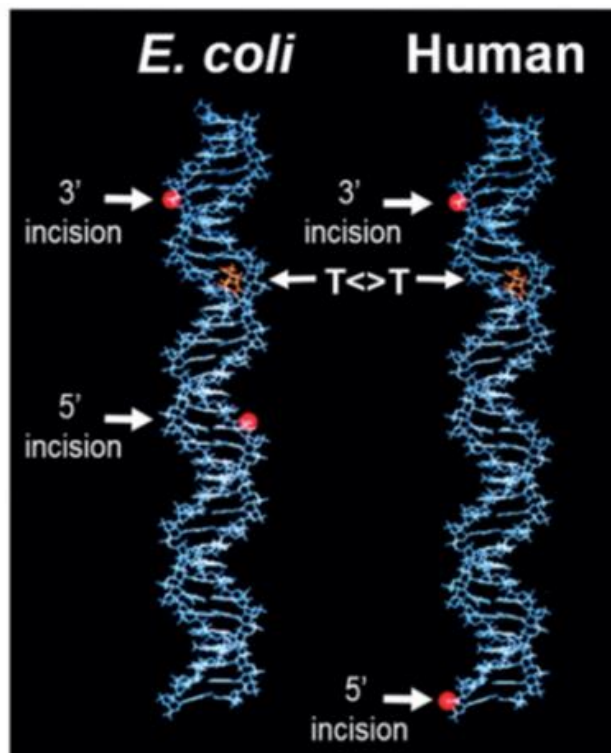


Figure 3. Excision repair in *E. coli* and humans. In both organisms, excision is by dual incisions. However, the proteins required for the dual incisions, the mechanisms for damage recognition, and the dual incision patterns are entirely different (Huang *et al.*, 1992; Sancar, 2016). Adapted from (Sancar, 2016).

2.2 Direct repair: photolyase

Photoreactivation (Dulbecco, 1949; Kelner, 1949) is the reversal of the harmful effects, such as growth delay, mutagenesis, and death of far UV (200-300 nm) on organisms by concurrent or subsequent exposure to blue light (350-450 nm).

The photoreactivation was independently discovered in two American laboratories. In early studies cells survival was predominantly used as a biological characteristic. Later on an *in vitro* photoreactivation system, DNA transformation assay, was taken. With this methodology, Rupert found that photoreactivation is an enzymatic process, mediated by an enzyme named photoreactivating enzyme (Setlow and Carrier, 1966), which was later called photolyase. Rupert continued to study the repair reaction in some details and finally demonstrated that the photoreactivation follows Michaelis–Menten reaction kinetics with the notable exception that catalysis is absolutely dependent on light. Photolyase binds to UV-damaged DNA in the dark and is released from the repaired DNA upon illumination with visible light (Rupert, 1962; Sancar, 2000).

Photolyases from *E. coli* and budding yeast that were studied by Rupert, Dulbecco and others could repair only CPDs (Dulbecco, 1949; Rupert, 1962; Sancar, 2000). Forty four years after the discovery of CPD photolyase, the photolyase that repairs (6-4) photoproducts was discovered from *Drosophila melanogaster* by Takeshi Todo (Todo *et al.*, 1993).

3 Photolyase/cryptochrome family

So far a vast number of photolyase and photolyase-like genes in all three domains of life are known, their encoded proteins sharing a structurally highly conserved core domain and the active cofactor. These proteins form a huge flavoprotein family, termed cryptochrome/photolyase family (CPF).

Phylogenetically, proteins of photolyase/cryptochrome family are sorted into 7 different groups (Figure 4): class I CPD photolyases which comprised the founding member *E. coli* photolyase and mainly bacterial homologs, the class II CPD photolyases

with mainly eukaryotic members (Okafuji *et al.*, 2010), the class III CPD photolyases (Todo, 1999), another group with mainly bacterial members, the Cry-DASH proteins, which are CPD photolyases that repair only single stranded DNA (Tagua *et al.*, 2015), the eukaryotic (6-4) photolyases and animal cryptochromes, plant cryptochromes and a group of prokaryotic (6-4) photolyases that is termed (6-4) BCP proteins.

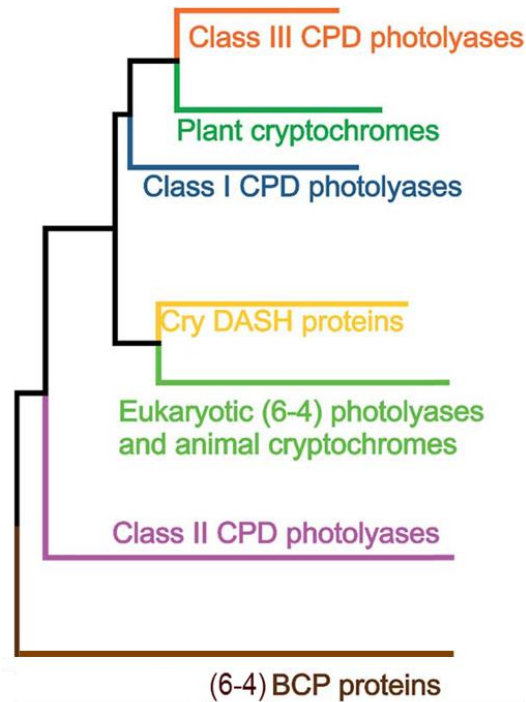


Figure 4. Phylogenetic tree of photolyases and cryptochromes. The tree is a simplified version of trees shown in previous publications (Tilman Lamparter *et al.*, 2014; Scheerer *et al.*, 2015) in which only the groups of photolyase and cryptochromes are shown. Adapted from (Holub *et al.*, 2018).

These members that are able to repair CPD and (6-4) PPs are called photolyases . There are also CPF members that are incapable of repairing UV-induced DNA damage, which are called cryptochromes. Cryptochromes regulate blue light responses in plants, the circadian rhythm in animals and possibly also function as magnetoreceptors in birds

and insects. The first cryptochrome was found in *Arabidopsis thaliana* (Ahmad and Cashmore, 1993) and later discovered in humans (Hsu *et al.*, 1996). However, The discrimination between photolyases and cryptochromes became recently blurred as cryptochromes, such as the DASH-type or CryA from *Aspergillus nidulans*, exert dual functions by being competent in signaling and DNA repair (Bayram *et al.*, 2008; Pokorny *et al.*, 2008). The other example is CryB from *Rhodobacter sphaeroides* which acts as photoreceptor (Hendrischk *et al.*, 2009; Geisselbrecht *et al.*, 2012) and also has DNA repair function (von Zadow *et al.*, 2016).

3.1 Photolyases

Photolyases have been reported in all three domains of life, except in placental mammals including humans. DNA photolyases are monomeric repair enzymes with a molecular weight of 50 to 65 kDa and a length of 454 to 614 amino acids (Weber, 2005; Essen and Klar, 2006). They generally contain two noncovalently bound chromophoric cofactors. The first cofactor is a flavin adenine dinucleotide (FAD). Only the fully-reduced form of FAD (FADH⁻) is enzymatically active. FADH⁻ functions as the catalytic cofactor and electron donor. The second cofactor is an antenna chromophore functioning in absorbing light and transferring the excitation energy to the catalytic cofactor, which varies depending on the protein (Sancar, 2003). Nowadays 10-methenyltetrahydrofolate (MTHF, $\lambda_{\max} \approx 380$ nm) (Johnson *et al.*, 1988) and several nucleotide-like compounds such as 8-hydroxy-5-deazariboflavin (8-HDF, F0, $\lambda_{\max} \approx 445$ nm) (Eker *et al.*, 1990), flavin mononucleotide (FMN, $\lambda_{\max} \approx 446$ nm) (Ueda *et al.*, 2005) and FAD (Fujihashi *et al.*, 2007) have been described as antenna chromophores in photolyases (Figure 5). In recent years, a new antenna chromophore DMRL in *Rhodobacter* CryB and *Agrobacterium* PhrB from (6-4) BCP has been found (Geisselbrecht *et al.*, 2012; Zhang *et al.*, 2013).

Figure 5. Antenna chromophores of photolyases. The left drawings show the chemical structures of the antenna chromophores, the panels in middle show the 3D structure and the right panel shows the UV-Vis spectra of the protein, usually with FAD in the reduced FADH- form. (A) *E. coli* photolyase (PDB code 1DNP) with 10-methenyltetrahydrofolate (MTHF) as antenna chromophore (Park *et al.*, 1995; Sancar and Sancar, 2006). (B) *A. nidulans* photolyase with 8-hydroxy-5-deazaflavin (8-HDF, F0) as antenna chromophore (PDB code: 1QNF) (Sancar and Sancar, 2006; Fujihashi *et al.*, 2007). (C) *T. thermophilus* photolyase with flavin mononucleotide (FMN) as antenna chromophore. (PDB code: 2J09). The UV-Vis spectrum is taken after purification (FADH and FMN) (Klar *et al.*, 2006). (D) *S. tokodaii* photolyase with FAD as antenna chromophore (PDB code: 2E0I). The UV-Vis spectrum is taken immediately after purification (Fujihashi *et al.*, 2007). (E) *Agrobacterium fabrum* photolyase with 6,7-dimethyl-8-ribityllumazine (DMRL) as antenna chromophore (PDB code: 4DJA) (Zhang *et al.*, 2013).

The presence of the antenna chromophore is not an absolute requirement for photolyases activity, since the photolyases lacking this chromophore are still biologically active (Zhang *et al.*, 2017). However, the antenna chromophore absorbs blue light and transfers excitation energy to the catalytic cofactor, consequently improving the DNA repair efficiency (Sancar, 2003; Selby and Sancar, 2012; Zhang *et al.*, 2017).

3.2 Photoreduction

Photoreduction exists in both cryptochromes and photolyases, it means under the trigger of blue light the cofactor FAD gradually change its redox state to fully reduced state. During this process, electrons flow from the surface via conserved amino acid residues to FAD (Figure 6). Typically, the electron transfer pathway consists of 3 conserved tryptophane and tyrosine residues (normally Trp-triad) in the protein moiety that is located within the C-terminal α -helical domain. The Trp-triad is conserved in most of the DNA photolyases subfamilies except class II photolyases, in which an alternative Trp-triad was identified at different position (Figure 6) (Kiontke *et al.*, 2011; Maul *et al.*, 2008; Park *et al.*, 1995).

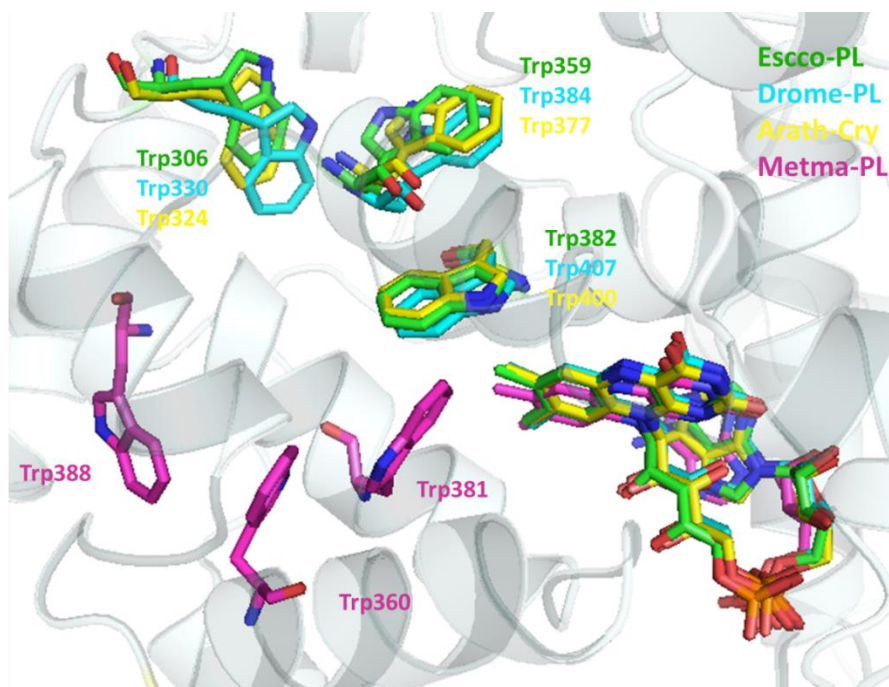


Figure 6. The electron transfer chain that reduces photoexcited oxidized FAD via a conserved tryptophan triad (Trp-triad). The Trp-triads and FAD of *E. coli* CPD I photolyase (1DNP), *Drosophila melanogaster* (6-4) photolyase (3CVV), *Arabidopsis thaliana* Cry1 (1U3C) and *Methanosarcina mazei* CPD II photolyase (2XRY) are shown in sticks. *Escherichia coli* photolyase is illustrated in cartoon.

Flavin bound to proteins may exist in any one of the three redox states in five different forms: oxidized (*e.g.* FAD), semireduced semiquinones (*e.g.* neutral radical FADH^\bullet , anion radicals $\text{FAD}^{\bullet-}$) or fully reduced hydroquinones (*e.g.* FADH^- or FADH_2) (Figure 7) (Kao *et al.*, 2008). Because of the different spectral properties, the flavin redox states of flavoproteins can be analyzed *in vitro* by monitoring protein absorption spectra.

In photolyase, the catalytically active form of flavin is FADH^- , which is the predominant form *in vivo*. During the purification of photolyases under aerobic conditions the flavin cofactor is usually oxidized to the semireduced and eventually to the fully oxidized form (Payne *et al.*, 1987). Exposure of such inactive photolyases to light in the presence of a reducing agent, such as dithiothreitol (DTT), ethylenediaminetetraacetic

acid (EDTA) or β -mercaptoethanol, can convert the photoexcited flavin to the active FADH^- form (Heelis and Sancar, 1986; Sancar *et al.*, 1987). Nicotinamide adenine dinucleotides can turn the photoexcited flavin to the semiquinoid $\text{FAD}^{\cdot-}$ State (Ignatz *et al.*, 2018). In addition, Based on our measurement, TCEP can also convert the oxidize FAD to FADH^- State.

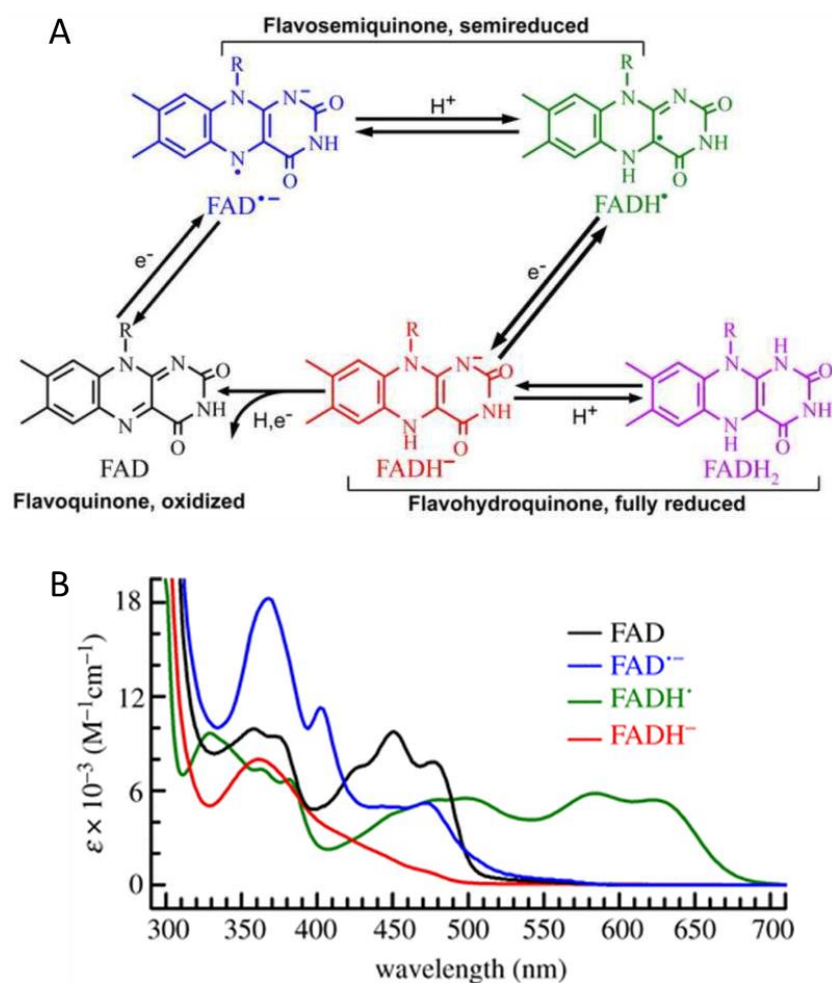


Figure 7. Oxidoreduction of flavins. (A) Five possible redox forms of flavins are shown. R indicates different side groups in different flavins. The two different forms of semiquinone radicals: anion radical (*e.g.* $\text{FAD}^{\cdot-}$) and neutral radical (*e.g.* FADH^{\cdot}), and two forms of reduced flavins: protonated hydroquinone (*e.g.* FADH_2) and anionic hydroquinone (*e.g.* FADH^-) are shown. (B) Absorption spectra and extinction coefficients (ϵ) of different redox forms of the

following cryptochrome/photolyase (Kao *et al.*, 2008). Mosquito AgCRY1 (*Anopheles gambiae*) containing oxidized FAD (black line) or anion radical semiquinone ($\text{FAD}^{\bullet-}$, blue line), and *E. coli* photolyase containing neutral radical semiquinone (FADH^{\bullet} , green line) or fully reduced flavin (FADH^- , red line). Adapted from (Liu *et al.*, 2010).

3.3 Reaction mechanism of photolyases

Based on previous studies, such as crystallography and ultrafast spectroscopy, the major part of the DNA photolyase repair mechanism has been resolved both structurally and dynamically (Mees *et al.*, 2004; Maul *et al.*, 2008; Glas *et al.*, 2009b; Li *et al.*, 2010; Liu *et al.*, 2011). The light-harvesting chromophore of photolyases absorbs blue light to excite the fully-reduced FADH^- and then FADH^- transfers an electron to either the CPD or the (6-4) lesion which drives the dimer into the monomers. The electron finally returns back to restore the active state of FADH^- (Stuchebrukhov, 2011).

For CPD lesions (Figure 8), the single electron reduced cyclobutane ring undergoes a thermally forbidden [2+2] cycloreversion reaction followed by back transfer of the ‘enabling electron’ to the semireduced FADH^{\bullet} (Muller and Carell, 2009). The initial electron transfer to the dimer takes 250 ps, the ring opening occurs in two steps, the first in less than a few picoseconds and the second with a time constant of 90 ps. After the dimer is split, the electron returns back to FADH with a time constant of about 700 ps (Liu *et al.*, 2011).

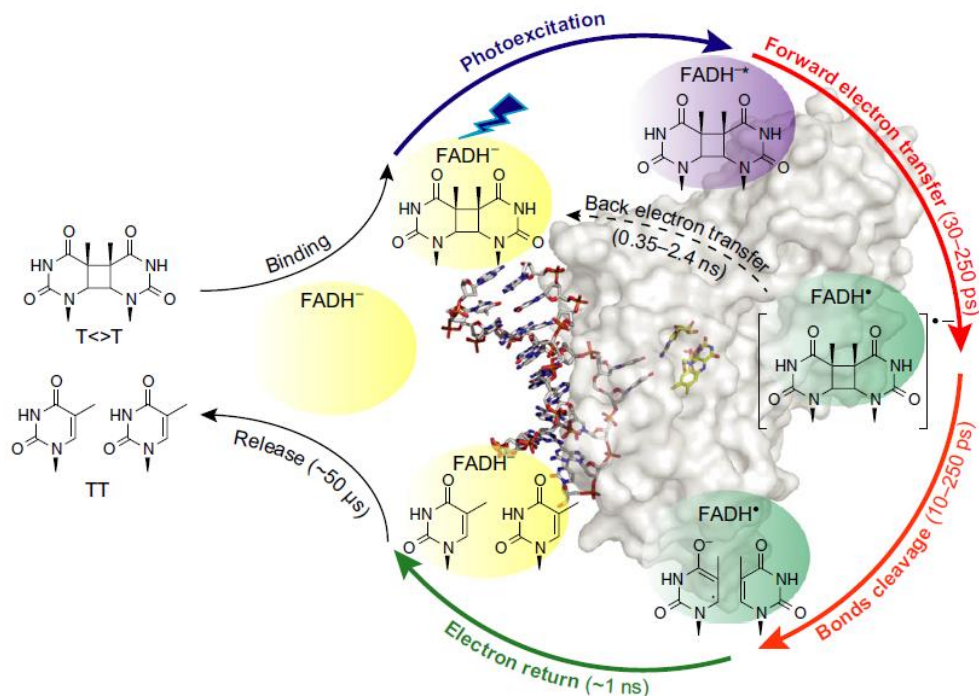


Figure 8. Sketch of the reaction cycle for photorepair of CPD lesion by CPD PL. The indicated ranges of time constant cover results obtained by different groups (Yamamoto *et al.*, 2017). Inside the repair cycle, a structural overview is shown of CPD PL from *Anacystis nidulans* (surface representation in gray; the FAD cofactor is highlighted in sticks representation) bound to a double-stranded oligomer (in sticks representation on the left side) that initially contained a CPD lesion, which is flipped out of the double helix into the enzyme's binding pocket. In the X-ray crystal structure (PDB code 1TEZ) (Mees *et al.*, 2004), the two intradimer bonds are broken, presumably due to the synchrotron irradiation. Figure from (Yamamoto *et al.*, 2017).

In (6-4) photolyases (Figure 9), upon excitation the FADH⁻ donates an electron to the (6-4) PPs to generate a charge-separated radical pair (FADH[•] + (6-4) PP^{•-}), which subsequently induces proton transfer from an essential His residue of the photolyase to the (6-4) PPs. These successive steps naturally proceed to an intramolecular proton transfer from the -OH group on the C5 of the 5' base to the N3 at the 3' base to form a transient zwitterion. Then, the oxygen atom attacks the C4 position at the 3' base to form a transient oxetane-type structure. The transient oxetane formation facilitates the oxygen-atom transfer from the 5' to the 3' base followed by the splitting of the C6-C4 bond. After oxygen transfer and C-C bond

cleavage the proton returns to the His residue and the electron returns to FADH• to restore the active form of the enzyme and the two pyrimidine bases (Li *et al.*, 2010).

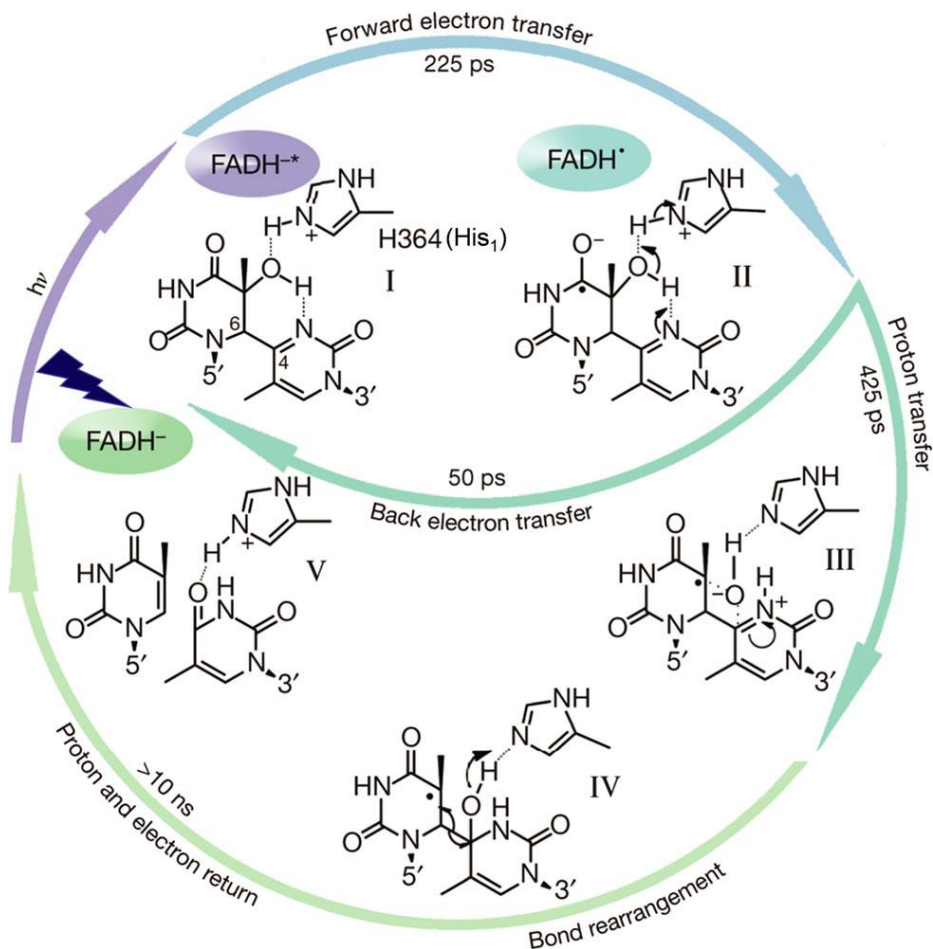


Figure 9. Reaction cycle for photorepair of a T(6-4)T lesion by the (6-4) photolyase of *Arabidopsis thaliana* (Li *et al.*, 2010), on the basis of an experimental study of the reaction by ultrafast fluorescence and transient absorption spectroscopy. Figure from (Li *et al.*, 2010).

4 PhrB from *Agrobacterium fabrum*

In previous studies the crystal structure of PhrB has been solved in our group (Zhang *et al.*, 2013). PhrB has been experimentally confirmed to be able repair (6-4) photoproduct

in vitro, so PhrB is a bacterial (6-4) photolyase. Before this finding, (6-4) photolyase was thought to be restricted to eukaryotes. Based on sequence analysis we propose that (6-4) photolyases are broadly distributed in prokaryotes which are sorted as (6-4) BCP proteins. The (6-4) BCP proteins are most distantly related to the other groups. (6-4) BCP photolyases (CryB and PhrB) share a common fold with primase, which is an ancient enzyme that synthesizes RNA oligonucleotides during replication. We therefore assume that the (6-4) BCP proteins represent the most ancient group of photolyases and cryptochromes. About this new type of (6-4) photolyase, several topics are interesting:

(1) The two (6-4) BCP proteins investigated so far, *Rhodobacter* CryB and *Agrobacterium* PhrB, have Fe-S cluster and DMRL antenna chromophore. Photolyases and cryptochromes of other groups have MTHF, 8-HDF or other antenna chromophores, but never DMRL. Proma-PL of *Prochlorococcus marinus* belongs to the subgroup of (6-4) BCP which has no Fe-S cluster.

(2) According to crystal structure of the two (6-4) BCP members (PhrB and CryB), they have a C-terminal extension, a feature in common with cryptochromes and some photolyases, although the sequences reveal no homology between the different groups. The C-terminal extension of cryptochromes is relevant for signal transduction, and both CryB and PhrB could serve as photoreceptors for bacterial light responses.

(3) A loop between helix 7 and 8 of PhrB interacts with the DNA. This DNA interaction is replaced by another loop in other photolyases.

(4) Photoreduction of PhrB differs from the typical pattern because the amino acid of the electron cascade next to FAD is a tyrosine (Tyr391), whereas photolyases and cryptochromes of other groups usually have a tryptophan as direct electron donor of FAD.

5 Aim of this project

In this work, we aimed at further investigate of PhrB to find out the role of the new cofactor DMRL, find out the electron transfer chain of PhrB photoreduction, check the impact of divalent metal ions on different photolyases, and reveal the role of magnesium in the mechanism of DNA repair.

Results

1 Different (6-4) DNA lesions affect the repair efficiency of PhrB

1.1 Different length of (6-4) single stranded DNA lesions

In order to test the impacts of different DNA substrates on DNA repair and choose the suitable DNA substrate for further repair assay, I tested the impact of different length oligonucleotides and the difference between single and double stranded oligonucleotides in Mg^{2+} free conditions. In previous work (Zhang *et al.*, 2013; Ma *et al.*, 2017), the oligonucleotide "t_repair" with 8 nucleotides was always used, whereas for experiments with double stranded DNA, 15mer were used (the larger size was necessary because shorter DNA would not form stable double strands at the assay temperatures). Length variations of single stranded oligonucleotides have however not been performed before. I therefore compared the repair activities for single stranded oligonucleotides with 8, 10, 12 and 15 bases (Figure 10 and Table 12). Under conditions of the present work, no repair of the 8mer "t_repair" was detectable by HPLC for irradiation times of up to 40 min and a 60 min irradiation resulted in a repair of only (0.9 ± 0.1) % repair. For the ODN4 (6-4) photoproduct, which has 10 nucleotides, there was no detectable signal of repaired DNA for illumination times up to 20 min, and after 40 min irradiation (4.2 ± 0.2) % were repaired. With ODN5 and ODN6, which have 12 and 15 oligonucleotides, respectively, about half of the lesion DNA was repaired after 20 min and the repair was complete after 40 min of irradiation. We concluded that the weak repair in our previous studies (Ma *et al.*, 2017) was not only due to the lack of Mg^{2+} but also due to the short length of the oligonucleotide. The more efficient repair with longer oligomers is most likely due to an increased binding of the oligomers to PhrB. Because there was no increase between ODN5 and ODN6, we assume that there would be no further improvement for larger oligomers.

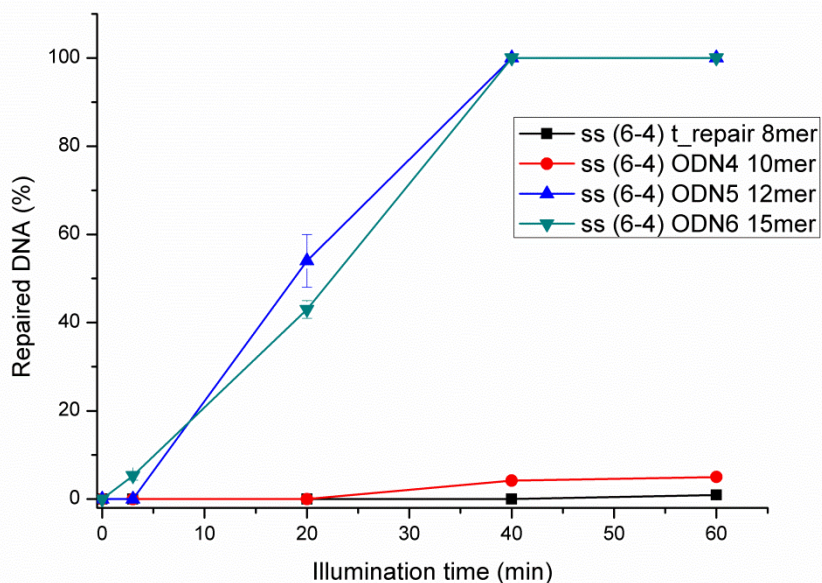


Figure 10. Repair of single stranded (6-4) photoproducts of different lengths. The repair assays were performed in the absence of divalent cations. Proportion of repaired DNA of (6-4) photoproducts of single stranded DNA oligonucleotides "t_repair" (8mer, black squares), ODN4 (10mer, red circles), ODN5 (12mer, blue up-pointing triangles), ODN6 (15mer, down-pointing triangles) Irradiation times were 0, 3, 20, 40 and 60 min. Mean values \pm SE from 3 independent experiments. In those cases where SE error bars are invisible, the errors are smaller than the symbols.

1.2 Single and double stranded (6-4) DNA lesions.

The melting temperature of ds (6-4) ODN5 is about 10 °C higher than the reaction temperature of 22 °C such that the DNA would not melt into single strands. In the absence of Mg^{2+} in the reaction mixture, after 20 min irradiation (54 ± 6) % ss (6-4) ODN5 and (10 ± 0.5) % ds (6-4) ODN5 were repaired, respectively, while in the presence of Mg^{2+} both ss (6-4) ODN5 and ds (6-4) ODN5 were completely repaired within 20 min. Because this result did not allow us to make a quantitative comparison, I reduced the repair time for the assay with Mg^{2+} . When the reaction mixture was irradiated for only 2

min in the presence of Mg^{2+} (81 ± 2) % of ss (6-4) ODN5 and (35 ± 0.5) % of ds (6-4) ODN5 were repaired. When the experiments were repeated in the absence of Mg^{2+} there was no detectable repaired DNA in the HPLC profiles.

When a repair assay was performed with double stranded (6-4) ODN5 for 20 min, the repair efficiency was lower than with single stranded (6-4) ODN5 (Figure 11 and Table 2). In a control experiment, ds (6-4) ODN5 was heated to $95\text{ }^{\circ}\text{C}$ and suddenly cooled on ice to let most of the DNA remain in the single strand state. With this substrate the DNA repaired percentage was ~ 32 % lower than with ss (6-4) ODN5, but still ~ 25 % higher than with ds (6-4) ODN5. This result may be explained either by a part amount of DNA to still form ds DNA or by the complementary ss DNA interfering with repair of the ss (6-4) DNA, and it also confirms that PhrB repairs ss (6-4) ODN5 more efficiently than ds (6-4) ODN5.

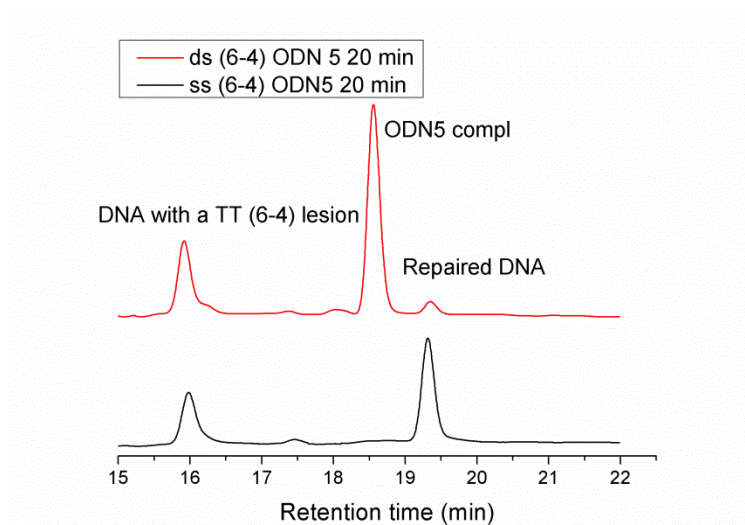


Figure 11. Repair of single stranded (6-4) photoproducts and ds (6-4) ODN5 by the PhrB photolyase. Reaction mixture irradiated for 20 min in the absence of Mg^{2+} . Two examples of HPLC profiles of DNA repair by PhrB-WT: ds (6-4) ODN5 as substrate (upper red curve) and ss (6-4) ODN5 as substrate (lower, black curve).

2 Divalent cations stimulate DNA repair activities of bacterial (6-4) photolyases

In the present study, I focus on the role of divalent cations in biochemical activities of five photolyases out of three different phylogenetic groups (Figure 12) and they are 3 members of (6-4) BCP group, PhrB of *Agrobacterium fabrum*, CryB of *Rhodobacter sphaeroides* and Proma-PL from *Prochlorococcus marinus*, a eukaryotic (6-4) photolyase from *Ostreococcus tauri* OtCPF1, and a member of the class III CPD photolyases PhrA from *Agrobacterium fabrum*. Except PhrA is a CPD photolyase, all of the rest 4 proteins are (6-4) photolyases (Table 1).

It is proposed that in the activated form of photolyase the FAD chromophore is in its fully reduced state FADH⁻ (Muller and Carell, 2009), as our proteins were purified under aerobic condition and FADH⁻ gradually turned into oxidized state which can be verified by spectra measurement. Anyway, it is necessary to check whether divalent metal cations have impacts on photoreduction and photorepair, separately.

Table 1. Wild type proteins investigated in this project and their corresponding organisms.

Proteins	characterization	organisms
PhrB	with Fe-S cluster	<i>Agrobacterium fabrum</i>
CryB	with Fe-S cluster	<i>Rhodobacter sphaeroides</i>
Proma-PL	no Fe-S cluster	<i>Prochlorococcus marinus</i>
OtCPF1	eukaryotic (6-4) photolyase	<i>Ostreococcus tauri</i>
PhrA	CPD photolyase	<i>Agrobacterium fabrum</i>

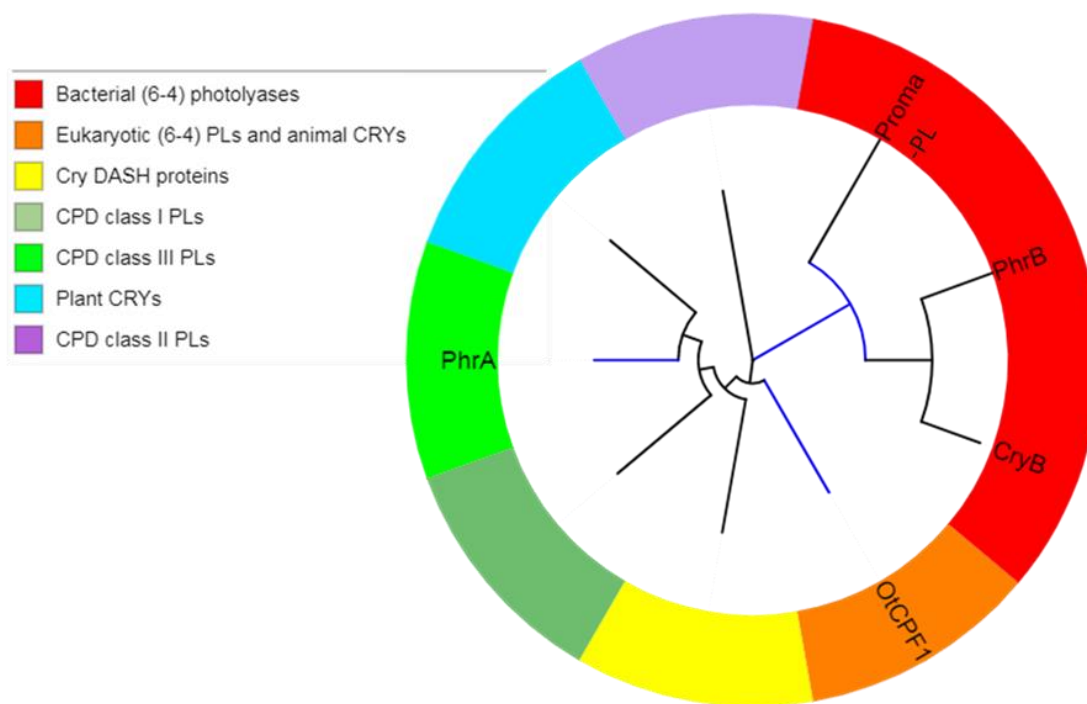


Figure 12. Phylogenetic tree of photolyases and cryptochromes. The tree is a simplified version (Scheerer *et al.*, 2015) which the groups of photolyase and cryptochromes are shown in different color. Proteins used in the present study are indicated by abbreviated letters in their corresponding group.

2.1 Photorepair and photoreduction of PhrB

Photorepair assays with PhrB from *Agrobacterium fabrum* have been performed in the absence of divalent cations (Zhang *et al.*, 2013), according to common practice in photolyase research (Maul *et al.*, 2008; Hendrischk *et al.*, 2009). In our previous assays we used a high protein: DNA ratio of 1:1 (Zhang *et al.*, 2017). Single stranded (6-4) t_{repair} DNA was only incompletely repaired (ca. 27 %) after 2 h. In experiments of this subchapter I concentrated on the repair of single stranded (6-4) t_{repair} DNA, which allows higher throughput of measurements with varying biochemical parameters. After it turned out that divalent cations increase the repair efficiency, I changed the initial DNA/protein ratios and HPLC conditions, because in the presence of Mg²⁺ the original

high protein/DNA ratios resulted in the completion of DNA repair being too fast for any quantitative assessment. Examples for HPLC profiles obtained under new conditions are shown in (Figure 13A). From such measurements, the percentages of repaired DNA were calculated and used for comparisons between different reaction conditions and between different photolyases. The (6-4) DNA lesion repair activity of PhrB in the absence of divalent cations was quantified after illuminating the sample for 120 min with strong blue light (400 nm, $250 \mu\text{mol m}^{-2} \text{s}^{-1}$), and after 30 min irradiation, the yield of repaired DNA could not be detected. After 120 min illumination, we found that (3 ± 0.1) % of the (6-4) DNA lesions were repaired (Figure 13B). However, when Mg^{2+} or Mn^{2+} was added to the reaction solution, the (6-4) lesions were completely repaired within 10 min. I thus reduced the repair time further. After an illumination time of 3 min, (48 ± 3) % and (68 ± 2) % of the (6-4) DNA lesions were repaired in the presence of 4 mM free Mg^{2+} and 4 mM free Mn^{2+} , respectively (Table 4). In the presence of Ca^{2+} , DNA repair was also promoted: after 20 min illumination, (13 ± 0.8) % DNA was repaired. Based on these data and the given illumination conditions, we calculated the rate constants of DNA repair in the presence and absence of divalent cations, considering a simple exponential decay of the substrate concentration during the enzymatic reaction (Table 4). According to these calculations, Mg^{2+} , Mn^{2+} and Ca^{2+} enhanced the DNA repair activity of wild type PhrB 879 ± 62 , 1530 ± 16 , and 28 ± 0.5 times, respectively.

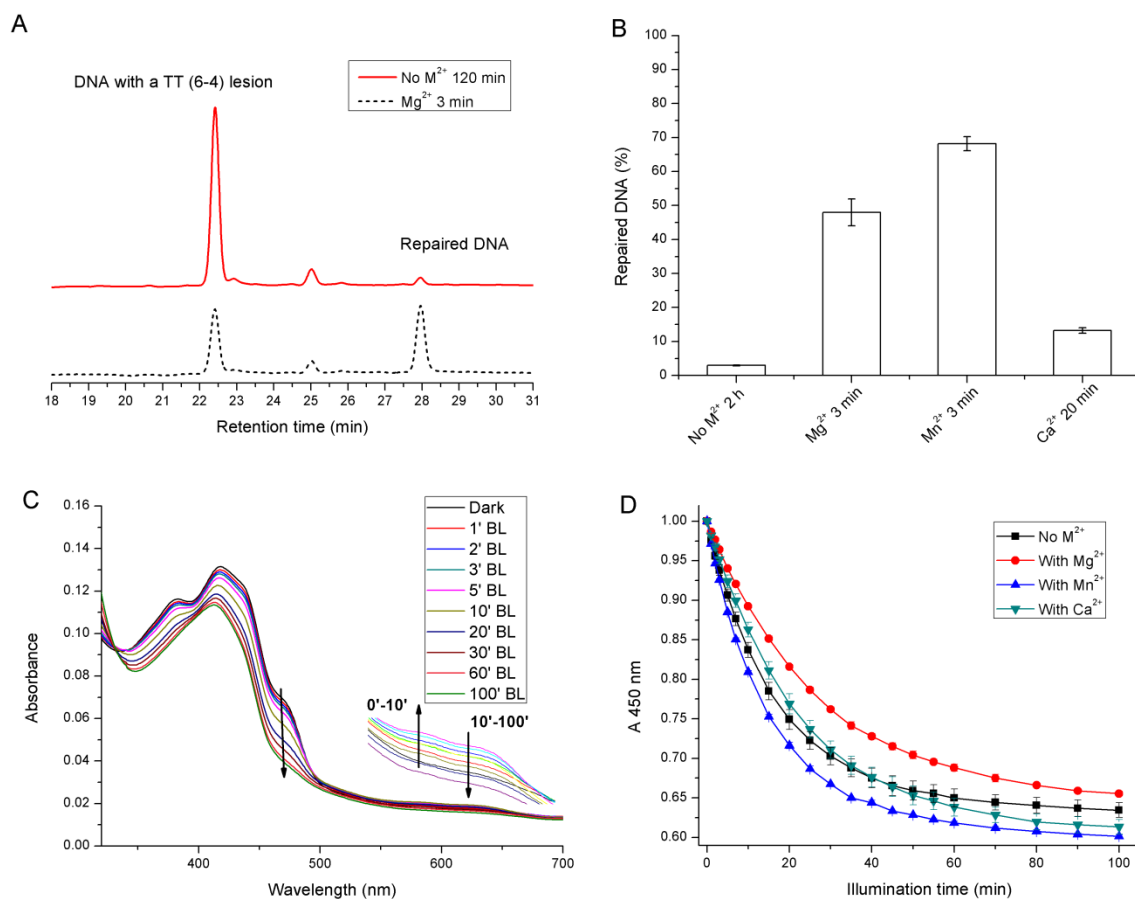


Figure 13. (A) HPLC assay after (6-4) DNA repair by PhrB without (upper red curve) and with Mg^{2+} (lower, dashed curve). Irradiation times for the assays without and with Mg^{2+} were 120 min and 3 min, respectively. (B) DNA repair activity of PhrB with and without divalent metal ions. Repair mixture contained 5 μ M of the purified (6-4) photoproducts of t_repair, 850 nM wild type PhrB, 14 mM DTT and 4 mM free Mg^{2+} , Mn^{2+} or Ca^{2+} in the corresponding reaction mixture. The percentages of repaired DNA after illuminating 120 min, 3 min, 3 min, 20 min for repair mixture without divalent metal ions (no M^{2+}) and with Mg^{2+} , Mn^{2+} and Ca^{2+} are shown, respectively. Mean values \pm SE of 3 experiments. (C) Photoreduction of wild-type PhrB. UV-Vis spectra during irradiation with 470 nm LED light. The inset shows spectra $>$ 550 nm in an enlarged y-axis. (D) Photoreduction of wild-type PhrB with and without divalent metal ions. From series of spectra, the A450 values were extracted at each time point. These values were normalized to the value measured at $t = 0$ min. Mean values \pm SE of 3 experiments.

I next estimated whether and how photoreduction of PhrB is affected by divalent cations. The transition from oxidized FAD to semi-reduced and fully reduced FADH⁻ during irradiation with blue light was followed by UV-Vis spectrometry (Figure 13C) (see also (Graf *et al.*, 2015)). Loss of oxidized FAD results in a continued absorbance decrease at 450 nm. The transient formation of the semiquinone is detected by the increase during the first 10 min of irradiation. The subsequent decrease in this wavelength range shows the formation of fully reduced FADH⁻. The decrease of the absorbance at 450 nm (A₄₅₀) was taken to compare photoreduction under different conditions (Figure 13D). During the first 10 min, the decrease was approximately linear, and the slopes were used for comparisons of initial rates. Compared to the assay without divalent cations, Mg²⁺ decreased the initial rate by (39 ± 3) %, but Mn²⁺ promoted the initial rate by (41 ± 0.3) % and Ca²⁺ diminished the initial rate by (17 ± 1) %. However, after 40 min illumination, the reduction with Ca²⁺ was faster than without divalent metal ions. Such a pattern in the presence of Ca²⁺ could be due to a reduced rate of semiquinone formation and an accelerated conversion into the fully reduced form. However, we could not confirm this upon inspection of the spectra. For the whole illumination period Mg²⁺ slowed down the photoreduction and Mn²⁺ promoted photoreduction.

2.2 Photorepair of CryB and Proma-PL

CryB from *Rhodobacter sphaeroides* (Geisselbrecht *et al.*, 2012) is another member of the (6-4) BCP proteins. PhrB and CryB have highly similar structures. In earlier studies no repair activity was found for CryB. In the present study the (6-4) DNA lesion repair efficiency of CryB was very low in the absence of divalent metal ions. After illuminating the reaction mixtures for 120 min, (3.3 ± 0.07) % of (6-4) DNA lesions were repaired. Upon addition of Mg²⁺ or Mn²⁺ to the reaction mixture, (82 ± 4) % and (97 ± 3) % of the (6-4) DNA lesions were repaired during an illumination time of 3 min, respectively. The addition of Ca²⁺ also improved the activity of CryB, (12 ± 1) % of DNA lesions were repaired upon 20 min illumination (Figure 14). According to the turnover rates as given in (Table 4), Mg²⁺ and Mn²⁺ and Ca²⁺ improved the DNA repair activity 2060 ± 20, 3400

± 100 and 24 ± 2 times, respectively. This pattern of divalent metal ion effects corresponds well to the pattern observed for PhrB.

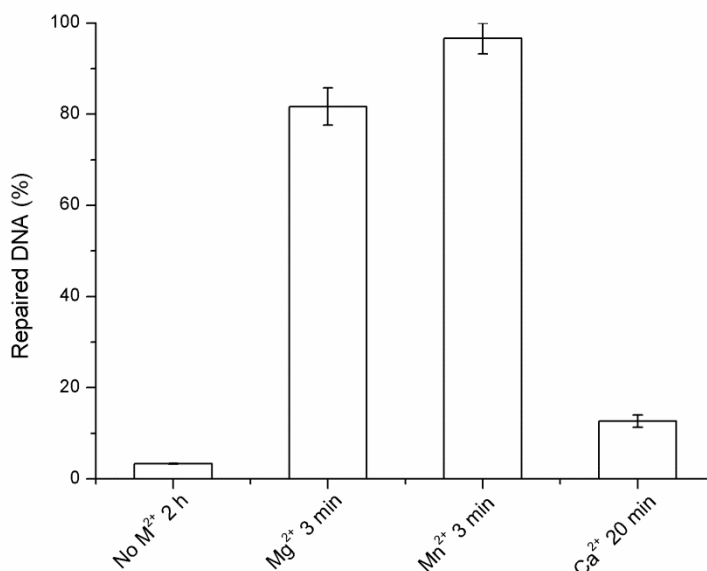


Figure 14. DNA repair activity of CryB with and without divalent metal ion. Repair mixture contained 5 μM of the purified (6-4) photoproducts of t_repair, 850 nM CryB, 14 mM DTT and 4 mM free Mg²⁺, Mn²⁺ or Ca²⁺ in corresponding reaction mixture. The percentages of repaired DNA after illuminating 120 min, 3 min, 3 min, 20 min, respectively for repair mixture without and with Mg²⁺, Mn²⁺ and Ca²⁺ are shown. Mean values \pm SE from 3 independent experiments.

Proma-PL from *Prochlorococcus marinus* is also a member of the (6-4) BCP proteins, PhrB has 4 conserved cysteines covalent binding to the Fe-S cluster whereas Proma-PL have no 4 cysteines and its 1000 homology also contains no 4 cysteines for Fe-S cluster binding, which means that Proma-PL represents another subgroup of (6-4) BCP protein that has no Fe-S cluster. As the solubility of Proma-PL is very poor, after purification we only get very less Proma-PL in the supernatant, despite of several rounds of optimizations which were performed by Gero Kaeser. After affinity chromatography,

the highest purity of Proma-PL I got is about 30 %. Since *E. coli* expressed proteins do not have (6-4) DNA repair ability, the (6-4) DNA repair activity can be assigned to the Proma-PL fraction in the supernatant. The single stranded ODN5 was used for repair assays with and without Mg^{2+} . In the presence of Mg^{2+} , we observed a clear repair activity (Figure 15). Without Mg^{2+} , no repair was detected. Thus, the Mg^{2+} effect is also present in prokaryotic (6-4) photolyases without Fe-S cluster.

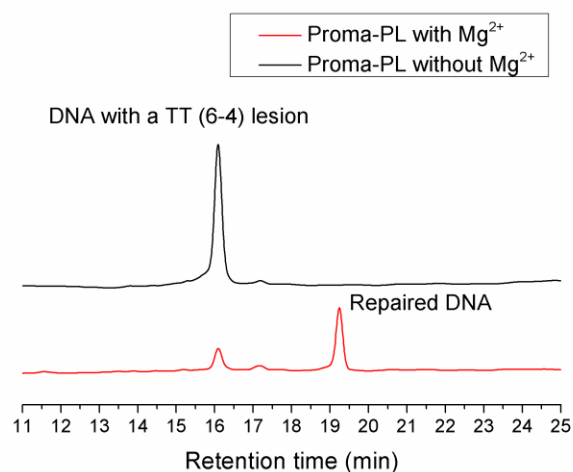


Figure 15. DNA repair HPLC profile of Proma-PL with and without Mg^{2+} . 30 μ l repair mixture contained 5 μ M of the purified (6-4) photoproducts of ODN5, soluble Proma-PL about 10 % purity ($A_{280} = 0.66$, 27 μ l), 14 mM DTT or 1.5 mM free Mg^{2+} .

2.3 Photorepair and photoreduction of PhrA

The CPD DNA lesion repair ability of PhrA from *Agrobacterium fabrum* was very efficient. Under the given conditions, CPD DNA lesions were repaired within 3 min, although the enzyme concentration was significantly lower than in the above assays. There was only a minor effect of divalent metal ions on the repair. After an illumination time of 1 min, the percentages of repaired DNA in the assays without divalent metal, with

Mg^{2+} , with Mn^{2+} and with Ca^{2+} were $(38 \pm 2) \%$, $(44 \pm 1) \%$, $(38 \pm 2) \%$ and $(42 \pm 3) \%$ respectively (Figure 16A).

I also studied the effects of Mg^{2+} , Mn^{2+} and Ca^{2+} on photoreduction of PhrA (Figure 16B). All three metal ions had a positive effect on photoreduction. In the presence of Mg^{2+} the initial rate of photoreduction was increased by $(74 \pm 2) \%$. Mn^{2+} and Ca^{2+} increased the initial rate by $(39 \pm 3) \%$ and $(25 \pm 6) \%$, respectively.

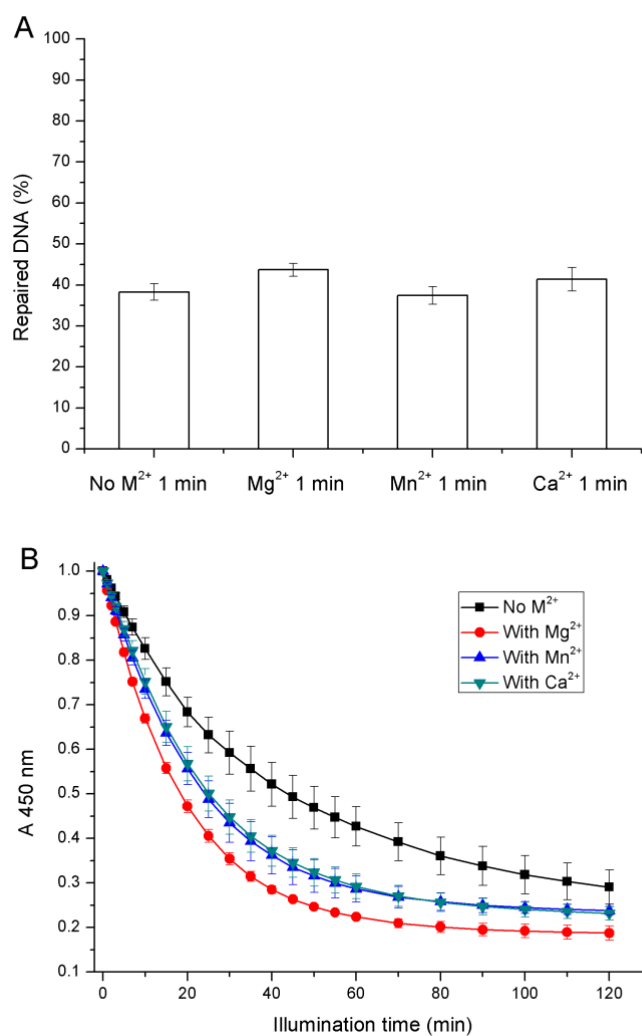


Figure 16. (A) DNA repair activity of PhrA with and without divalent metal ions. The repair mixture contained $5 \mu\text{M}$ of the purified CPD photoproducts of “t_repair” oligonucleotides, 50 nM

PhrA, 14 mM DTT and 4 mM free Mg^{2+} , Mn^{2+} or Ca^{2+} ; the illumination time was 1 min. (B) Photoreduction of PhrA with and without divalent metal ion. Spectra were recorded from 250 nm to 700 nm; A450 values were extracted at each time point and normalized to t 0 min. Mean values \pm SE from 3 independent experiments.

2.4 Photorepair and photoreduction by OtCPF1

The (6-4) photolyase of a green alga *Ostreococcus tauri* was chosen as representative of eukaryotic (6-4) photolyases. Although this group and (6-4) BCP proteins catalyze the same enzymatic reaction by possibly the same mechanism of electron transfer, their primary structures are only 17 % identical. Without divalent metal ion, the (6-4) DNA repair activity of OtCPF1 was higher than that of PhrB, whereas an effect of divalent metal ions on DNA repair was not obvious. Illuminating for 60 min, (21 \pm 2) % of the (6-4) DNA lesions were repaired in the assay without divalent metal ion, and (22 \pm 1) %, (18 \pm 1) %, and (20 \pm 2) % were repaired in the assays with Mg^{2+} , Mn^{2+} and Ca^{2+} , respectively (Figure 17A). After correcting for the different protein concentrations used in our experiments, the repair rates of OtCPF1 were lower than those of both other (6-4) photolyases presented in this work in the presence of Mg^{2+} (Table 4). Considering the missing antenna chromophore in OtCPF1, the repair rates per absorbed photons are probably similar in OtCPF1 and (6-4) BCP proteins in the presence of Mg^{2+} . We also investigated the divalent metal ion effect on the photoreduction of OtCPF1. The transition to the fully reduced form $FADH^-$ was completed after 240 min illumination, as there was no further decrease of absorbance at 450 nm afterwards. As shown in Figure 17B, there was no significant effect of Mg^{2+} on photoreduction, the curves with and without Mg^{2+} are almost identical.

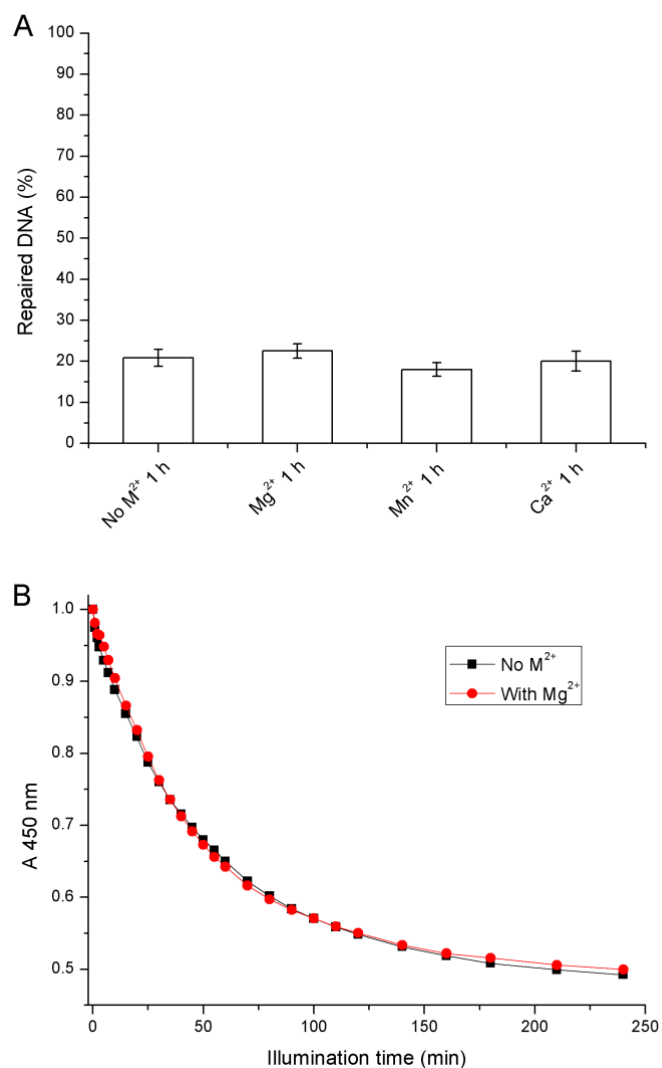


Figure 17. (A) DNA repair activity of OtCPF1 with and without divalent metal ion. The repair mixture contained 5 μ M of the purified (6-4) photoproducts of t_{repair}, 50 nM OtCPF1, 14 mM DTT and 4 mM free Mg^{2+} , Mn^{2+} or Ca^{2+} in the respective reaction mixture. The percentages of repaired DNA after illuminating 60 min for repair mixture with and without divalent metal ion were shown. Mean values \pm SE of 3 experiments. (B) Photoreduction of OtCPF1 with and without magnesium. Spectra were recorded from 250 nm to 700 nm and A₄₅₀ values were extracted at each time point and normalized to t = 0 min.

2.5 Summary of DNA repair

I found that an improvement of DNA repair by divalent cations is restricted to members of the (6-4) BCP group, and the repair activities of photolyases belonging to other groups in our assay are not affected by divalent cations. Although minor positive and negative divalent cations effects on photoreduction were found in different groups, they are without clear correlations.

Table 2. Summary of PhrB repair of single and double stranded oligonucleotides.

Oligo DNA	Length (nt)	ss/ds substrate	With Mg ²⁺	Irradiation time	Repair (%)	k (s ⁻¹)
t_repair	8	ss	no	2 hour	3 ± 0.1	(4.2 ± 0.2) x 10 ⁻⁶
t_repair	8	ss	yes	3 min	48 ± 3	(3.7 ± 0.4) x 10 ⁻³
ODN5	12	ss	no	20 min	54 ± 6	(6.6 ± 1) x 10 ⁻⁴
ODN5	12	ss	yes	2 min	81 ± 2	(1.4 ± 0.1) x 10 ⁻²
ODN5	12	ds	no	20 min	10 ± 0.5	(9.3 ± 0.4) x 10 ⁻⁵
ODN5	12	ds	yes	2 min	35 ± 0.5	(3.7 ± 0.1) x 10 ⁻³

Notes: Based on example measurements at different time points, we assume that the repair reaction can be treated as first order reaction. Based on the formula for exponential decay, $c(t) = c_0 e^{-kt}$, where c_0 and $c(t)$ are substrate concentrations before illumination and after a given time (t) of illumination, we obtained the specific reaction rate k (s⁻¹).

Table 3. Comparison of Mg²⁺ increased times on the DNA repair of different (6-4) DNA lesions.

	Increased times of repair activity by Mg ²⁺
single stranded 8mer	879 ± 62
single stranded 12mer	21 ± 2
double stranded 12mer	40 ± 1

Table 4. DNA repair activity of the four photolyases with and without divalent metal ion.

	Lesion DNA	Protein	Divalent	k (s ⁻¹)
PhrB	5 μM	850 nM	-	(4.2 ± 0.2) x 10 ⁻⁶
PhrB	5 μM	850 nM	Mg ²⁺	(3.7 ± 0.4) x 10 ⁻³
PhrB	5 μM	850 nM	Mn ²⁺	(6.4 ± 0.3) x 10 ⁻³
PhrB	5 μM	850 nM	Ca ²⁺	(1.2 ± 0.1) x 10 ⁻⁴
CryB	5 μM	850 nM	-	(4.7 ± 1) x 10 ⁻⁶
CryB	5 μM	850 nM	Mg ²⁺	(9.7 ± 1) x 10 ⁻³
CryB	5 μM	850 nM	Mn ²⁺	(1.5 ± 0) x 10 ⁻²
CryB	5 μM	850 nM	Ca ²⁺	(1.1 ± 0.1) x 10 ⁻⁴
OtCPF1	5 μM	50 nM	-	(6.5 ± 0.7) x 10 ⁻⁵
OtCPF1	5 μM	50 nM	Mg ²⁺	(7.1 ± 0.6) x 10 ⁻⁵
OtCPF1	5 μM	50 nM	Mn ²⁺	(5.6 ± 0.6) x 10 ⁻⁵
OtCPF1	5 μM	50 nM	Ca ²⁺	(6.3 ± 0.8) x 10 ⁻⁵
PhrA	5 μM	50 nM	-	(8.0 ± 0.5) x 10 ⁻³
PhrA	5 μM	50 nM	Mg ²⁺	(9.6 ± 0.4) x 10 ⁻³
PhrA	5 μM	50 nM	Mn ²⁺	(7.9 ± 0.5) x 10 ⁻³
PhrA	5 μM	50 nM	Ca ²⁺	(8.9 ± 0.8) x 10 ⁻³

From these results we draw the following conclusions: (1) Mg²⁺ dramatically enhances the repair activity of PhrB with single stranded DNA and double stranded DNA (Table 3); (2) PhrB repairs single stranded DNA more efficiently than double stranded DNA, irrespective of the presence or absence of Mg²⁺. (3) Both Mg²⁺ and the longer DNA substrates can improve the binding (see 3.2.3) of (6-4) DNA to PhrB.

3 Key amino acids involved in DNA repair of PhrB

3.1 Key amino acids involved in metal ion-stimulated effect.

Based on former results we expected that the action of Mg^{2+} in PhrB is close to the DNA lesion. Because the Mg^{2+} effect is only found in PhrB and CryB, but not in other groups of photolyases, the most probable site for Mg^{2+} action seemed to be at a specific interdomain loop which is only present in relatives of PhrB, and replaced by another loop in other photolyases. In PhrB, the loop contains 4 negatively charged amino acids, Asp179, Glu181, Asp189, and Asp201. Of these, only Asp179 is highly conserved in the (6-4) BCP proteins. Another Asp with its COOH side group ca. 7 Å distant from Asp179 and is highly conserved in (6-4) BCP proteins is Asp254 (Ma *et al.*, 2017). Both residues have been checked to be candidates for Mg^{2+} binding close to the DNA lesion. We therefore generated both relevant mutants, PhrB-D179N and PhrB-D254N in which the negative side chain of each Asp was replaced by a neutral side chain of Asn. These mutants were used for repair assays with and without Mg^{2+} (Figure 18). In these repair assays ss (6-4) t_{repair} was used as the substrate. Without Mg^{2+} and after 2 h irradiation, the repair efficiencies of the 3 proteins PhrB-WT, PhrB-D179N and PhrB-D254N were $(3.5 \pm 0.3) \%$, $(4 \pm 0.1) \%$, and $(5 \pm 2) \%$, respectively. When Mg^{2+} was added and the reaction mixture irradiated for 3 min, PhrB-WT repaired $(80 \pm 1) \%$ of ss (6-4) t_{repair}, but for PhrB-D179N and PhrB-D254N no signal from repaired DNA was detectable. The irradiation time was therefore prolonged to 2 hours, and it turned out that the yields of repaired DNA were almost the same no matter if the repair assays were conducted with or without Mg^{2+} . In the presence of Mg^{2+} PhrB-D179N and PhrB-D254N repaired $(4 \pm 0.5) \%$ and $(5 \pm 0.2) \%$ of DNA, respectively, which were similar to the results obtained for PhrB-WT in the absence of Mg^{2+} . Our results prove that both Asp179 and Asp254 are crucial for enhancement of the catalytic activity of PhrB by Mg^{2+} , which is likely due to binding of the divalent cation to these residues during the reaction cycle of DNA repair.

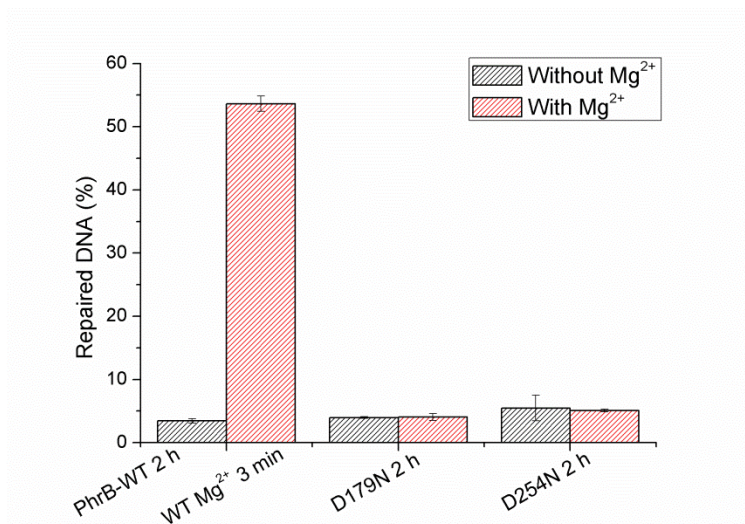


Figure 18. DNA repair activity of PhrB-WT and its mutants PhrB-D254N and PhrB-D179N with and without Mg²⁺. 8 mer single stranded (6-4) DNA t_{repair} were used in the repair assays. The molar ratio between DNA and protein is ca. 10:1. Irradiation time for PhrB-WT without and with Mg²⁺ was 2 h and 3 min, respectively; for the two mutants PhrB-D179N and PhrB-D254N was always 2h. For all time points measurements were repeated 3 times and mean values \pm SE are shown.

3.2 Mutants with impaired repair activity

3.2.1 PhrB-I51W without DMRL cofactor

3.2.1.1 Generation of a mutant lacking DMRL

PhrB-I51W is the second mutant of which a crystal structure was obtained. Based on the PhrB structure, we reasoned that a replacement of Ile51 by Trp could result in a displacement of the DMRL antenna chromophore. Spectral characterizations showed that the mutant does indeed not incorporate DMRL.

The absorbance spectrum of PhrB-WT is characterized by a maximum at 415 nm and a shoulder at 450 nm. Free oxidized FAD has an absorbance maximum around 450 nm and an extinction coefficient of 11000 M⁻¹ cm⁻¹ (Whitby, 1953). Free DMRL has a

maximum at 408 nm and an extinction coefficient of $12100 \text{ m}^{-1} \text{ cm}^{-1}$ (Fischer *et al.*, 2002). We assume that the 415 nm peak primarily arises from DMRL, red shifted by tuning of the protein environment, with small contributions from FAD and the Fe-S cluster (Green *et al.*, 1996; Zhang *et al.*, 2011).

The UV-Vis spectrum of PhrB-I51W is characterized by weaker absorbance around 400 nm (Figure 19), indicating a reduced content or a complete loss of DMRL. For the calculation of the PhrB-WT –minus-PhrB-I51W difference, the spectra in Figure 19 were normalized to the estimated 280 nm extinction coefficients (protein and FAD in both and DMRL in the wild type) as given below. The shape of the difference spectrum is comparable with that of free DMRL but has a maximum at 415 nm. The comparison between wild type and mutant shows that the DMRL content in the mutant is low or zero and that the incorporation of DMRL into the protein results in a ~5 nm bathochromic shift.

For normalization of spectra we used the following extinction coefficients at 280 nm: PhrB-WT and PhrB-I51W apoproteins, $\epsilon_{280 \text{ nm}} = 86300 \text{ M}^{-1} \text{ cm}^{-1}$ and $\epsilon_{280 \text{ nm}} = 91790 \text{ M}^{-1} \text{ cm}^{-1}$, respectively; DMRL, $\epsilon_{280 \text{ nm}} = 10300 \text{ M}^{-1} \text{ cm}^{-1}$ based on (Fischer *et al.*, 2002) and own spectral measurements; FAD, $\epsilon_{280 \text{ nm}} = 17600 \text{ M}^{-1} \text{ cm}^{-1}$ based on (Whitby, 1953) and own spectral measurements. PhrB-WT and PhrB-I51W holoproteins, $\epsilon_{280 \text{ nm}} = 10300 \text{ M}^{-1} \text{ cm}^{-1}$ and $\epsilon_{280 \text{ nm}} = 10300 \text{ M}^{-1} \text{ cm}^{-1}$, respectively. The absorbance spectrum of PhrB samples are above zero in the entire visible range (Graf *et al.*, 2015), which is no absorption in the other photoactive proteins. We attribute this overall absorbance to the Fe-S cluster. Because the values are very small as compared to absorbance of DMRL, FAD or Trp residues, quantifications are only affected in a little extent.

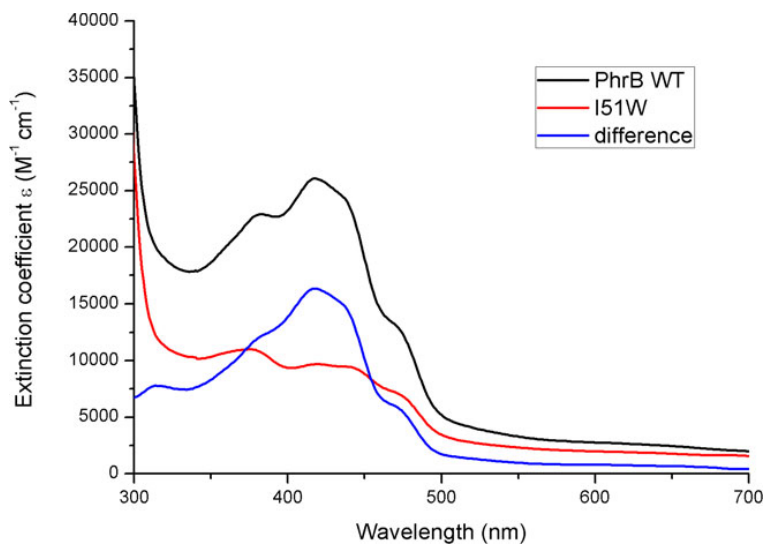


Figure 19. UV-Vis absorbance spectra of PhrB (black line) and PhrB-I51W (red line), normalized to the 280 nm value. Blue line: difference between both spectra. Based on the added extinction coefficients of protein and FAD at 280 nm, the extinction coefficient of DMRL at 415 nm was estimated to be $12000 M^{-1} cm^{-1}$.

3.2.1.2 Biochemical properties of PhrB-I51W

To find out whether PhrB-I51W contains residual DMRL, I performed an HPLC-based assay. For PhrB-WT, both FAD and DMRL were clearly recognized as separate peaks based on their absorbance spectra, which were measured continuously in this setup. When the PhrB-I51W mutant extract was applied to HPLC under the same conditions, the FAD peak was present, and there was no DMRL peak (Figure 20), indicating that PhrB-I51W is indeed free of DMRL.

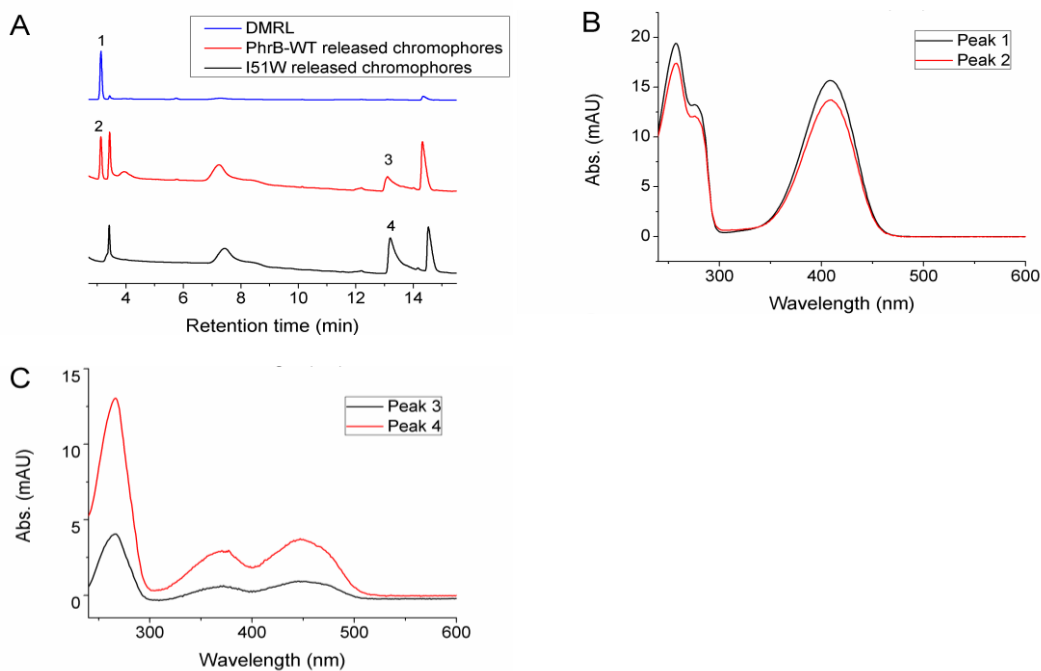


Figure 20. HPLC analysis of cofactors released from PhrB-WT and PhrB-I51W. (A) HPLC profiles of pure DMRL (blue line) and factors released from PhrB-WT (red line) and PhrB-I51W (black line); detection wavelength 380 nm. (B) Spectra of peaks 1 and 2, DMRL. (C) Spectra of peaks 3 and 4, FAD.

Energy transfer between spectrally different chromophores can be estimated by steady state fluorescence. When fluorescence emission of PhrB-WT was measured at 520 nm, the approximate emission maximum of FAD (Huang, 2003), the maximum of the excitation spectrum was at 411 nm, which coincides with the absorbance maximum of DMRL (Figure 21). The corresponding excitation spectrum of PhrB-I51W was completely different: there was no maximum at 411 nm but two maxima at 368 and 444 nm. These peaks relate to oxidized FAD. In PhrB-WT, theoretically light energy absorbed by DMRL is transferred to FAD, but actually the emission spectrum of PhrB-WT has a maximum at 488 nm and a shoulder at 540 nm and the emission spectrum of PhrB-I51W has the shape of a typical FAD emission with a maximum at 540 nm This

result shows that some energy absorbed by DMRL is emitted as fluorescence and therefore not efficiently transferred to FAD. Since the fluorescence quantum yields of DMRL and FAD embedded in the protein are unknown, the transfer efficiency cannot be quantified presently.

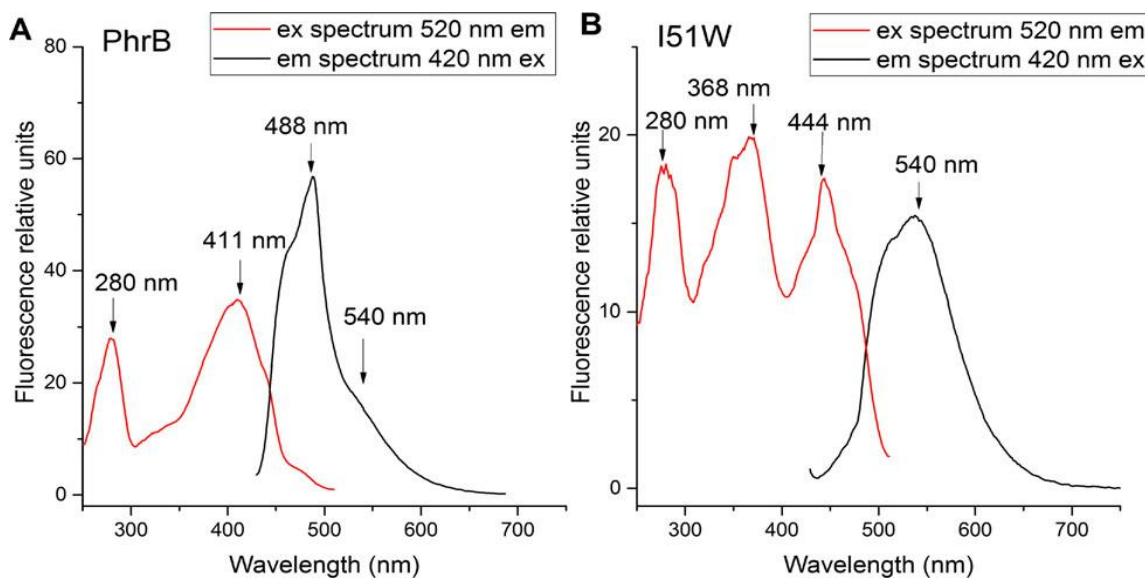


Figure 21. Fluorescence spectra of PhrB-WT and PhrB-I51W. Excitation spectra are measured with an emission wavelength of 520 nm and emission spectra with an excitation wavelength of 420 nm.

I also investigated how the two light triggered reactions of PhrB, photoreduction and photorepair, are affected by the loss of DMRL. In comparative photoreduction assays, two phenomena were observed. First, the irradiation with 470 nm led to a slower absorbance loss at 450 nm, the absorbance maximum of FAD, in the PhrB-I51W mutant. Second, the semiquinone intermediate as identified by its absorbance around 600 nm was present after 90 min in PhrB-I51W but not in PhrB-WT (Figure 22). A comparison between the difference spectra of PhrB-WT and PhrB-I51W suggests that only FAD but not DMRL undergoes light induced spectral changes. The lower photoreduction efficiency of PhrB-I51W indicates that the DMRL-FAD energy transfer in PhrB-WT

results in the excitation and subsequent reduction of FAD, although the absorbance of DMRL in this spectral range is very low.

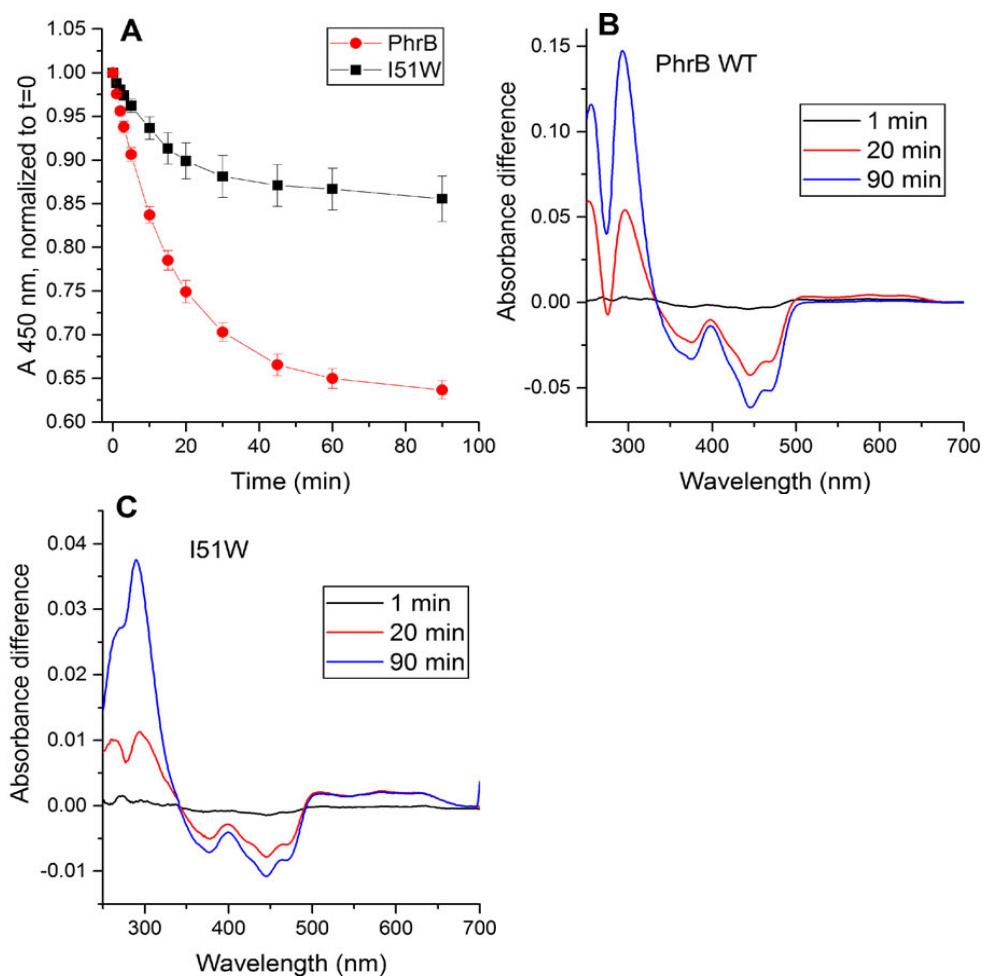


Figure 22. Photoreduction of PhrB-WT and PhrB-I51W. Dark-adapted protein samples of A450 nm = 0.1 were irradiated with 470 nm light of $100 \mu\text{mol m}^{-2} \text{s}^{-1}$. (A) Time course of photoreduction as measured by absorbance at 450 nm, normalized to $t = 0$. (B) and (C) Light-dark difference spectra of PhrB-WT and PhrB-I51W, respectively. The absorption spectra of dark-adapted protein samples were subtracted from the spectra measured at 1, 20 or 90 min after illumination.

To test the repair of DNA lesions, I used a single stranded oligonucleotide “t_repair” with a central (6-4) T-T lesion. PhrB-WT repaired 21 % after 1 h and 27 % after 2 h of irradiation, whereas the repair rates for PhrB-I51W were reduced to only 3 % and 7 %, respectively (Figure 23 and Table 5). PhrB-I51W can still repair (6-4) lesions but less efficient than the PhrB-WT. This indicates that in the wild type, DMRL is required for efficient excitation of FADH[•]. An indirect DMRL effect via photoreduction also has slightly possibility (based on the reason indicated in the Methods part with DNA repair assay). A five-fold difference in repair activity between protein with and protein without antenna chromophore has been described for the *Drosophila melanogaster* (6-4) photolyase (Glas *et al.*, 2009a).

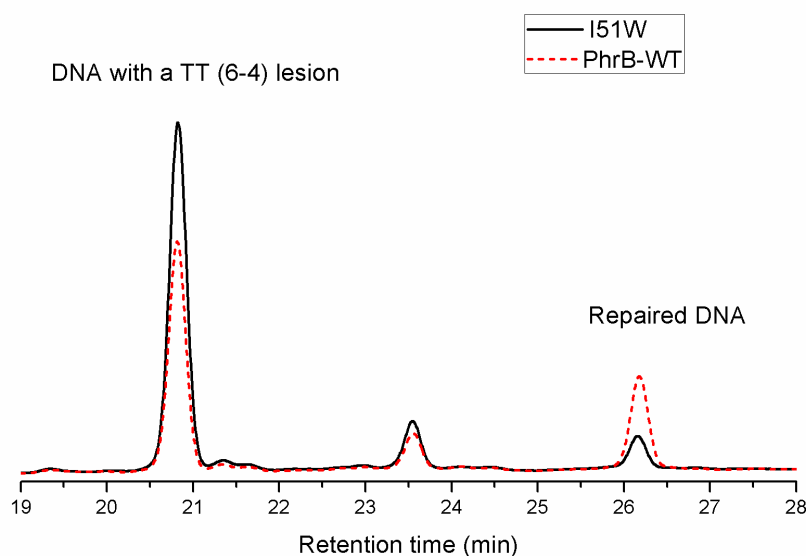


Figure 23. HPLC profiles for DNA repair assay of PhrB-WT (dashed line) and PhrB-I51W (solid line). The DNA t_repair with (6-4) lesion was incubated with the protein under the ratio of DNA: protein ca. 1:1 and irradiated with blue LEDs ($\lambda_{\text{max}} = 400 \text{ nm}$, $250 \mu\text{mol m}^{-2} \text{ s}^{-1}$) for 2 h. After separating DNA from protein, the DNA was subjected to HPLC. The position of damaged and repaired DNA is indicated above the relevant peaks. Detection wavelength was 264 nm.

Table 5. DNA repair by PhrB-WT and PhrB-I51W.

Protein	Irradiation time		
	0h	1 h	2 h
	Repair (%)		
PhrB-WT	0 ± 0	21 ± 0.9	27 ± 2
PhrB-I51W	0 ± 0	3.1 ± 0.2	6.7 ± 0.3

3.2.2 DNA repair of PhrB-Y430F

As Fe-S cluster in photolyase is a recently founded cofactor in photolyase (Zhang *et al.*, 2013) and its function in photolyase is still unclear. As Fe-S cluster acts a role in electron transfer of respiratory chain, so we speculate Fe-S might involve in the electron transfer in DNA repair and then we mutated the Tyr 430 and Tyr424 which those amino acids most likely involved the electron transfer in PhrB (Figure 24). Tyr424 and Tyr430 of PhrB are highly conserved in (6-4) BCP proteins. According to previous work (Graf *et al.*, 2015), the DNA repair activity of the Y430F mutant of PhrB is impaired under no Mg^{2+} condition.

In the present study, only (1.1 ± 0.09) % of (6-4) DNA was repaired by the mutant protein when illuminating for 120 min in the absence of Mg^{2+} , whereas (3 ± 0.1) % of (6-4) DNA was repaired by the wild-type protein under the same condition (Figure 25). After adding Mg^{2+} to the repair assay of Y430F, about (12 ± 1.2) % of the (6-4) DNA lesions were repaired in 3 min; Mg^{2+} promoted the repair activity of Y430F 440 ± 20 times.

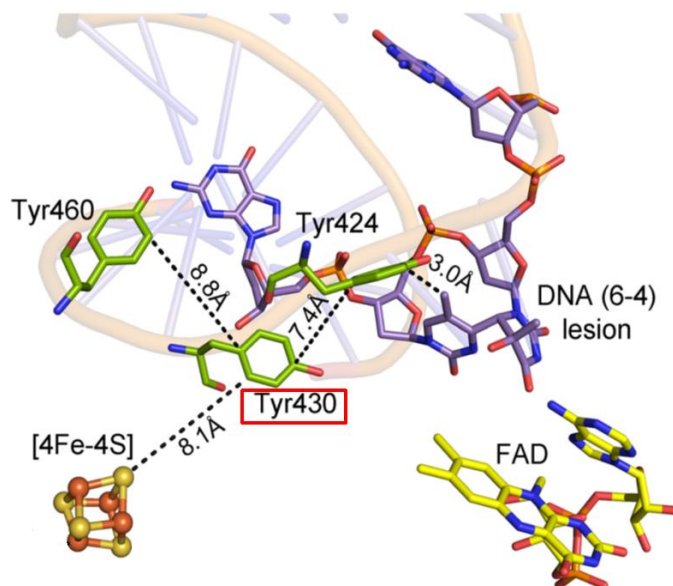


Figure 24. Position of tyrosines between the DNA lesion and the Fe-S cluster of PhrB (4DJA). The DNA is from the *Drosophila melanogaster* (6–4) photolyase co-crystal structure (3CVU). Modified from (Graf *et al.*, 2015).

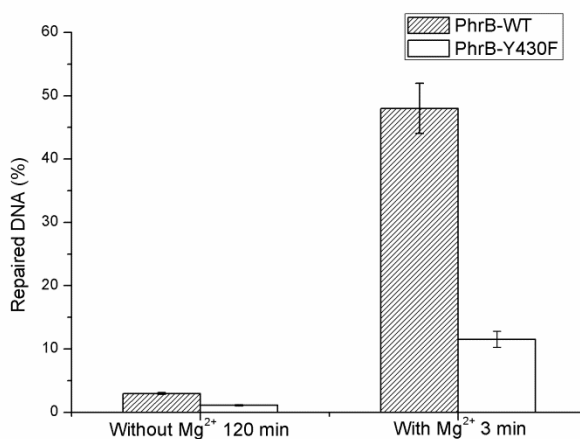


Figure 25. DNA repair activity of PhrB wild type and the mutant PhrB-Y430F with and without Mg²⁺. Repair mixtures contained 5 μ M of the purified (6–4) photoproducts of t_{repair}, 850 nM wild-type PhrB or its Y430F mutant, 14 mM DTT and 4 mM free Mg²⁺ in the respective reaction

mixture. The percentages of repaired DNA after illuminating 120 min and 3 min, respectively, for repair mixture with and without Mg^{2+} are shown. Mean values \pm SE of 3 experiments.

3.2.3 DNA repair of PhrB-Y424F involved in DNA binding

The Y424F mutant was previously generated to test for possible electron transfer between the iron sulfur cluster of PhrB and the DNA lesion. According to DNA binding model Tyr424 interacts with the DNA. This binding of lesion DNA to this mutant was found to be very weak, and no repair activity was found. The crystal structure of PhrB-Y424F showed that the folding of the protein is unaffected by the mutation and effects can be directly assessed to this amino acid. In order to test for Mg^{2+} effect in this mutant, I performed repair assays with increased protein concentrations.

In order to compare the DNA repair activities of wild-type PhrB and the Y424F mutant, the repair assay was carried out using a protein concentration that was 5 μ M, *i.e.* about 10 times higher than in the remaining experiments presented in this work.

The PhrB-Y424F mutation is characterized by a great loss of binding affinity for damaged DNA (Table 6) and DNA repair as compared to PhrB-WT (Graf *et al.*, 2015). In this work, ss (6-4) ODN5 was chosen as the substrate as PhrB can repair it with rather high efficiency. It was found that PhrB-Y424F does not completely lose its ability to repair damaged DNA, but its repair efficiency is very low (Figure 26), since after 60 min irradiation when repair of damaged DNA with PhrB-WT was complete (even with 10 times less protein, Figure 10) PhrB-Y424F repaired only (3.2 ± 0.06) % DNA. As observed for PhrB-WT addition of Mg^{2+} markedly increased the DNA repair efficiency of PhrB-Y424F. In the presence of Mg^{2+} and after 2 min irradiation (45 ± 1) % DNA were repaired, which is still low compared to the 100 % repair efficiency of PhrB-WT under the same conditions. In Table 3 with Mg^{2+} enhanced PhrB wild type DNA repair activity about 21 times, but for PhrB-Y424F enhanced by Mg^{2+} about 545 times (Table 7). We conclude that in PhrB-Y424F the lower binding affinity for (6-4) DNA (Graf *et*

al., 2015) (Zhang *et al.*, 2017) greatly impairs repair efficiency and the lower binding and repair ability can be improved by Mg^{2+} .

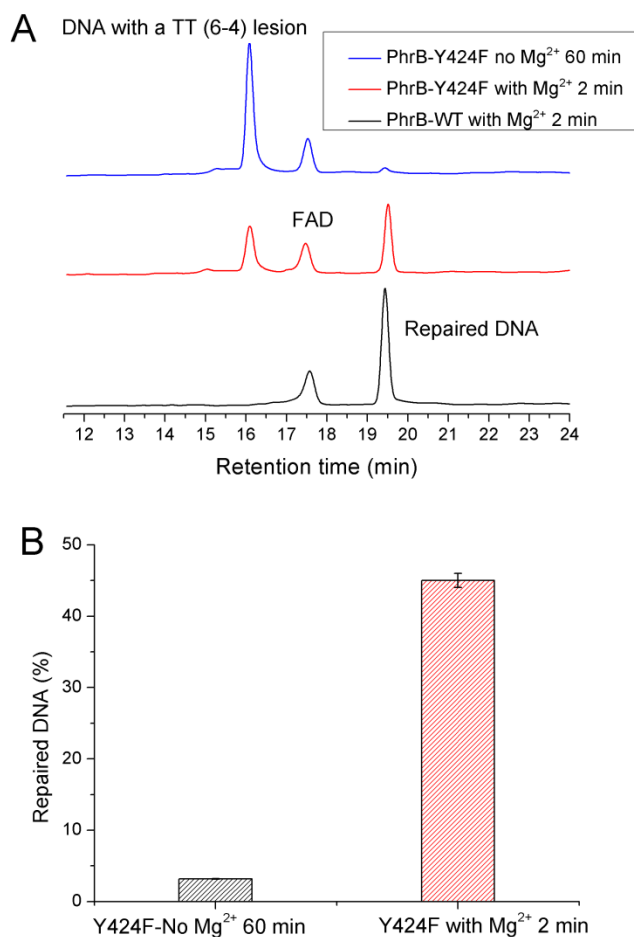


Figure 26. DNA repair activity of PhrB wild-type and the mutant PhrB-Y424F with and without Mg^{2+} . (A) One example of HPLC profile was shown for each type of experiment: DNA repair (top blue line) by PhrB-Y424F without Mg^{2+} irradiated for 60 mn, (middle red line) by PhrB-Y424F with Mg^{2+} irradiated for 2 min, (bottom black line) by PhrB-WT with Mg^{2+} irradiated for 2 min. (B) 12 mer single stranded DNA ss (6-4) ODN5 was used in the repair assays. The molar ratio between DNA and protein was ca. 1:1. The repair mixtures contained 5 μM (6-4) ODN5, 5 μM protein, 14 mM DTT and 4mM free Mg^{2+} if with Mg^{2+} . Irradiation time with and without Mg^{2+} were 2 min and 60 min, respectively. For every time point the

measurements were repeated 3 times and the yields of repaired DNA are shown as percentages of total DNA (mean values \pm SE).

Table 6. DNA binding of PhrB and Y424F (Graf *et al.*, 2015).

	ss EMSA_1, KD	(6-4) ss EMSA_1, KD
PhrB	$(25 \pm 3) \times 10^{-6}$ M	$(13 \pm 2) \times 10^{-9}$ M
Y424F	$(28 \pm 3) \times 10^{-6}$ M	$(18 \pm 2) \times 10^{-6}$ M

Table 7. ss (6-4) ODN5 DNA repair specific reaction rate of PhrB-Y424F with and without Mg^{2+} .

no Mg^{2+} k (s^{-1})	with Mg^{2+} k (s^{-1})	Increased times of repair activity by Mg^{2+}
$(9 \pm 0.03) \times 10^{-6}$	$(5 \pm 0.1) \times 10^{-3}$	545 ± 14

4 Electron transfer pathway in photoreduction of PhrB

Photoreduction of PhrB differs from the typical pattern because the amino acid of the electron cascade next to FAD is a tyrosine (Tyr391), whereas photolyases and cryptochromes of other groups have a tryptophan as direct electron donor of FAD. For PhrB the distance between the isoalloxazine ring and Trp390 is roughly 8 Å (Figure 27). Trp390 is quite far from FAD and there is no other Trp in the structure that can complete the triad, which implies the role of the closest residue of FAD involved in charge transfer.

Mutagenesis studies have identified Trp342 and Trp390 as essential for charge transfer (Graf *et al.*, 2015). Trp342 is located at the periphery of PhrB while Trp390 connects Trp342 and Tyr391. The role of Tyr391, which lies between Trp390 and FAD (Figure 27), is however unclear as its replacement by phenylalanine did not block photoreduction (Figure 29). Experiments reported here, which replace Tyr391 by Ala, show that photoreduction is blocked, underlining the relevance of Tyr/Phe at position 391 and indicating that charge transfer occurs via the triad 342-390-391 (Holub *et al.*, 2018).

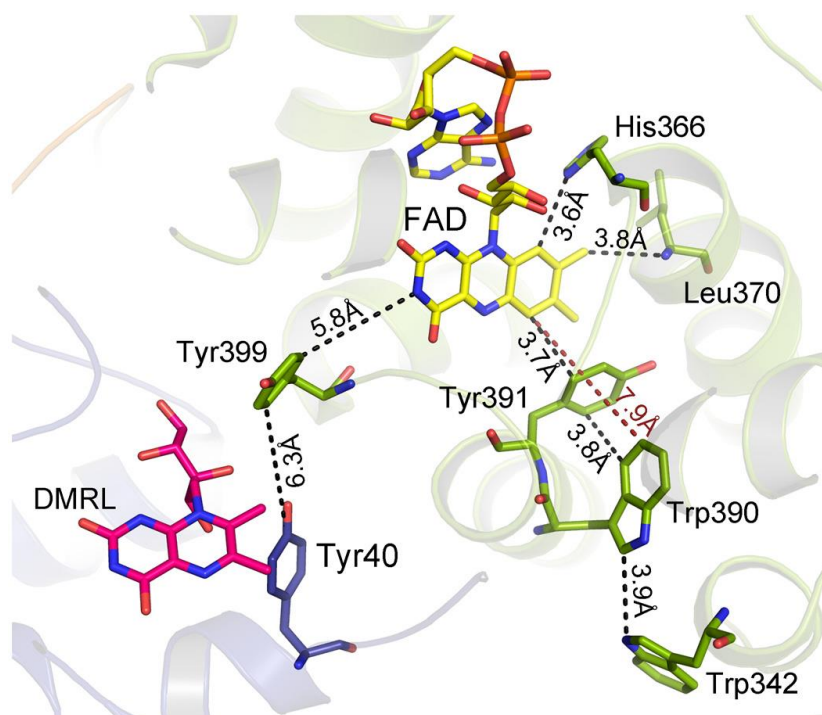


Figure 27. Orientation of FAD and amino acids that might be relevant for photoreduction in the structure of PhrB (PDB entry 4DJA). Protein structure is illustrated in cartoon. The cartoon FAD chromophore (yellow), DMRL cofactor (pink) and relevant amino acids are shown as stick models. Trp342 is located close to the surface. Distances are given in Å. Adapted from (Graf *et al.*, 2015).

For photoreduction studies, I generated the Y391F, Y391W and Y391A mutants of PhrB. All mutants and PhrB-WT were expressed in *E. coli* and purified by Ni²⁺ chromatography and size exclusion chromatography. Whereas protein yields of Y391F and Y391A are comparable to those of WT, the yield of Y391W is ca. 10 times lower. Absorbance spectra of Y391A and Y391F in the oxidized FAD state are comparable with WT (Figure 28), although detailed analyses reveal different chromophore to protein ratios and/or different fractions of reduced FAD at starting time. The absorbance of the Y391W in the blue spectral range is very weak (Figure 28). Chromophore analyses show that this mutant contains only (1.3 ± 0.1) % FAD and (1.8 ± 0.2) % DMRL as compared to WT. These values are (94 ± 1) % and (87 ± 3) % for FAD and DMRL of Y391F, respectively, and (53 ± 2) % and (53 ± 2) % for FAD and DMRL of Y391A, respectively. We propose that the replacement of Tyr 391, which is located close to FAD, by bulky Trp in Y391W results in opening of the FAD pocket and loss of FAD binding capacity. The DMRL pocket is formed by amino acids of the N-terminus and more distant from the mutation. The loss of DMRL results therefore probably from FAD depletion. The partial loss of both chromophores to equal percentages in the Y391A mutant supports this idea. The 410 nm peak in the spectrum of the Y391W mutant is assigned to the iron sulfur cluster.

During blue light irradiation, the spectra of WT PhrB and the Y391F mutant change in a characteristic manner. The transient increase at 580 nm, the maximum of the protonated FAD semiquinone, and the loss of absorbance at 450 nm, characteristic for the loss of oxidized FAD (Figure 29), are comparable to data published earlier (Graf *et al.*, 2015). Here, the relative A_{450 nm} decrease at t = 90 min in the Y391F mutant appears smaller than in WT. This can be due to slower photoreduction or smaller fraction of oxidized vs. total FAD in the mutant. Both decay curves can be treated with

monoexponential decay functions which yielded time constants of 36 ± 1 min and 32 ± 1 min for WT and Y391F, respectively. Thus, the rate of overall photoreduction is not affected by the Tyr to Phe replacement, but the oxidation state of Y391F was incomplete at the start of the photoreduction experiments. Formation and decay of the semiquinone intermediate absorbing at 580 nm is slower in Y391F. This result show that the role of Tyr or Phe differs in the first and second electron transfer. In summary, the present show clearly that the replacement of Tyr by Phe into the proposed electron path does not block photoreduction. We do not observe any light induced absorbance changes in the Y391A mutant (Figure 28). This result suggests that position 391 is critical for photoreduction, as proposed above.

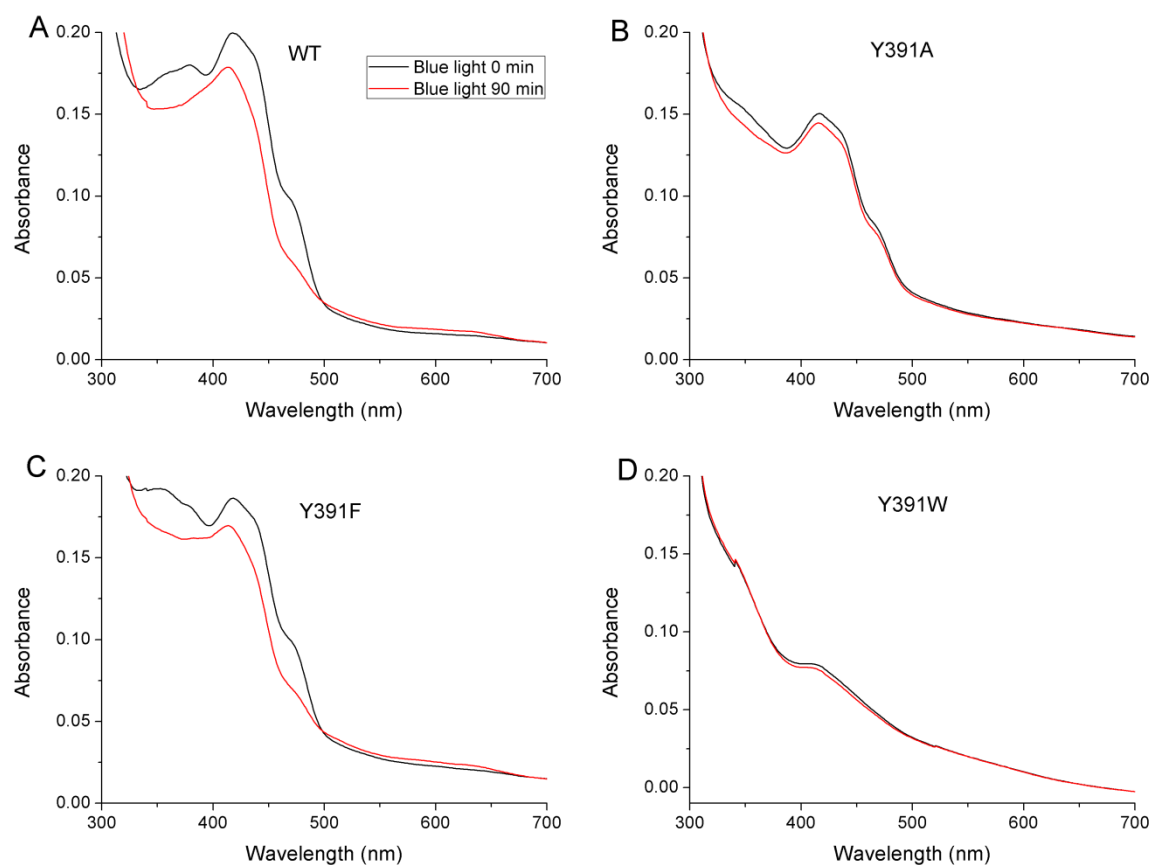


Figure 28. UV-Vis spectra of PhrB WT and mutated proteins Y391A, Y391F and Y391W. Black line: without illumination; red line: illuminated by 470 nm blue light for 90 min.

DNA repair in the presence of Mn^{2+} is completely repaired in 5 min for WT PhrB and Y391F mutant, whereas no repair activity was observed for Y391A and Y391W mutants under these conditions. When the repair time was prolonged to 120 min, Y391W repaired about (8.7 ± 0.7) % of damaged t_{repair} DNA, whereas with Y391A still no repair was observed.

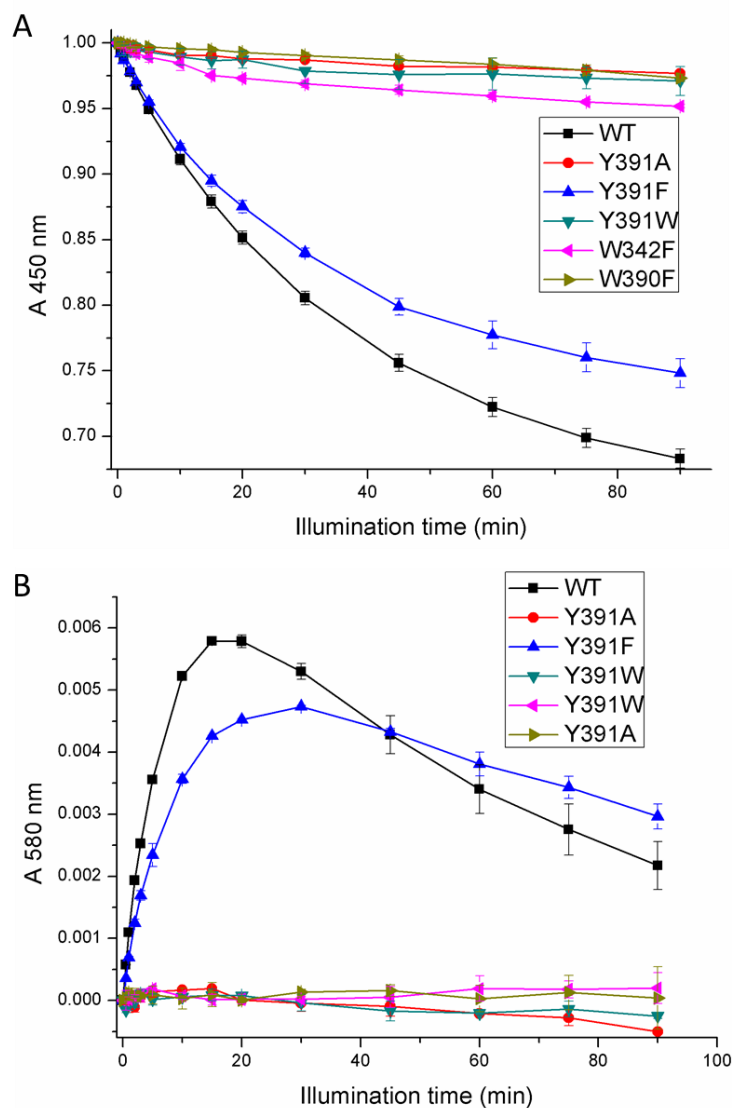


Figure 29. Photoreduction of PhrB and its mutants. Absorption values at 450 nm (upper picture) were taken from UV-Vis spectra measured at indicated time points upon onset of blue-light illumination. For each protein, these values were normalized against the value measured at $t = 0$ min. Absorption values at 580 nm (lower picture) after subtraction of the $t = 0$ value and normalization to the absorbance at 280 nm.

5 Crystal Structures of PhrB

5.1 Crystal structure of PhrB mutants with impaired DNA repair activity

In the present subchapter I describe crystal structures of two point mutants of PhrB: PhrB-Y424F and PhrB-I51W. Both mutants have a reduced DNA repair capacity, related to different sub-functions of PhrB. Tyr424 and Tyr430 are part of a Tyr bridge between the DNA lesion and the Fe-S cluster; both Tyr residues are highly conserved among Fe-S-BCP proteins. At first, the mutants PhrB-Y424F and PhrB-Y430F are characterized by loss of DNA repair and reduced DNA repair (30 % of wild type), respectively (Graf *et al.*, 2015). According to a superposition with the *Drosophila* (6-4) photolyase/lesion DNA cocrystal structure, Tyr424 but not Tyr430 is also part of the proposed lesion binding site. The binding affinity of PhrB-Y424F for lesion DNA was significantly lower than that of PhrB-WT, whereas the affinity of PhrB-Y430F for lesion DNA was as high as that of PhrB-WT (Graf *et al.*, 2015). Although both PhrB-Y424F and PhrB-Y430F mutants have clear phenotypes, the functions of these highly conserved Tyr residues are yet unclear. We obtained the crystal structure of PhrB-Y424F to find out the loss of Tyr424 have either direct or indirect effects on the lesion-DNA binding capacity.

5.1.1 Crystal structure of PhrB-Y424F

The structure of PhrB-Y424F could be solved at resolution 2.5 Å (PDB entry 5LFA). The cubane Fe-S cluster, FAD and DMRL ligands were clearly visible in the electron density after initial rounds of refinement. The finally refined model of PhrB-Y424F (Figure 30A) superposes with a very low RMSD of 0.343 Å to the crystal structure of the PhrB-WT as determined with the program PROSMART (Nicholls *et al.*, 2014). Initial electron density after molecular replacement confirmed the Tyr to Phe substitution (Figure 30B). Similar to PhrB-WT, the loop region connecting $\alpha 7$ and $\alpha 8$ is highly flexible which is reflected by missing electron density for the residues Asp179 to Arg192.

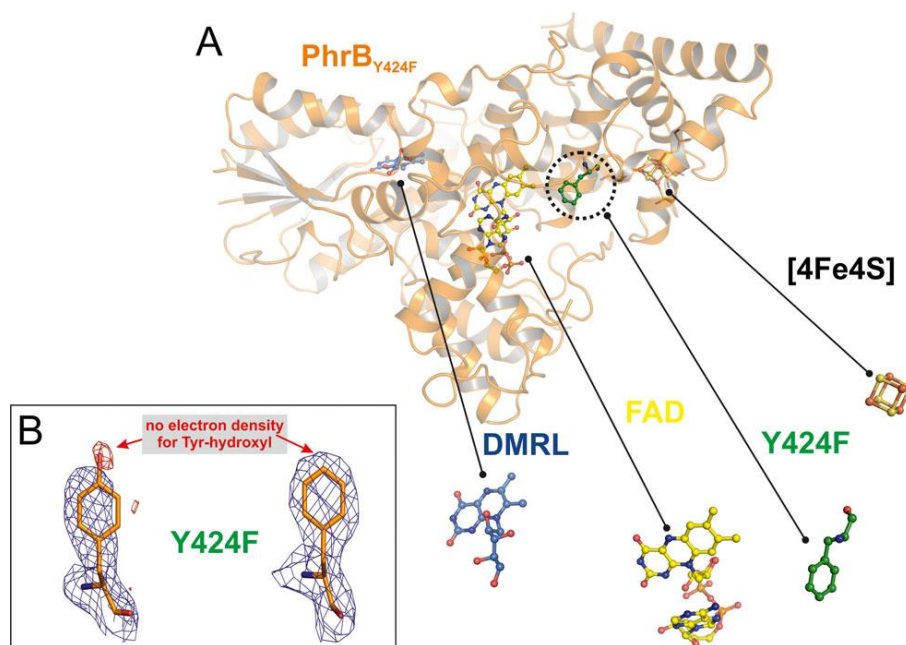


Figure 30. (A) Structure of PhrB-Y424F. Cofactors and the mutated amino acid residue are highlighted by sticks presentation. (B) Electron densities around Tyr424 of PhrB-WT (left) and Phe424 of PhrB-Y424F (right) confirm that the mutation resulted in a Tyr-Phe transition. Figure from (Zhang *et al.*, 2017).

The structural comparison of PhrB-WT and PhrB-Y424F indicates several remarkable differences in the close proximity of Tyr424. In PhrB-WT, Tyr424 is engaged in an extended water molecule and hydrogen bonding network primarily to the two highly conserved amino acids His366 and Arg476 (Figure 31A, B). Obviously, in PhrB-Y424F this water/hydrogen bonding chain is abolished. The water molecule that connects Tyr424 and Arg476 in PhrB-WT is not visible in PhrB-Y424F (Figure 31B). The reduced number of water molecules in PhrB-Y424F compared to PhrB-WT might also be a result from the different resolution of both crystal structures (1.45 Å in PhrB-WT vs. 2.48 Å in PhrB-Y424F), but in this position the missing electron density for water is most likely due to the missing OH residue of the Phe side chain. Furthermore, the electron density of Arg476 is not visible in the PhrB-Y424F structure. The loss of the Tyr424 hydroxyl group and of the water/hydrogen bonding chain probably results in a flexible rotamer

conformation for Arg476, which is not resolved in the PhrB-Y424F structure (Figure 31A, B). In order to see in which way the observed alterations could affect the interaction with DNA lesion, we superimposed the PhrB-WT and PhrB-Y424F crystal structures with that of the *Drosophila* (6-4) photolyase in complex with photo-damaged DNA (PDB entry 3CVU) (Maul *et al.*, 2008). According to these models, the DNA/protein interaction in the mutant is affected twofold. Tyr424 forms a contact with the lesion, and its loss can directly explain why the affinity to lesion DNA is lowered. In the wild type a short distance of Arg476 to the DNA backbone is observed. This contact point is probably also lost in the mutant (Figure 31C, D). The model indicates also a potential involvement of the extended hydrogen network involving Tyr424, in binding and adjustment of the DNA lesion (Figure 31C).

The wild type and mutant crystal structures show that Tyr424 is not only involved in the interaction with the lesion but also with other amino acids such as the highly conserved His366 that interacts with lesion DNA and the DNA interacting Arg476, through hydrogen bonding and water stabilizing.

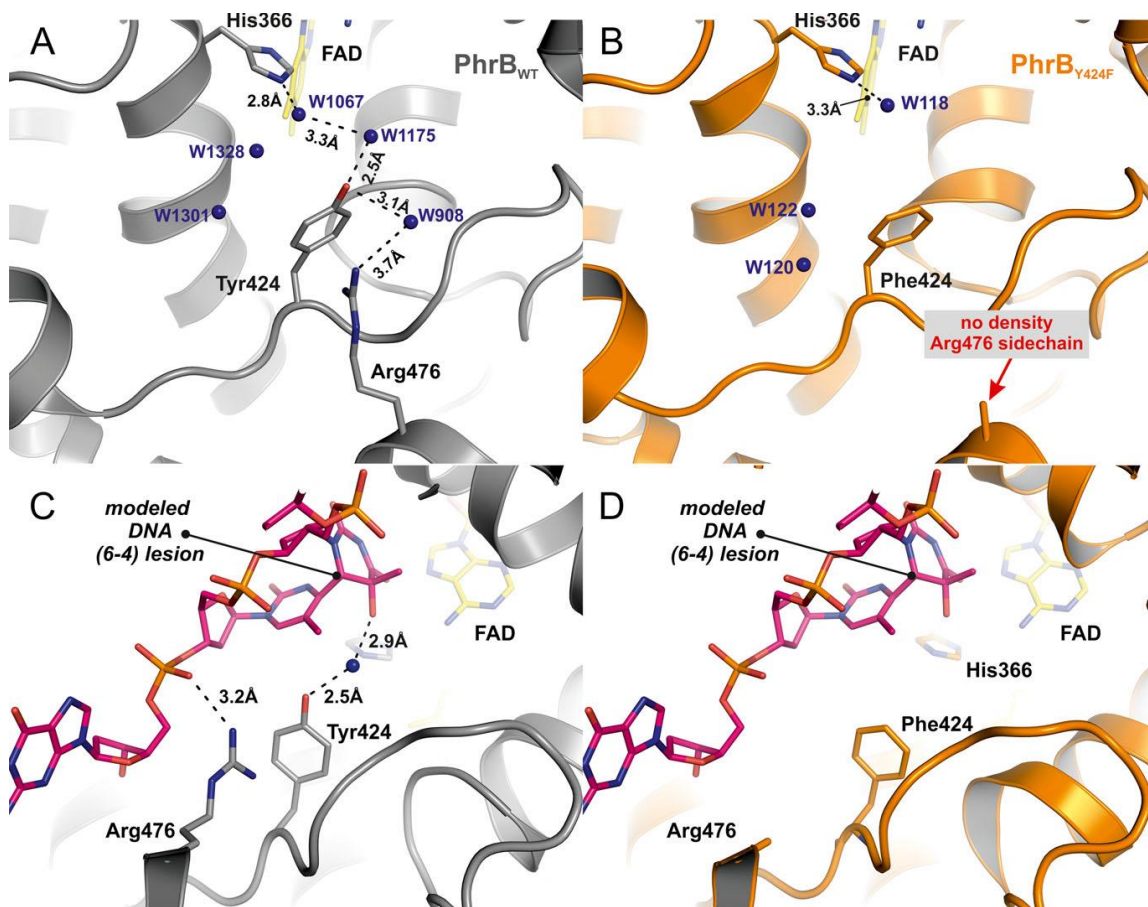


Figure 31. Structure details of PhrB-WT (A and C) and PhrB-Y424F (B and D). The water molecules of the hydrogen-bonding network from His366 via Tyr424 to Arg476 in PhrB-WT (A) are not detected in PhrB-Y424F; the Arg476 side chain is also not resolved (B). In the simple DNA–protein model, Tyr424 forms a contact to the DNA lesion via a water molecule. Arg476 interacts directly with the DNA backbone (C). In the DNA–protein model of PhrB-Y424F, the water-bridged contact is abolished (D), while the Arg476 side chain of PhrB-WT is not detected in PhrB-Y424F. Figure from (Zhang *et al.*, 2017).

5.1.2 Crystal structure of PhrB-I51W

This crystal structure was analyzed by the cooperation group mentioned in the published paper (Zhang *et al.*, 2017). The crystals of the PhrB-I51W mutant were obtained under similar conditions to those of PhrB-WT. The crystal structure was determined at

resolution 2.15 Å (PDB entry 5KCM). There are two nearly identical molecules in the asymmetric unit with a RMSD value of ~0.21 Å. The overall crystal packing and structure of the PhrB-I51W mutant are closely similar to those of PhrB-WT (Zhang *et al.*, 2013) that contains only one molecule per asymmetric unit. PhrB-I51W and PhrB-WT exhibit similar molecular packing in the crystal lattice, although they differ in space group and the cell dimension, which are resulted from breakdown of a crystallographic symmetry in the PhrB-I51W crystals.

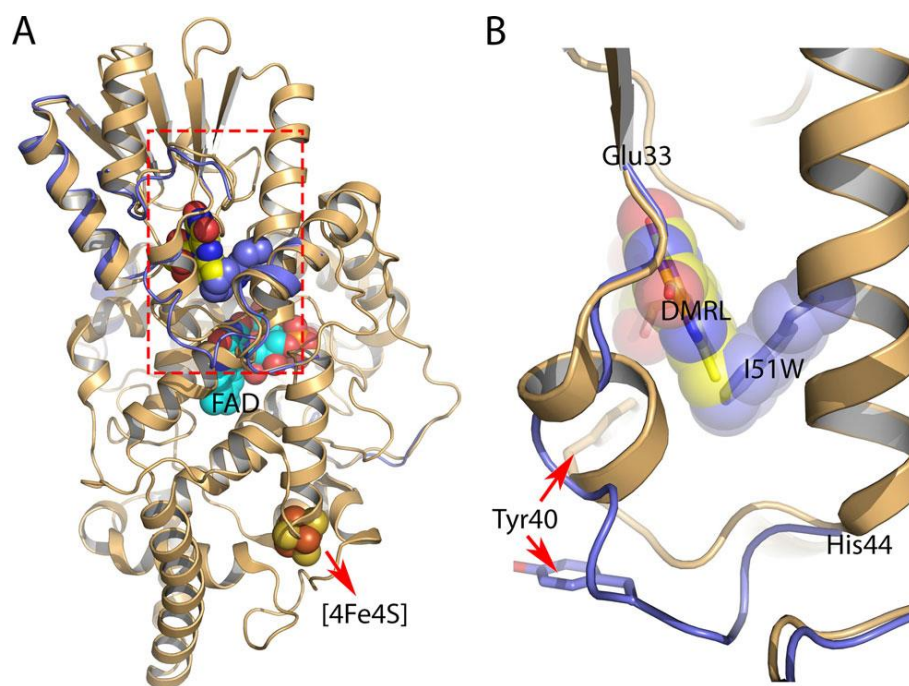


Figure 32. Structural differences between PhrB-WT and PhrB-I51W. (A) Ribbon diagram of the PhrB-WT (light orange) structure. Also shown are segments of the PhrB-I51W structure (blue) that deviate from the PhrB-WT structure by an RMSD > 0.5 Å. All cofactors shown in space-filling representation are from the PhrB-WT structure. A close-up view inside the rectangular box (outlined in red dashed line) is shown in B. (B) Substitution of Ile51 with Trp51 (blue spheres) in PhrB-I51W leads to a direct steric clash with DMRL (yellow spheres) in the PhrB-WT structure. The resulting loss of DMRL is accompanied by extensive structural rearrangements near the binding pocket with significant displacements in the segment between Glu33 and His44. The PhrB-WT structure is highlighted in yellow and gray, PhrB-I51W in blue.

There is no visible electron density for DMRL in the PhrB-I51W crystal structure, which confirms our above interpretations of the UV-Vis spectra and HPLC profiles. Superposition of the PhrB-WT and PhrB-I51W structures shows no significant differences in the overall structure except in the region near the DMRL binding pocket (Figure 32). The Trp51 side chain of PhrB-I51W overlaps with a methyl side chain of the DMRL aromatic ring system (Figure 32B). Such a steric clash is most likely the cause for displacement of DMRL in PhrB-I51W. Significant structural rearrangements have been observed in the protein segment between Glu33 and His44 in PhrB-I51W near the DMRL binding pocket of the PhrB-WT structure (Figure 32), likely via two mechanisms. The first mechanism is reorganization of hydrogen bonding networks. Some residues involved in hydrogen bonding interactions with DMRL reorient in the PhrB-I51W structure and form new hydrogen bonds or salt bridges with other residues and/or to become exposed to the solvent (Figure 33). For example, Glu37, a residue in hydrogen bonding contact with DMRL in the PhrB-WT structure, is displaced by approximately 6 Å from its original C α position. Glu37 breaks the salt bridges with Arg108 and forms a new salt bridge interaction with Arg389 at the surface of the protein (Figure 33). This new interaction between Glu37 and Arg389 in PhrB-I51W also helps stabilizing the side chain conformation of Arg389, which was modeled in two alternate conformations in the PhrB-WT structure (Zhang *et al.*, 2013). The second mechanism is the movement of structural segments due to steric repulsion caused by the mutation. Specifically, the side chain of His43, which is in van der Waals contact with DMRL in the PhrB-WT structure, is pushed ~3 Å away from its original position by the bulky side chain of Trp51 in PhrB-I51W (Figure 33). All these structural rearrangements are achieved not only by amino acid side chains assuming different rotameric conformations, but also by the polypeptide backbone adopting a different conformation (Figure 32 and Figure 33). In the absence of DMRL, the segment ranging from Val34 to His43 that shields the DMRL chromophore from the solvent exhibits a significantly different fold in PhrB-I51W (Figure 32B). In particular, a short helix (residues 35-39) refolds to become part of a well-ordered extended loop conformation in PhrB-I51W (Figure 32B). And the phenolic side chain of Tyr40 that forms a hydrogen bond with the ribityl side chain of DMRL in the PhrB-WT

structure moves away from the vacant DMRL pocket by about 6.5 Å in the C position in the PhrB-I51W mutant and exposes its side chain hydroxyl group to the solvent (Figure 32B). The refolding of the Val34-to-His43 segment also leads to formation of a channel connecting the DMRL binding pocket to the solvent. As a result, DMRL is released, and the vacated cavity is largely occupied by potential water molecules in the crystal structure of PhrB-I51W. The structural changes induced by binding of the antenna chromophore are comparable with those in *Drosophila* 6-4 photolyase upon binding of its antenna chromophore, deazaflavin, where the chromophore insertion induces rotations of side chains and displacement of water (Glas *et al.*, 2009a).

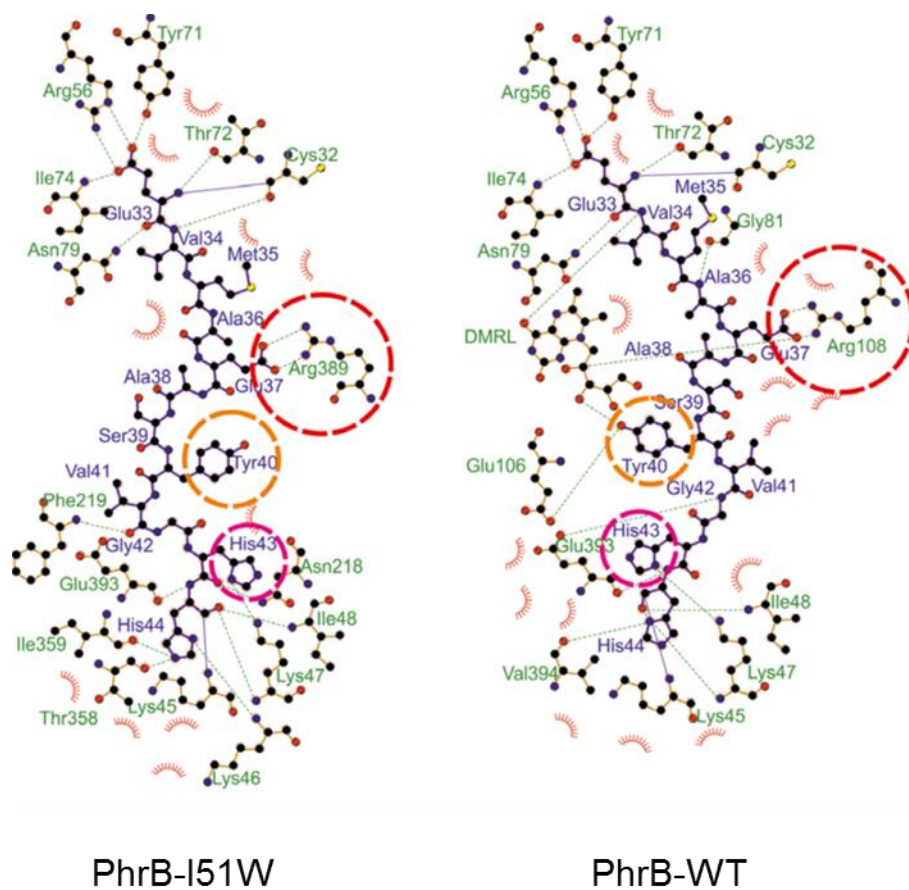


Figure 33. Structural reorganization and interactions of the Glu33-His44 region in the PhrB-WT (right) and PhrB-I51W (left) structures near the DMRL pocket. Three residues Glu37, Tyr40 and

His43 that are close to DMRL in the PhrB-WT structure are highlighted in red, orange and magenta circles, respectively. For clarity, hydrogen bonds involving water molecules are not shown. Adapted from (Zhang *et al.*, 2017)

Beyond the DMRL pocket, the PhrB-I51W and PhrB-WT structures match very well with an overall RMSD value of 0.49 Å. An amino acid region (residue 174-190) within the extended loop near the putative DNA binding site of PhrB becomes more ordered with well-defined electron density in the PhrB-I51W structure (Zhang *et al.*, 2017). Ala180, Glu181 and Asn182 are disordered in the PhrB-WT structure, indicating flexibility in this region (Zhang *et al.*, 2013). Superpositions show that the loop segment ranging from Arg183 to Leu190 assumes different positions in PhrB-WT and PhrB-I51W crystals (RMSD between the corresponding C α atoms = 1.0 Å). Such structural variations in the long inter-domain linker (Zhang *et al.*, 2013) arise probably from subtle differences in crystal packing due to crystallization and/or cryo-cooling conditions, which are almost similar in both crystal forms but never exactly identical.

5.2 Crystallization of PhrB under blue light

Oxidized PhrB crystals which grow under dark condition have been well researched by the former member in our group, but its reduced state crystal has never been gained. PhrB's homology CryB has been confirmed that it has dual function photorepair and photoreceptor. Normally as photoreceptor, under its photoreduction process it will undergo conformational change. As this conformational change might be able to track and observe from the crystal structure, I conducted the crystallization experiment under blue light try to gain the crystals in reduced state. After primary crystallization screening of 96 different conditions, I got four positive conditions (Figure 34). The buffer condition in (Figure 34A) and (Figure 34D) can successfully gain crystal of PhrB under both dark, oxidized stated and blue light, reduced state, and for the buffer condition in (Figure 34B) and (Figure 34C) only successfully gain crystal of PhrB under blue light, and reduced state, which means the crystal structure under these two condition might different from the dark conditions. The buffer condition in (Figure 34C) contains 10 mM magnesium

chloride which means the PhrB crystal growing under this solution probably also contains magnesium in their binding site, which may give us a direct evidence of magnesium action site in PhrB then help reveal the mechanism of divalent cations stimulated effect in (6-4) bacterial photolyases.

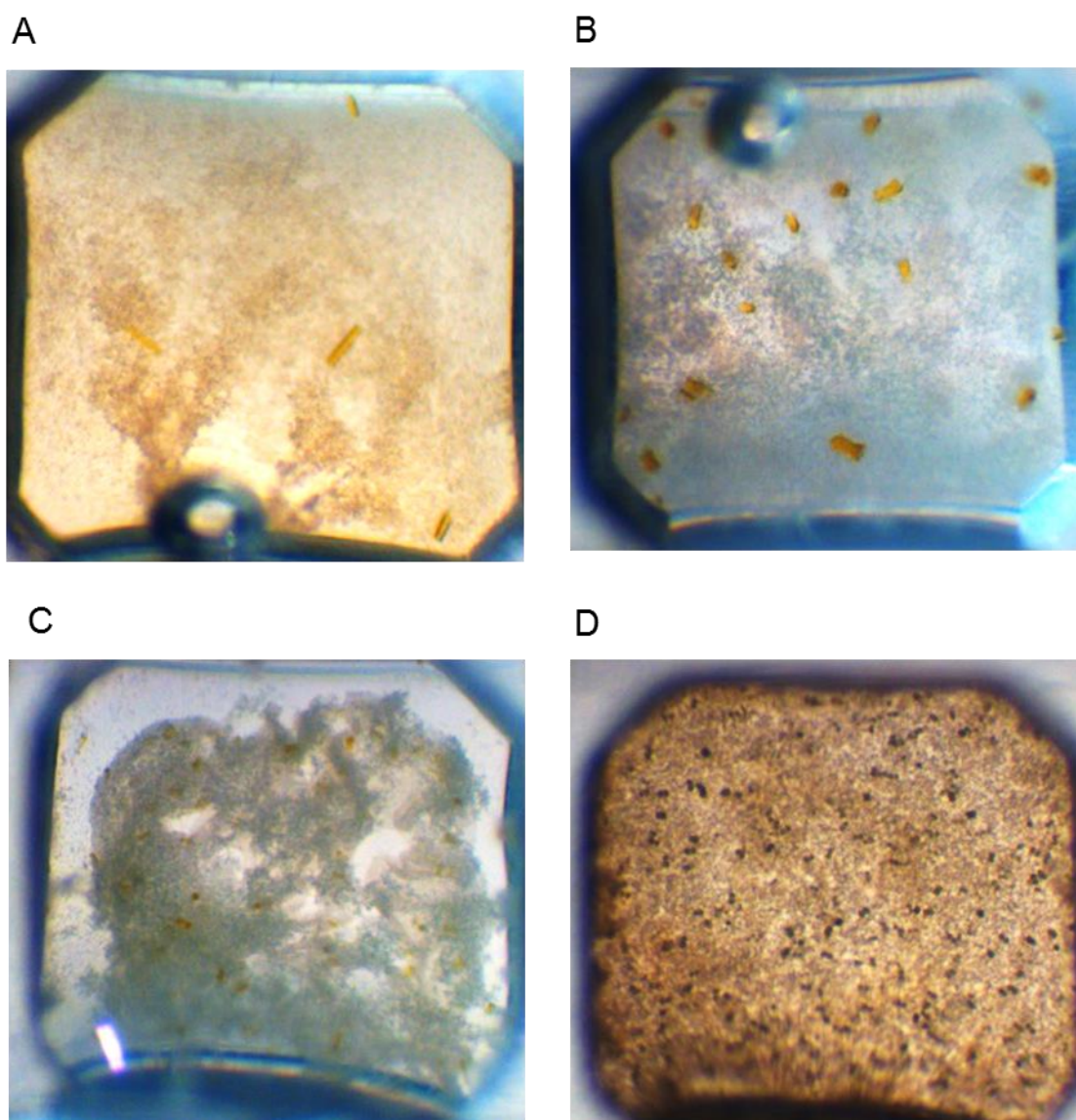


Figure 34. Positive crystal results from the primary screen under blue light. The protein concentration was 6 mg/mL and the temperature was 298 K. Drops were made by mixing of 2 μ l protein solution (protein solution contained 4mM TCEP with 2 μ l reservoir solution. The blue

light is $20 \mu\text{mol m}^{-2} \text{s}^{-1}$ and the buffer conditions of the positive wells were: (A) 15 % PEG 400, pH 6.5, 100 mM MES sodium chloride, (B) 20 % PEG 3000, pH 7.5, 100 mM HEPES sodium salt, 200 mM sodium acetate, (C) 15 % PEG 6000, 50mM potassium chloride, 10 mM magnesium chloride, (D) 8 % PEG 4000.

Discussion

1 Divalent metal ion effects on bacterial (6-4) photolyases

Many DNA processing enzymes like nucleases, polymerases and phosphonatasases (Zhang *et al.*, 2004) require Mg^{2+} or Mn^{2+} for catalytic function. Mg^{2+} is also required for interactions between proteins, for ribosome subunit association, ATP-dependent reactions and many other functions. The impact of divalent cations on photolyase DNA repair has not been reported by other group. In my project, I found that DNA repair by a bacterial CPD photolyase and a eukaryotic (6-4) photolyase is indeed not dependent on Mg^{2+} , whereas the repair activities of three (6-4) BCP photolyases were stimulated by Mg^{2+} or to a similar extent by Mn^{2+} . This stimulated effect that could partially be imitated by Ca^{2+} . This finding explains why the repair activities of PhrB in initial assays were found to be very poor and required protein concentrations exceeding those of the DNA. At first, DNA repair experiments with CryB hence erroneously suggested that this protein does not act as photolyase because no repair activity was found (Geisselbrecht *et al.*, 2012). However, further studies showed that CryB strongly affects the UV-survival rate of *R. sphaeroides* and also been checked out some degree of (6-4) photolyase activity *in vitro* (von Zadow *et al.*, 2016). If consider the amount of protein, in the presence of Mg^{2+} or Mn^{2+} the activities of both PhrB and CryB were promoted to the range of the eukaryotic (6-4) photolyase OtCPF1 from *Ostreococcus tauri*, however still about 10 times lower than CPD photolyase from *Agrobacterium fabrum* (Table 4).

Based on the CPF proteins I studied in this project, the Mg^{2+} stimulation effect is only restricted to (6-4) BCP proteins. Based on my experiment results that a eukaryotic (6-4) photolyase and a class III CPD photolyase have no Mg^{2+} stimulation effect, so this effect could commonly exist in other groups of photolyases, because Mg^{2+} is absent in all the other standard assays, where DNA repair activities have been determined. In evolutionary terms, the loss of Mg^{2+} stimulation should correlates with the loss of the Fe-S cluster or the other properties described in (Table 8).

Table 8. Comparison between (6-4) BCP proteins and other groups of photolyases

	DNA Repair effect of Mg ²⁺	Fe-S cluster	Antenna chromophore	C-terminal extension	DNA stabilization loop
(6-4)BCP proteins	Increased	Yes/No	DMRL	Long, 2 helices	between helix 7 and 8
Other photolyases	No effect	No	MTHF, 8-HDF or other but not DMRL	Either no, short (Arath (6-4) PL) or long (<i>e.g.</i> plant cryptochromes) but in this case no homology with (6-4) BCP proteins	Between helix 17 and 18

Photoreduction assays that were also performed with all 3 types of photolyases *i.e.* a (6-4) BCP protein, a eukaryotic (6-4) photolyase and a CPD photolyase. The photoreduction results showed that divalent cations can exert a positive or negative effect on the rate of photoreduction, but that there is no correlation with the effect on photorepair and in PhrB, Mg²⁺ slows down photoreduction but highly improving the DNA repair. So we could exclude that the reason of stimulation on DNA repair is because of divalent cations promoting the photoreduction .

The fact that Mn²⁺ enhances the repair activity of PhrB and CryB to a similar extent as Mg²⁺, whereas the effect of Ca²⁺ on the catalytic activity of these enzymes is less pronounced correlates well with the six-coordinate geometry of Mn²⁺ displaying a similar effective ionic radius (0.83 Å in its high spin state) as Mg²⁺ (0.72 Å) whereas Ca²⁺ ions are significantly larger (≥ 1 Å), irrespective of their coordination number (Shannon, 1976). These observations suggest that PhrB and CryB in complex with (6-4) photoproducts or intermediates of the catalytic repair cycle share homologous binding sites for the metals responsible for enhancement of repair activity that are selective for divalent cations abundantly found in the cytosol.

We could then imagine the Mg^{2+} effect that is due to provide a bridge between the protein and DNA lesions and form a stable reaction complex during the catalytic process by binding of the metal ion at the protein DNA interface or close to it (Zhang *et al.*, 2004). A most obvious structural difference between (6-4) BCP proteins and other photolyases or cryptochromes is the long linker region between helices 7 and 8, which according to (Zhang *et al.*, 2013) is likely to interact with the DNA lesion. This loop, also named interdomain linker because it connects the antenna binding domain and the catalytic domain, is much longer than in other photolyases or cryptochromes and structurally unique to (6-4) BCP proteins as shown by a multiple structural alignment of representatives of the different classes of CPF proteins (Figure 38). It appears to functionally replace a loop between helices 17 and 18 of *Drosophila* (6-4) photolyase (PDB entry 3CVU).

Interestingly, this loop harbors one negatively charged residue, an aspartate (CryB: Asp175; PhrB: Asp179; Proma-PL: Asp177) that is absolutely conserved among the (6-4) BCP subfamily of photolyases (Figure 38, Figure 36, Figure 39). Another highly conserved aspartate (CryB: Asp250; PhrB: Asp254; Proma-PL: Asp252) is found in the neighboring C-terminal helix. The closest distances between oxygen atoms of both amino acids are 7.1 Å in PhrB and 5.2 Å in CryB. Although both distances are slightly too large to fit in a Mg^{2+} ion, Mg^{2+} -O distances are in the range of 2.0 – 2.1 Å, a Mg^{2+} has been here tentatively modeled into the CryB structure (PDB code 3ZXS). The proposed Mg^{2+} -O distances to Asp175 and Asp250 range from 2.9 to 3.0 Å and from 3.2 to 3.3 Å, respectively, for the three copies of the molecule in the asymmetric unit. However, a significant degree of disorder for this site cannot be excluded, as CryB crystals were cultured in the presence of 0.3 M $MgCl_2$ and soaked with $GdOAc_3$ then the crystals were cryo-protected with buffer containing 0.3M $MgCl_2$ prior to structure determination. In any case, this loop region could also slightly move upon DNA binding so that both amino acids form a defined binding site for Mg^{2+} or Mn^{2+} . Flexibility of the loop has been proposed before based on missing electron densities of three amino acids in PhrB (Zhang *et al.*, 2013). In case that the (6-4) lesion binds analogously like in conventional (6-4) photolyases this Mg^{2+} would neighbor the pyrimidine-pyrimidine (6-4) DNA lesion and

hence being capable to stabilize its radical state after light-driven electron transfer from the catalytic FADH^- (Ma *et al.*, 2017). In addition, I also tested the different magnesium concentration also had impact on DNA repair (Table 9), which indicated probably not only one magnesium molecule involved in DNA repair.

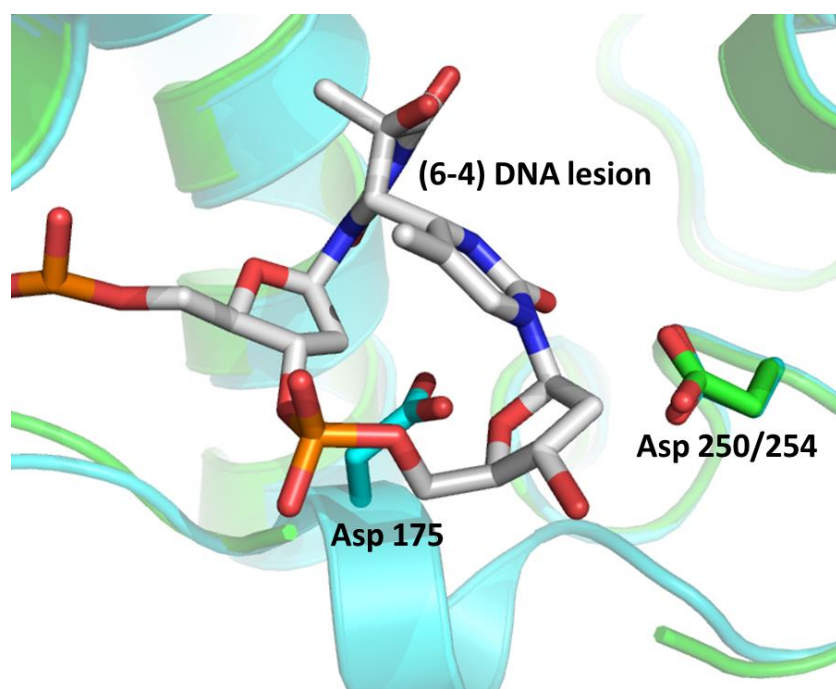


Figure 35. Pairs of highly conserved residues Asp175-Asp250 in CryB (PDB code 3ZXS, polypeptide chain A, blue) and Asp179-Asp254 in PhrB (PDB code 4DJA, green) at the putative DNA binding site. Asp175/179 in CryB/PhrB, respectively, is located in the long loop that is part of the interdomain linker. Asp179 of PhrB is modeled in two conformations ((Ma *et al.*, 2017)) in order to make the figure clear, Asp179 was not shown in stick, and the segment from Ala180 to Asn182 in PhrB is not visible in the crystal structure due to disorder. The view shown in this figure was obtained by superposition of the respective polypeptide chains of CryB and PhrB with the structure of (6-4) photolyase from *Drosophila melanogaster* in complex with photo damaged DNA (PDB code 3CVU). Of the latter structure, only the damaged DNA site of the (6-4) DNA is shown as stick.

Table 9. DNA repair comparison of different Mg^{2+} concentration.

	Repair (%)	
	0.06 mM Mg^{2+}	4 mM Mg^{2+}
PhrB-Y424F for ss (6-4) ODN5 (2min repair)	18.7 ± 1	45 ± 1
PhrB-WT for t_repair (3min repair)	20 ± 3	48 ± 3

Based on sequence analysis of PhrB and Proma-PL (Figure 36), PhrB contains the two conserved aspartates (Asp 179 and Asp 254) and Fe-S cluster (4 cysteines which act as covalently bonding the Fe-S cluster). The alignment results of more than 4000 PhrB homology protein show that not only the two conserved aspartates but also the 4 cysteines existed in all of the 4000 homology proteins, so PhrB could be treated as a representative protein in the subgroup of (6-4) BCP proteins which contains Fe-S cluster, whereas Proma-PL only has two conserved aspartates (Asp 177 and Asp 252) (Figure 39) and without the 4 cysteine which act as bonding the Fe-S cluster and the alignment of more than 900 Proma-PL homology proteins show that the two conserved aspartates conserved in all of these 900 homolog proteins and the 4 cysteines were not there, hence Proma-PL could be treated as a representative protein in the other subgroup of (6-4) BCP proteins which are without Fe-S cluster.

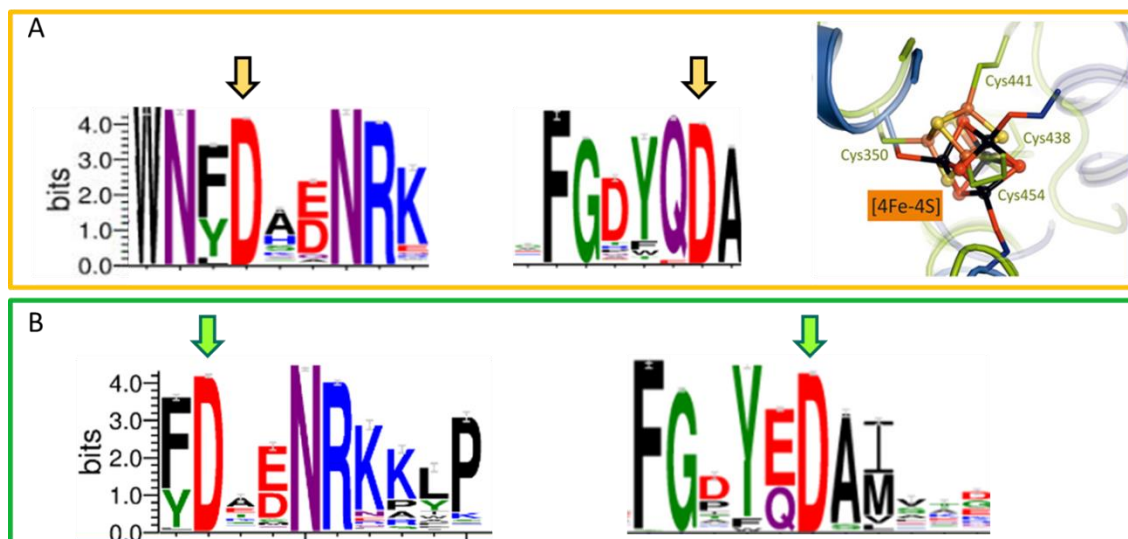


Figure 36. Weblogo (Crooks *et al.*, 2004) presentation of conserved amino acids near the DNA binding site in the (6-4) BCP members. Arrows pointed out the most conserved aspartates which may involve in binding with divalent cations. (A) Amino acid conservation based on an alignment of >4000 (6-4) BCP homologs with Fe-S cluster. The sequences blast (NCBI) with PhrB amino acids as template and then aligned with MEGA4 (Tamura *et al.*, 2007). (B) Amino acid conservation based on an alignment of >900 (6-4) BCP homologs without Fe-S cluster. The sequences blast (NCBI) with Proma-PL amino acids as template and then aligned with MEGA4 (Tamura *et al.*, 2007).

Alternatively, another pair of strictly conserved acidic residues (PhrB: Glu152/Glu301, CryB: Glu148/Glu297), which may serve as magnesium ligands near the active site can be delineated. However both structures of PhrB and CryB show that this pair forms already polar interactions with a conserved arginine (PhrB: Arg309; CryB: Arg305). Overall, the precise mechanism of (6-4) lesion repair and binding by members of the (6-4) BCP subfamily may differ in this regard substantially from other members of CPF proteins.

2. Model predicted for Mg^{2+} effect on DNA repair

2.1 Crystal structure analysis of CPF proteins

Based on my experiment results of magnesium stimulated effect in DNA repair, we can conclude that this stimulated results only existed in (6-4) bacterial photolyases. In order to find out the differences between the (6-4) BCP group and the other CPF proteins, I selected one representative protein which crystal structures have been reported from every other group to compare with the two (6-4) BCP proteins. The following sequence alignment is based on crystal structure. Positively charged site 1 and 2 are labeled by orange arrow (Figure 37, Figure 38). Based on structure alignment, I found that except the two (6-4) BCP proteins CryB and PhrB, all the other representative proteins have positively charged site 1 and 2 which means there are two positive charged amino acids at site 1 and site 2 separately, however both CryB and PhrB have two aspartates which are absent in all the rest selected proteins near the DNA binding site (Figure 35).

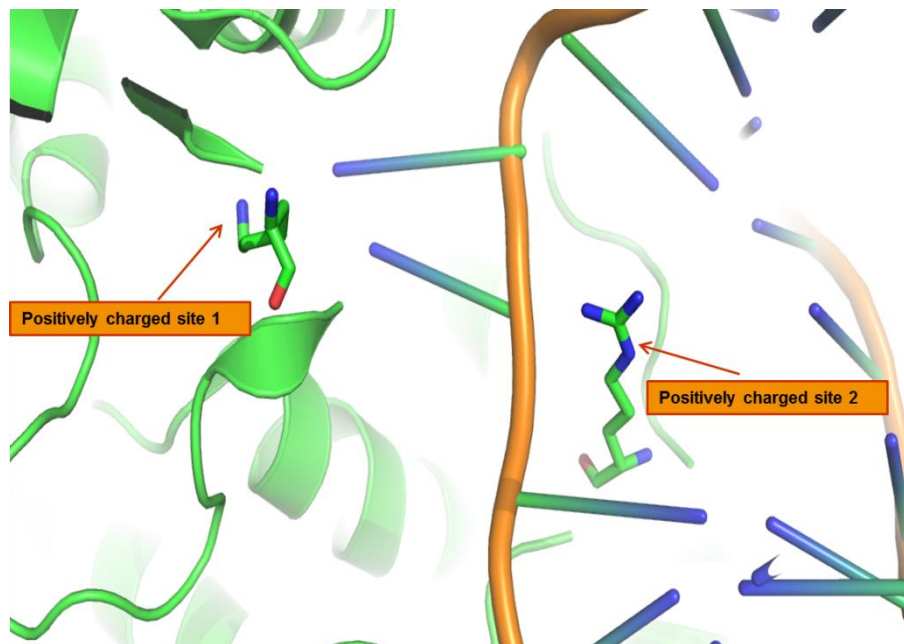


Figure 37. *Drosophila melanogaster* photolyase (3CVU) (Maul *et al.*, 2008) active site containing the (6-4) photoproduct, and positively charged site 1: Lys 246, positively charged site

2: Arg 421. The possible electrostatic interactions is those positively charged sites near the DNA lesion binding site can interact with the phosphate group of DNA chain.

```

4djaA -----MSQLVLLIGDQLSP-SIAALDGV---DK-----KQDILVLCV-VM- 35
3zxsA -----LRRLILVLDQLSD-DLPALRAA---DP-----AADLVVMAE-VM- 35
4u63A -----SIIASSLKTAPVIVWFR-KDLRLSDNLALLAAVE-H-G-----GPVIVPVIIE- 45
3cvuA -----R-----SILVHWFR-KGLRLHDNPALSHIF-AANA-APGRYVFRPIFILDPG- 45
1u3cA -----CSIWVFR-RDLRVEDNPALAAAVR-A-----GPVIALFVWA-P- 35
1np7A -----MKHV-----PPVVLVWFR-NDLRLHDHEPLHRAK-S-G-----LAIHAVCYD-P- 42
1dnpA -----TTHLVWFR-QDLRLHDNLALAAACR-N-S-----ARVLALYIAT-P- 38
3umvA -----SPAPFPRVRIHPGGGK-----GGPVVYVWML-RDORLADNWALLHAAGLA--AASA--SPLAVAFALPFRP 62
1.....10.....20.....30.....40.....50.....60.....70.....80
    
```

```

4djaA A-EA-S-YV---G--HKKKIAPFISAMRHPAEBLRGEGYRVRVTRIDDADNAG---SFTGEVKRAIDDLTPERICVT 102
3zxsA E-EG-G-YV---P--HHPQKIALILAAMRKPARRLOERGFVRVAVSRLLDDPTGPF---SIGAELLRRAAETGAREAVT 102
4u63A KSA-----GPLGGAQEWLHHSLAALSSSLEKAGGRLVLA-----SG---DAERILRDLISITGADTVVWN 103
3cvuA ---ILDW-----M-QVGANRWRFLQQLLELDLNOQLRKLNSRLVAVV---RG---KPAEVFPRIFKSWRVMELTFE 104
1u3cA EEE---GHY-----HPGRVSRWMLKNSLAQLDSSLSRSLGTCLIK-----RST---DSVASLVDVVKSTGASQIFPN 96
1np7A R-DF-A-QTHGCFPA-KGCPWRSNFIQQSVQNLAESLQKVGKLLVTV---EG---LPEQVIPIQIAKINAKTIYYH 107
1dnpA RHW---A-TH-----NMSPRQAEILINAQNLGLQIALAEKGIPLLFR-----EVDLFAVSVVEIVKQCAENSVTHLFIN 102
3umvA F-L-----L-----SARRRQLGFLRLGLRRLAADAARHLPPFLF-----TG---GP-ABIIPALVQRLGASTLVAD 118
.....90.....100.....110.....120.....130.....140.....150.....160
    
```

```

4djaA -----EPGEWRVRSEMDGFAGAFGIQV-----DIRSDFRF-LSSHGE-FRN-WA-----AGRKS--LTMVIFYREMR--RRTG 163
3zxsA -----RPGDWRLTEALEAM--PL-P-V-----RFLPDRDF-LCPADP-FAR-WI-----EGRKQ--LRMEWIFYREMR--RRTG 159
4u63A -----RRYDPTGMATDKALKQ-K-LR-D-D-GLTVRSFSGQLL-HEPSR-L-----QIKSG-G---PYRVVTPFWRALV--GS-D 164
3cvuA -----TDIEPYSVTRDAAVQK-L-AK-A-E-GVRVETHCSHTI-VNPEL-VIA-KN-L-GK---APITYQKFLGIV--EQ-- 164
1u3cA -----HLVYDPLSLVRDHRADK-V-LT-A-Q-GIAVRSFNADLL-YEPWE-V-----TDELG-R---PFSMPAFAWFERCL--SM- 156
1np7A -----REVVTQELDVERNLVK-Q-LT-I-L-GIEAKGYWGSILCHP--EDL--PF--SID--LPDLFTKFRKDIKXKII-S 170
1dnpA -----YQYEVNERARDVEVER-A-L-R--NVVCEGFDSDVI-LPPGA-V---MIGNH--E---MYKVFVTPFKNAWL--KRLR 162
3umvA -----FSPLRVREALDAVVG-D-LR-RAPGVAVHVDVAVN-VFVWT-ASA---K---MEYSAKIFRQKVS--KVM 179
.....170.....180.....190.....200.....210.....220.....230.....240
    
```

Asp179/175

```

4djaA -----LLMNGECPVGGRWNFDAENRQPARPDLRLPKHPVFAPDKIKK----- 205
3zxsA -----LLMEGDEPAGGKWNFDENRKPAAFDLLRPRPLRFEPDAEVR----- 201
4u63A -----EPHAPADPP--KSL--I-----APKVV-P-----K- 184
3cvuA -----LK-VPKVLGVP-EKLNK--P-TPPKDEV--EQ- 190
1u3cA -----PYDPESPLLP--KKI-I-----SGDVS-K-C-V- 179
1np7A -----I--IRPCFFAP--SQL-L-----PSFNIXL--P- 190
1dnpA -----EGM-PECVAAP--KVRV-SGSIEP-----SPS- 185
3umvA -----E-MLVEFPFLPA--VV-P-----WDREQ--P-E- 200
.....250.....260.....270.....280.....290.....300.....310.....320
    
```

```

4djaA -----E-VIDT---VERLPPDNF--G--KLEN---FG-FAVTRIDAERALS---AFI--DI--PLC 247
3zxsA -----A-VLDL---VEARPPRF--G--RLRF---FH-WATDRAEALRALD---HPI--RE--SLP 243
4u63A -----SEK--LS--NWK-LL-P-----NK--PDWAKD---FS-DIWPGETGALDKLD---DPID--G--ALK 228
3cvuA -----KDSAAAYD-C-PTM-K-Q-LV-K-----R-PE-ELGP-----N-KFPGGETEALRRME---ESLK--DEIWA 238
1u3cA -----ADP-----LV-FE-D-----DSE-K-GSNAL---LARA-WSPGWSNGDKALT---TFIN--G--PLL 221
1np7A -----LTA--P--P-PEFF-----P-Q--INFHRSV---LAFQGGTAGLARLQ---DYFWGD--RLK 234
1dnpA -----I--I--LN-IP-----R--QS---FDTAHFVVEKKAIAQLR---QFCQ--N--GAG 220
3umvA -----G-VDWDALI--AR-V--C-SEA--E--NV--PE---ID-W-CEPGHEAAIEALLGSKDGFLT-K--RIK 248
.....330.....340.....350.....360.....370.....380.....390.....400
    
```

Asp254/250

```

4djaA -----NFG--ATQDAMLODDPNLNHLLSIFYINCGLLDALDVCKAAE-RAY-HEGGA-----P-----LNAVE---GFIRCIIG 309
3zxsA -----RFG--DEQDAMLADDFPLSHALLSSMNLGLLGPMVECRRAE-TEW-REGRA-----P-----LNAVE---GFIRCIIG 305
4u63A -----GYE--EGRDFP--AK-PATSLLSPHLAAGEISPAAVWHATKGL--SR-HI-----A--SNDIS--RFRKEI-V 283
3cvuA -----RFE---KPNITAPNSLEPSTTVLSPYLKFGCLBARLNFQKLE-IYKR--QP--K-----HS--QPPVSLICQL-M 297
1u3cA -----EWS--KNRKA--DS-ATTSFPLSPHLHFGEVSVRKFVHLVRI-KQVA--WANEGNEAG-----EESVN--LPLKSI-G 283
1np7A -----DYK--ETRNGM--VGADYSSKFPWLAGCLSPRFIYQEVKRYE--QE-RV-----S--NDSH--WLIFEL-L 291
1dnpA -----EYE--QQRDFP--AV-EGTSRLSASLATGGLSPRQCLHRLLAEPQ-----ALDGG--AGS--VWLNEL-I 276
3umvA -----SVE--TDRNDP--TKPRALSGLSPLYLHFCHISAQRCALEAKCCR--H--L-----S--PKSVD--AFLEELVV 304
.....410.....420.....430.....440.....450.....460.....470.....480
    
```

Positively charged site 1

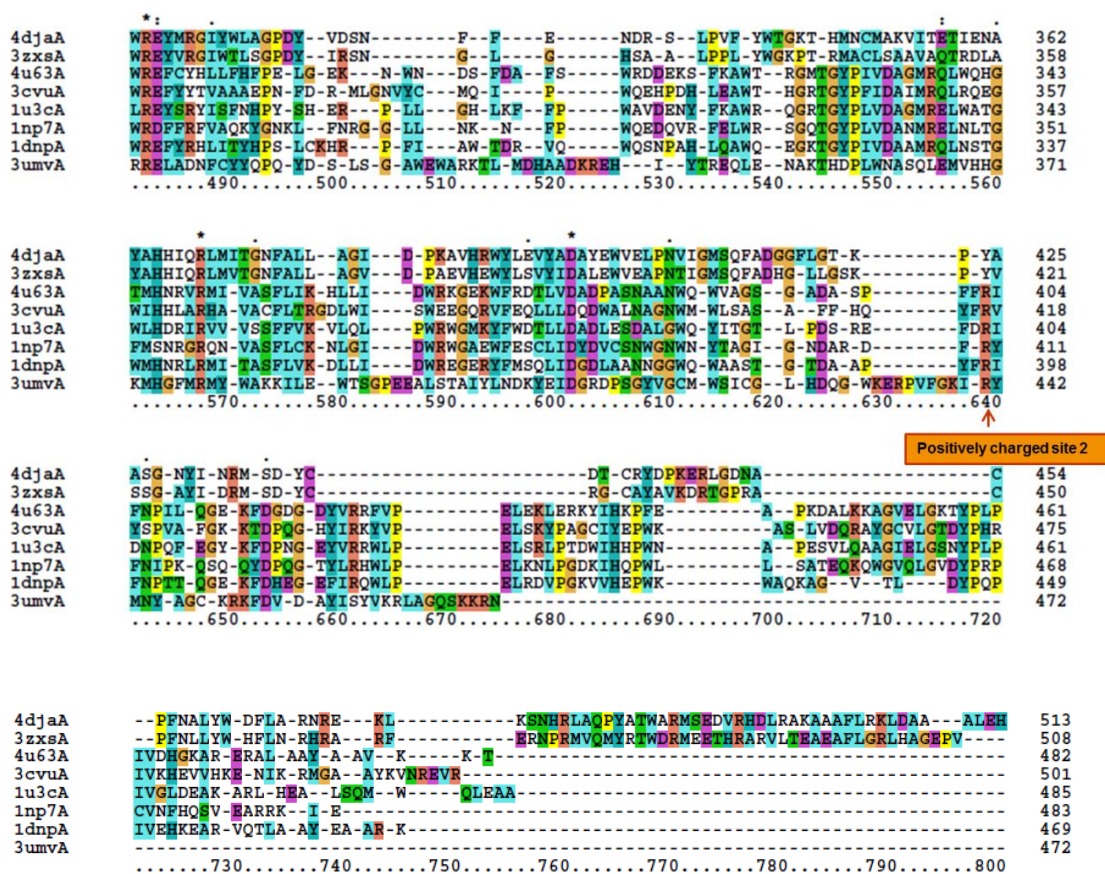


Figure 38. Multiple structure alignment of representatives of the photolyase cryptochrome family proteins, generated by using the SALIGN server (<http://salilab.org/salign>) (Braberg *et al.*, 2012). The PDB codes used for the aligned structures are: 4DJA, (6-4) photolyase PhrB from *Agrobacterium fabrum*; 3ZXS, CryB from *Rhodobacter sphaeroides*; 4u63, class III CPD photolyase PhrA from *Agrobacterium fabrum*; 3CVU, (6-4) photolyase from *Drosophila melanogaster*; 1u3c, cryptochrome 1 from *Arabidopsis thaliana*; 1np7, cryptochrome from *Synechocystis* sp. PCC 6803; 1dnp, class I CPD photolyase from *Eschericia coli*; 3umv, class II CPD photolyase from *Oryza sativa japonica*. These PDB codes are followed by a capital letter and the letter identifying the polypeptide chain used in the alignment. For those structures of the selected proteins, which contain more than one copy of the polypeptide chain per asymmetric unit, only the first chain (A) was used. The interdomain linker in PhrB and CryB is indicated by the red bar above the sequences. The blue bar indicates the flexible region. The two conserved Asp residues (175/179 and 250/254 in CryB/PhrB, respectively) are labeled by purple arrow.

Positively charged site 1 and 2 are labeled by orange arrow (The original crystal structure of PhrB has three missed amino acids, and I added them into the above figure).

2.2 Homology modeling and simulation prediction

For Proma-PL from *Prochlorococcus marinus*, its structure was predicted by software Swiss Model (<https://swissmodel.expasy.org/>) (Nicolas *et al.*, 2009; Benkert *et al.*, 2011; Bertoni *et al.*, 2017; Bienert *et al.*, 2017; Waterhouse *et al.*, 2018) and the results of Proma-PL superimposed with CryB was shown below (Figure 39).

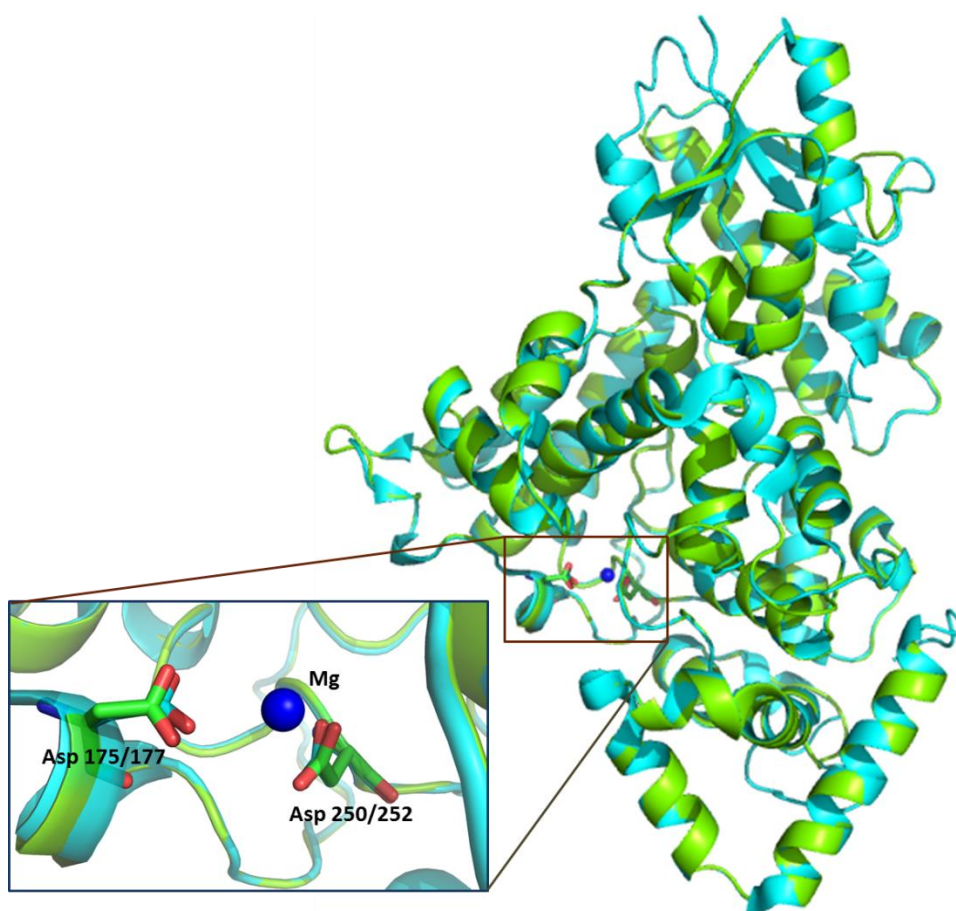


Figure 39. Predicted Proma-PL structure superimposed with CryB (PDB code 3ZXS, chain A).

The enlarged window part clearly indicated that in Proma-PL there are also two aspartates at the DNA binding area and they may involve in the coordinating of magnesium.

In order to analyze the connection between Mg^{2+} effect and the conserved amino acids, we cooperate with other laboratory (Institute for Physical Chemistry from, Karlsruhe Institute for Technology), performed simulations on possible location of Mg^{2+} in PhrB with bound lesion DNA. The stimulation we got is as following: Mg^{2+} cations reach the neighborhood of the (6-4) photoproduct in the active site pocket in the first nanoseconds of the simulations. However, the obtained Mg^{2+} complexes differ depending on the charge state of His366 and the presence of Asp179 and Asp254 residues.

In simulations where His366 was attributed a positive charge ($His366^+$), we observe two stable positions of Mg^{2+} close to the (6-4) photoproduct (see Figure 40 and Figure 41). One position, called Mg_a^{2+} , is close to the phosphate group of the 3' thymine and can interact with Asp179 and Glu181. The second one, called Mg_b^{2+} , is deeper buried in the active site and interacts with the phosphate of 3' thymine, the oxygen atom of the 3' thymine and the aspartic acid Asp254 (Table 10).

A structural comparison with eukaryotic (6-4) photolyase from *Drosophila melanogaster* showed that these two Asp positions are closely related to Arg421 and Lys246, respectively (Figure 40). These amino acids have a key role in binding of lesion DNA (Maul *et al.*, 2008; Korol and Solov'yov, 2017). To determine the degree of conservation of these two residues in eukaryotic (6-4) photolyases, we performed an alignment with 1000 nearest BLAST (Uniprot Dec 2017) homologs of *Drosophila* (6-4) photolyase. At the position of Lys246 (of Drome (6-4) PL) there was a Lys in 42 % and an Arg in 53 % of all sequences. The positive charge at this spatial position is thus highly conserved in eukaryotic (6-4) photolyases. The remaining 5 % sequences were annotated as animal cryptochromes or proteins with unknown functions. At the position of Arg421, 35 % of the sequences also had an Arg residue, 57 % had a His and 1 % a Lys residue. Although on the sequence level there is no clear criterion for distinguishing between photolyase and animal cryptochromes (which do not repair DNA), this survey suggests

that the positive side chain at position 421 of *Drosophila* (6-4) photolyase is not required for DNA repair.

According to our PhrB simulations, Mg_a^{2+} interacts with phosphate groups of the DNA at the periphery of the active site and should help to maintain the lesion in an optimized conformation to facilitate its flipped-out conformation. A presence of a positive charge in direct interaction with the damage as Mg_b^{2+} or Lys246 in *Drosophila* (6-4) photolyase increases the electron affinity of (6-4) lesion. In the crystal structure, the Lys246 side chain is orientated to form hydrogen bonds with 5' cycle whereas Mg_b^{2+} interacts with 3' cycle. Nevertheless, recent molecular dynamics simulations of *Drosophila melanogaster* photolyase have shown a motion of the lysine toward the 3' phosphate group and thus closer to the 3' thymine cycle which is in better agreement with our Mg^{2+} binding conformation.

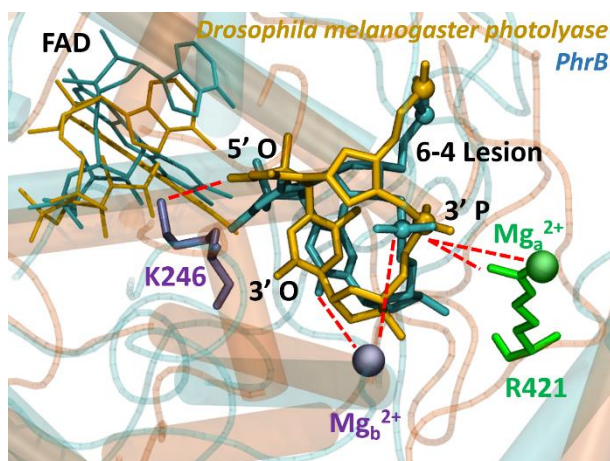


Figure 40. comparison between PhrB (cyan, MD snapshot) and *Drosophila melanogaster* photolyase (orange PDB 3CVU) (Maul *et al.*, 2008) active site containing (6-4) photoproduct (stick, phosphor atoms are represented by balls), FAD (smaller stick), and positively charge group: R421 (from *Drosophila melanogaster* photolyase) and equivalent Mg_a^{2+} (from PhrB) in green; K246 (from *Drosophila melanogaster* photolyase) and equivalent Mg_b^{2+} (from PhrB) in violet. The possible electrostatic or hydrogen interactions are represented with dashed red line. It

has been previously shown in MD simulation that K246 can interact with 3' P atom (Korol and Solov'yov, 2017). Image courtesy of Natacha Gillet.

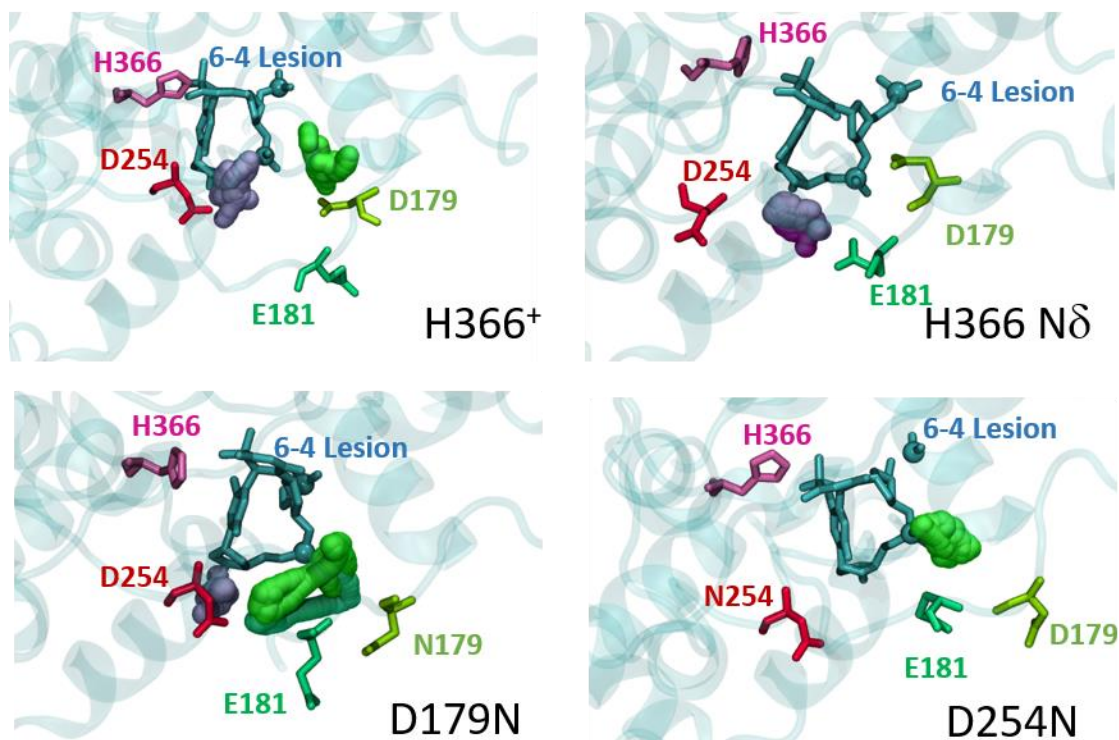


Figure 41. Positions occupied each nanosecond by magnesium cations along the 1 μ s simulations in PhrB with positively charged or neutral H366, D179N or D254N mutants. The cations in position Mg_a^{2+} and Mg_b^{2+} are represented in green and purple spheres respectively. Image courtesy of Natacha Gillet.

Table 10. Electrostatic interactions in kcal/mol between Mg^{2+} cations and (6-4) photoproducts or acid residues during molecular dynamic simulations. Averaged electrostatic interactions between the Mg^{2+} cations and the (6-4) photoproduct or D179, E181, D254 or the corresponding asparagine after mutation. Negative sign means attractive electrostatic interactions while positive sign refers to electrostatic repulsion. The error values correspond to the standard deviation of the interactions during the 1 microsecond molecular dynamic simulations.

	(6-4) PPs	D/N179	E181	D/N254
WT neutral H366	-18.7 \pm 6.1	-0.1 \pm 0.2	-12.3 \pm 7.4	-2.8 \pm 5.3
H366 ⁺	-27.9 \pm 5.2	-4.0 \pm 4.7	-3.3 \pm 5.5	- 10.0 \pm 5.3
D179N	-21.3 \pm 6.6	1.8 \pm 2.5	-7.4 \pm 7.5	-5.0 \pm 5.7
D254N	-13.3 \pm 5.1	-9.6 \pm 7.9	-9.8 \pm 7.4	-1.0 \pm 2.2

If we consider a neutral His366 in PhrB, the situation is different. We observe Mg^{2+} only in the deeper position, close to the thymine (Figure 41). No positive charge interacts with the phosphate as observed in the H366⁺ simulations or in the *Drosophila melanogaster* (6-4) photolyase. Moreover, the cations mainly interact with E181 (Table 10). The electrostatic interactions with D179 or D254 are very small and underline the absence of strong ionic interaction between Mg^{2+} and these two aspartates. Actually, D254 interacts with R187 during the first 750 ns of the simulation while D179 presents strong hydrogen bonds with R183. This is in contradiction with the impact of mutation described experimentally. The hypothesis of a neutral His366 has been consequently rejected.

Consequently, the simulations of D179N and D254N mutants have been performed including His366⁺. In both mutants, the stability of the Mg^{2+} cation around (6-4) photoproduct is affected by the lack of the aspartate negative charge, particularly in the D254N mutant (Table 10). One could expect that only the cation interacting with the mutated aspartate is no longer bound in the active site. Effectively, in D254N mutant, the Mg_b^{2+} position is no longer occupied while the Mg_a^{2+} is present, interacting even stronger with D179 or E181 than in WT (Figure 41 and Table 10). However, the D179N mutant

presents an unexpected behavior: the Mg_a^{2+} position is occupied all along the 1 μ s MD simulation, partially stabilized by an interaction with E181, while Mg_b^{2+} , present at the beginning, is released in the second half of the simulation (Figure 41 and Table 10). Thus, in both mutants, the cation insuring the (6-4) lesion binding still remains whereas the cation increasing the electron affinity of the substrate so decreasing the electron transfer barrier is not stable. Our computational results are in agreement with experimental data as both mutants affect the rate constant of DNA repair.

2.3 Conclusion

Based on the structural differences the major evolutionary transition between (6-4) BCP proteins and other photolyases/cryptochromes should be associated with a loss of the Fe-S cluster, replacement of the DMRL chromophore by other antenna chromophores and switch from the long interdomain linker between the antenna binding and catalytic domains to a region in the catalytic domain as DNA interacting loop (Zhang *et al.*, 2013). The present study shows that this kind of transition is also characterized by the loss of divalent cations dependency of the DNA repair function which only exists in bacterial (6-4) photolyase.

Bacterial (6-4) photolyase has 2 subgroups: one with Fe-S cluster, one without Fe-S cluster, and all the other CPF group members without Fe-S cluster, so they are more closed to Proma-PL the cyanobacteria photolyase (Figure 42). As Fe-S cluster is very ancient cofactor, and the (6-4) BCP proteins with Fe-S cluster can be treated as the original photolyase, the (6-4) photolyases which are widely spread in cyanobacteria did not contains Fe-S cluster, could be treated as a loss of Fe-S cluster during the evolution.

Here is the interesting hypothesis, during the evolution of bacteria, at first the environment can provide enough metal ions for them, as the environment change some bacteria suffer from a lack of metal ions living environment. They gradually evolved into a new type of CPF proteins that do not require metal ions. The Proma-PL can be treated as the middle of this evolution, as they contain no Fe-S cluster in their structures, but in DNA repair they still need metal ion to improve repair activity. Except the (6-4) BCP

proteins, all the other CPF members do not need Fe-S cluster in their structure fold and also do not need metal ions in their DNA repair process as they already have two positively charged amino acids near the DNA lesion binding site which replace the role of divalent cations as bridge between DNA and the proteins in (6-4) BCP proteins, and these two positively charged amino do not exist in the (6-4) BCP proteins which have divalent cations involved in their DNA repair process.

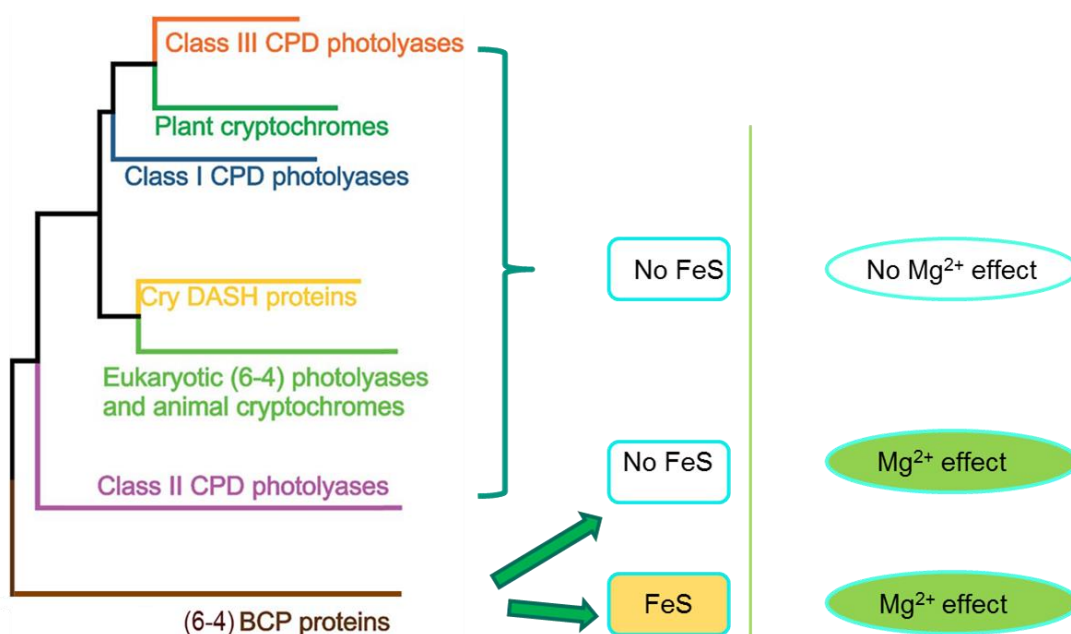


Figure 42. Phylogenetical tree of CPF proteins and typical characterizations of different group concluded from my work.

3 Structure analysis of PhrB-I51W and PhrB-Y424F

The crystal structures of two PhrB mutants, I51W and Y424F, give detailed insight into loss of DNA repair capacity. The PhrB-I51W mutation results in a loss of the DMRL chromophore, which can now be regarded as antenna chromophore for energy transfer to FAD. A comparable mutant has been described for *E. coli* photolyase in which the MTHF antenna was lost (Schleicher *et al.*, 2005; Kao *et al.*, 2008), whereas *Anacystis*

nidulans photolyase expressed in *E.coli* is lacking its 8-HDF antenna chromophore which is not synthesized in this host (Kort *et al.*, 2004). Both light dependent processes of photolyases, photoreduction and photorepair, are less efficient in the PhrB-I51W mutant and can be explained on the basis of energy transfer in the PhrB-WT. The HPLC assays and crystal structure show that PhrB-I51W is indeed completely free of DMRL. The mutant structure shows that the amino acid replacement and loss of chromophore results in a slightly different fold in the region of the DMRL pocket whereas other parts of the protein are not affected. Therefore the mutant effects are clearly due to loss of energy transfer and not the result of indirect structural changes. PhrB represents an ancient group of photolyases and the DMRL chromophore is probably the ancient type of antenna chromophore. As outlined before (Zhang *et al.*, 2013), the binding site of antenna chromophores is identical in PhrB and the related CryB from *Rhodobacter sphaeroides* (DMRL), *Anacystis nidulans* CPD photolyase (8-HDF), *Thermus thermophilus* CPD photolyase (8-HDF) and *Drosophila* (6-4) photolyase (8-HDF), whereas the MTHF chromophore in *E.coli* CPD photolyase or *Arabidopsis* Cry DASH it bound to another site. The MTHF binding site of the class III CPD photolyase PhrA from *Agrobacterium fabrum* is again different from the others (Scheerer *et al.*, 2015). The 8-HDF extinction coefficient is more than three times higher than that of DMRL or FAD (Eker *et al.*, 1990). This explains the replacement of DMRL by 8-HDF. Because some organisms do not produce 8-HDF, MTHF with intermediate extinction coefficient of $25000 \text{ M}^{-1} \text{ cm}^{-1}$ (Eker *et al.*, 1990) might have been selected as antenna chromophore; the establishment of new binding sites could have occurred in the presence of DMRL. We assume that our understanding of photolyase evolution could be advanced by investigating antenna chromophore exchange and binding sites in a comparative manner. We show that the energy transfer function marks already the early forms of photolyases.

The PhrB-Y424F mutation is characterized by a loss of DNA lesion binding and DNA repair (Graf *et al.*, 2015). The crystal structure of PhrB-Y424F gives new insight into a possible structural explanation for the loss of the DNA binding and repair function. It seems that Tyr424 is engaged in an extended hydrogen bonding network which could stabilize DNA lesion binding and allows DNA repair function (Figure 31A,C). The

mutation clearly abolishes part of the hydrogen bonding network, especially the interaction with the highly conserved Arg476 and His366 (Figure 31B,D). The impairment of DNA repair can be explained not only by the loss of lesion binding Tyr424 and the displacement of DNA backbone binding Arg476, but also by the loss of water/hydrogen bonding water chain around the lesion. The structures are in line with an electron transfer from the Fe-S cluster to the lesion via Tyr424 and Tyr430. The structural water around Tyr424 that was highlighted by the mutant could be important for this electron transfer. In addition in previous measurements, the photorepair rate of Y430F was only 30 % of the wild type. Tyr430 is located between the lesion binding Tyr424 and the Fe-S cluster. We hypothesized that Tyr430 and Tyr424 could provide an electron chain between the Fe-S cluster and the lesion which could be required for efficient repair (Graf *et al.*, 2015). However, the Mg^{2+} stimulation of DNA repair of the two mutants was comparable with that of the wild type; hence Mg^{2+} and Tyr430 act independently on DNA repair.

4 Electron transfer chain of PhrB

In most members of the cryptochrome-photolyase family, the electron transfer pathway contains a triad of Trp residues, from the surface of the protein to the FAD chromophore. The electron transfer in (6-4) BCP proteins differs from all other cryptochrome and photolyase groups. The presence of Tyr391 is interesting, as it is situated between FAD and Trp390 in a suitable place to take part in the electron transfer, but mutation of Tyr391 to a redox inert Phe residue reduces but does not block FAD photoreduction or DNA repair; the other phenomenon is in the > 400 PhrB homologs, this residue is either Tyr or Phe (Figure 43). However, experimental mutation of Tyr391 to Ala blocks FAD photoreduction (Figure 29) and DNA repair, underlining its relevance in the electron transfer process.

In the two members of (6-4) BCP proteins, PhrB from *Agrobacterium fabrum* (PDB 4DJA) and CryB from *Rhodobacter sphaeroides* (PDB code 3ZXS) photoreduction proceeds via Trp390 and Trp342 (PhrB numbering), was shown by site directed mutagenesis. These residues are highly conserved in (6-4) BCP members (Figure 43). In

both proteins, the Tyr391 side chain is directly located between Trp390 and FAD (Figure 27) suggesting that this Tyr must be part of the electron transfer chain. However, when the Tyr was replaced by Phe, the photoreduction rate of PhrB and CryB (Geisselbrecht *et al.*, 2012) only slightly affected, and in about 30 % of (6-4) BCP proteins, a Phe is placed at this position (Figure 43). These results favor an electron-tunneling mechanism of electron transfer (Sancar, 2003) and we also cooperated with others (Holub *et al.*, 2018) performed the theoretical computation and also support that the aromatic rings of Tyr or Phe in PhrB are included as bridges in electron tunnelling.

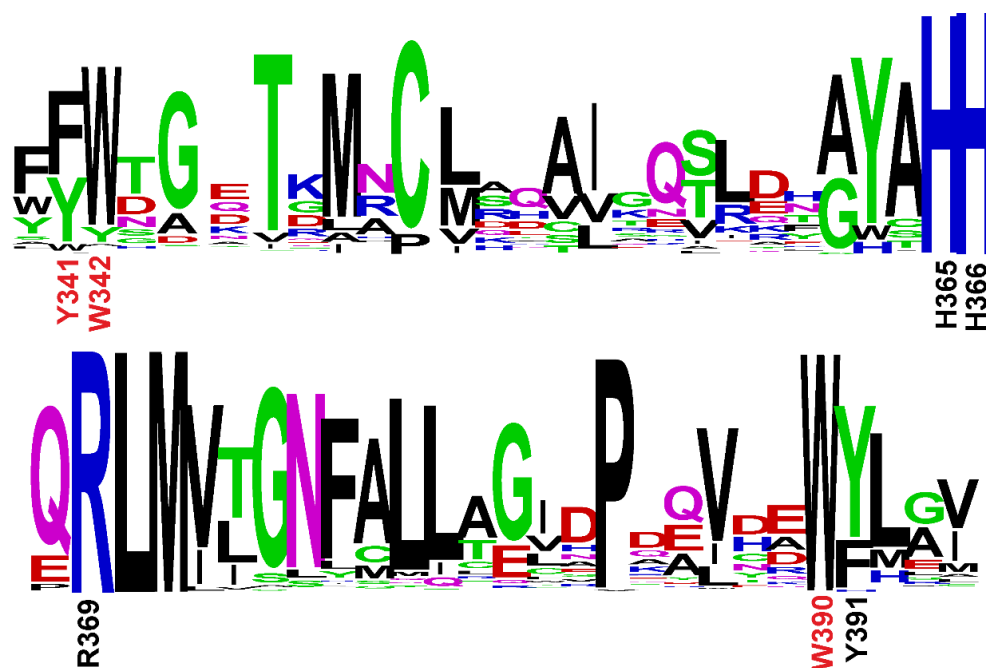


Figure 43. Sequence alignment of >450 PhrB homologs using WebLogo (Crooks *et al.*, 2004) web based application. The amino acids numbering is based on PhrB sequence.

Mutation of Tyr or Trp to Phe is often used in order to impede the charge transfer and identify redox active residues. Both our experimental and theoretical results (Holub *et al.*, 2018) show that tunnelling can also be involved in charge transfer through aromatic rings in residues such as Phe. Consequently, mutation of a member of the triad

to Phe does not necessarily prevent charge transfer even if it impacts the charge transfer rate and modifies the charge transfer mechanism.

Absorbance spectra of the Y391A mutant are comparable in terms of the wavelength of maximum absorption to the WT protein, but the relative heights of the absorbance maxima suggest a partial depletion of FAD in this mutant. Absence of FAD photoreduction in Y391A mutant supports the essential role played by the aromatic side chain in electron tunnelling in the Y391F mutant. Absorbance spectra of the Y391W mutant indicate almost complete deletion of FAD and DMRL, in case of FAD probably due to the presence of a Trp, larger than Tyr, in the FAD pocket. Although the small percentage of DNA repair in presence of Y391W mutant suggests that the few protein molecules that have bound the chromophore keep their DNA repair functions. This FAD loss and then the DMRL loss phenomenon, also observed in CryB (von Zadow *et al.*, 2016), therefore we concluded that the replace of Trp by Tyr is because of the need by the protein structure stability, as I also observed the PhrB-Y391W mutant was also very easy to be unfolded. Taken together, our experimental results shows the presence of a Tyr residue instead of a Trp at this site preserves the structure and therefore the function.

Materials and methods

1 Protein preparation

1.1 Site-directed mutagenesis

A PhrB expression vector based on the pET21b (Novagen) with a C-terminal poly-histidine-tag was used as DNA template (Oberpichler *et al.*, 2011). Site-directed mutagenesis was performed according to the Quik Change site-directed mutagenesis protocol (Agilent) using Q5 polymerase and two complimentary primers as shown in Table 11 for PCR amplifying and then digest the template DNA with *DpnI* and transformed into *E. coli* ER2566 by heat shock.

Table 11. Primers for site-directed mutagenesis of PhrB. The triplet of the mutation site is printed in bold.

	Sequence (5'→3')
Y391W fw	CGGTGCATCGGTGGT GG CTCGAGGTCTATGCG
Y391W rev	CGCATAGACCTCGAG CC ACCACCGATGCACCG
Y391A fw	CGGTGCATCGGTGGG CG CTCGAGGTCTATGCG
Y391A rev	CGCATAGACCTCGAG CG CCCACCGATGCACCG
Y391F fw	GCGGTGCATCGGTGGT TTT CTCGAGGTCTATGCG
Y391F rev	CGCATAGACCTCGAG AAA ACCACCGATGCACCGC
D179N fw	GGCGGGCGCTGGAATTT TA ATGCGGAGAACCGCCAACCC
D179N rev	GGGTTGGCGGTTCTCCGC ATT AAAATTCCAGCGCCCGCC
D254N fw	GGCGCCACGCAG AA TGCCATGCTGCAGGATGAC
D254N rev	GTCATCCTGCAGCATGGC ATT TCTGCGTGGCGCC
I51W fw	GATCGCCTTCT TGG TTTTCCGCCATGCG
I51W rev	CGCATGGCGG AAA CCAGAAGGCGATC

1.2 Protein expression and purification

Photolyase OtCPF1 was expressed with a GST tag. Photolyase CryB, Proma-PL, PhrA and PhrB were expressed with a 6 x His Tag. The expression strains and the recombinant plasmids were described in the paper (Geisselbrecht *et al.*, 2012) for CryB and (Oberpichler *et al.*, 2011) for PhrA and PhrB.

The chemicals used for preparing buffers and medium in this part were purchased from the company Roth (Karlsruhe), Roche (Mannheim), Sigma Aldrich (Seelze), Sigma (Taufkirchen), Invitrogen (Karlsruhe), Applichem (Darmstadt).

1.2.1 GST-tag protein OtCPF1 purification

The (6-4) photolyase gene of *Ostreococcus tauri*, cloned into the expression vector pGEX-6P1, was a kind gift from Thomas Carell (Glas *et al.*, 2009a). This vector was transferred into *E. coli* strain Rosetta-gami™. Cells were grown in 1 L of TB-medium at 37 °C, 180 rpm, until OD_{600 nm} = 1, protein overproduction was induced with 1 mM IPTG and further incubated for 22 h at 19 °C, 180 rpm. Cells were harvested by centrifugation (10000 g, 10 min, 4 °C), resuspended in 30 ml PBS buffer (pH 7.4, 140 mM NaCl, 2.7 mM KCl, 10 mM Na₂HPO₄, 1.8 mM KH₂PO₄) with 1 mM Phenylmethanesulfonyl fluoride (PMSF). Cells were broken with a French Press (America Instrument Company) at 1000 bar. Cell debris was removed by centrifugation (3000 g, 30 min at 4 °C). The supernatant was incubated with Glutathione Sepharose 4B by shaking over-night (150 rpm, 4 °C). Further purification was done as described previously (Usman *et al.*, 2009) with a modified elution buffer (100 mM Tris-HCl, 100 mM NaCl, 20 mM reduced L-glutathione, pH 8.0). The eluted fractions were pooled and concentrated by ultrafiltration using Amicon Ultra-15 (30 kDa cutoff). Finally, OtCPF1 was transferred in buffer A (50 mM Tris-HCl, 100 mM NaCl, 1 mM EDTA, 5 % glycerol, pH 7.5). The buffer transfer was performed using NAP-10 columns (GE Healthcare) according to manufacturer's instructions.

1.2.2 His-tag protein purification

Expression and purification followed the procedure described in (Oberpichler *et al.*, 2011) for PhrA, PhrB WT and mutants. In brief, *E. coli* cells from agar plates were used for the inoculation of 6 liters LB containing ampicillin. Following specific induction of recombinant expression with IPTG (isopropyl- β -D-1-thiogalaktopyranosid) 0.1 mM and continue shaken over night at 28 °C (PhrB and its mutants), or 14 °C till $OD_{600\text{ nm}} = 2$ (PhrA). Cells were harvested by centrifugation, suspended in 50 ml extraction buffer (50 mM Tris-HCl, 5 mM EDTA, 300 mM NaCl, 10 % glycerol, pH 7.8) and extracted after disruption of the plasma membranes of the cells with a French Press (America Instrument Company) at 1000 bar. Following centrifugation and precipitation of soluble protein by 93 % saturated ammonium sulfate, the protein pellet was suspended in EDTA-free buffer. Soluble protein was purified by Ni-affinity chromatography followed by size exclusion chromatography (Sephacryl S-300 HR from GE healthcare). CryB was purified by Lars Oliver Essen group which was performed as described before (Hendrischk *et al.*, 2009; Geisselbrecht *et al.*, 2012).

We selected a sequence from *Prochlorococcus marinus* ssp CCMP1986 (Uniprot identifier or the protein: Q7V2P7) (Rocap *et al.*, 2003) and synthesized a codon optimized gene (Genscript, see Appendix) for expression in the pET28a vector between the *NdeI* and *XhoI* enzyme cutting sites. The expressed gene has an N-terminal His tag. Protein was expressed in *E. coli* ER2566 in autoinduction medium (Studier, 2005) with 100 μ M IPTG. The culture was cultivated for 3-4 d at 14 °C under 180 rpm shaking. Cell density reached $OD_{600\text{ nm}} = 17-18$. The extraction buffer was 40 mM Tris-HCl, 240 mM NaCl, 20 % glycerol, 1 % Nonidet P-40, pH 7.4. Extraction and purification followed the PhrB protocol, but ammonium sulfate precipitation was omitted and for the binding to the nickel column the Ni-NTA resin (Qiagen) was shaken for 1 hour in the protein solution. The imidazol concentration of the washing and elution buffer was 40 mM and 250 mM, respectively.

2 DNA repair assay

2.1 Preparation of CPD and (6-4) photoproducts

Oligonucleotides (Sigma-Aldrich) used in the present study are given in Table 12 (Glas *et al.*, 2009b). To obtain the (6-4) photoproduct, the oligonucleotide was dissolved in Millipore water at a concentration of 12.5 μM and degassed with argon. The solution was poured into a Petri dish, and the thickness of the solution was 2 to 3 mm. The Petri dish was placed on a 4 $^{\circ}\text{C}$ cooling pack in an irradiation box under argon atmosphere and irradiated with UV-C (GE Healthcare, G15T87B, 15 W) for 6 h at a distance of 12 cm. The irradiated DNA was concentrated by vacuum centrifugation and purified by HPLC on a “series 1200 Agilent Technologies system” using a Gemini C18 column (50 x 4.60 mm, 110 Å , Phenomenex). Mobile phases were solution A (0.1 M TEAA in H_2O) and solution B (0.1 M TEAA in $\text{H}_2\text{O}/\text{ACN}$ 20/80), the gradient was 4-18 % B in 45 min, and the flow rate was set to 5 ml/min. The elution was monitored by recording UV-Vis spectra every second. The (6-4) photoproduct is identified by its 325 nm absorption maximum (Blais *et al.*, 1994). Relevant fractions of (6-4) photoproducts were collected and stored at -20 $^{\circ}\text{C}$. The purity of (6-4) photoproducts was checked by subsequent analytic HPLC assay as described below for the repair assay. If the (6-4) photoproduct was not pure, a second HPLC purification followed under the conditions as described for the repair assay.

Table 12. Oligo DNA for producing (6-4) photoproducts. The TT pairs that yield the (6-4) photo lesions are printed in bold. ODN5 annealed with ODN5 Compl to form ds DNA with (6-4) lesion.

Name	Sequence (5'—>3')	Length (nt)
t_repair	AGG TT GGC	8
ODN4	CAGG TT GGCA	10
ODN5	ACAGG TT GGCAG	12
ODN5 Compl	CTGCCAACCTGT	12
ODN6	ACAGCGG TT GCAGGT	15

In order to obtain double stranded ODN5 oligonucleotides, (6-4) ODN5 and its complementary oligonucleotide (ODN5-Compl) were mixed at equimolar concentrations, heated to 95 °C for 3 min, and cooled to 25 °C over a period of ca. 90 min. The samples were stored on ice or at 4 °C until they were ready to use.

2.2 Repair assay

The photorepair reaction mixture contained 5 µM of the purified (6-4) photoproducts and 0.5 µM protein (unless stated otherwise) in repair buffer (50 mM Tris-HCl, pH 7.0, 1 mM EDTA, 100 mM NaCl, 5 % (w/v) glycerol, 14 mM DTT).

As the preillumination effect of photolyases (Harm and Rupert, 1976). We find that photoreduced PhrB can slightly improve the repair efficiency which equals to about 0.5 min extra irradiation. Based on experiments, I found that this difference of pre-induced and without pre-induced protein is within reasonable error range, so we conduct the repair assay with the non-pre induced proteins and the non-pre induced proteins were also used in this paper (Li *et al.*, 2010) .

After 20 min pre-incubation in darkness at 20 °C, aliquots were irradiated with 400 nm light emitting diodes ($250 \mu\text{mol m}^{-2} \text{s}^{-1}$) for the given time. Thereafter, the reactions were stopped by heating to 95 °C for 10 min. Samples were centrifuged at $15,000 \times g$ for 10 min and the supernatants analyzed by HPLC. To this end, the Agilent system with a Gemini C18 column (50 x 4.60 mm, 110 Å, Phenomenex) was used. The buffer conditions were: 7 % acetonitrile in 0.1 M TEAA (pH 7.0) for 0–5 min; 7–10 % acetonitrile in 0.1 M TEAA (pH 7.0) for 5–35 min. The flow rate was set to 0.75 ml/min and the column temperature to 25 °C. Elution was monitored at 260 nm and 325 nm. The repair efficiency was estimated from the peak areas corresponding to photoproduct DNA and repaired DNA.

3 Photoreduction

In all photoreduction studies, UV-Vis spectra were measured with a Jasco V550 photometer. Each protein was dissolved in basic buffer (50 mM Tris-HCl, 300 mM NaCl, 5 mM EDTA, 10 % glycerol, pH 7.8) to a final concentration of ca. 10 μM . The samples were incubated overnight at 4 $^{\circ}\text{C}$ in darkness in saturated oxygen solution. During this treatment, reduced FADH⁻ is converted to oxidized FAD. Before the first spectroscopic measurement was performed, 10 mM DTT was added to the protein solution. In the reaction mixtures with divalent metal cations, MgCl₂, MnCl₂ or CaCl₂ was added to a final concentration of 9 mM. Since the buffers contained 5 mM EDTA, the concentration of free divalent cations was approximately 4 mM. Photoreduction was performed by illumination with blue light emitting diodes ($\lambda_{\text{max}} = 470 \text{ nm}$). The light intensities for the PhrA and OtCPF1 proteins were 20 $\mu\text{mol m}^{-2} \text{ s}^{-1}$, and 100 $\mu\text{mol m}^{-2} \text{ s}^{-1}$ for PhrB (unless stated otherwise). Spectra were recorded at a series of time points as given in the results section.

4 Fluorimetry

Fluorescence was measured in a Jasco FO 8300 fluorimeter, bandwidth of excitation and emission were set to 3 nm, and scan speed was 200 nm min⁻¹. In control measurements we always checked whether the shape of an excitation spectrum is different if the wavelength of the emission maximum is set to 10 or 20 nm higher or lower wavelengths. This was not the case, indicating that the signals are due to fluorescence and not to Raman scattering or other possible artifacts.

5 Cofactor analysis

For detection of FAD and DMRL, 85 μM protein was denatured by incubation at 95 $^{\circ}\text{C}$ for 5 min. The insoluble protein and the soluble chromophores were separated by 10 min centrifugation at 15,000 $\times g$, and 10 μL supernatant were analyzed by HPLC (Agilent system with a Gemini C18 column (50 x 4.60 mm, 110 \AA , Phenomenex)). The HPLC buffer conditions were: 5 % acetonitrile in 0.1 % formic acid for 0–5 min; 5–75 %

acetonitrile in 0.1 % formic acid for 5–25 min. The flow rate was set to 0.75 ml/min and the column temperature to 25 °C. Elution was monitored at 260 nm and 400 nm. FAD cofactor can also be checked under the same HPLC condition as DNA repair assay.

6. Crystallization

6.1 Crystallization assays

In my crystallization experiments of PhrB and its mutants, the purified proteins obtained by affinity chromatography described above should be further centrifuged at 40,000 rpm, 4 °C for 30 min, otherwise no protein crystal could grow.

For the crystallization of PhrB under blue light, the 6 mg/ml protein solution was mixed with reduced agent tris(2-carboxyethyl) phosphine (pH adjusted to 7.5 by NaOH) to a final concentration of 4 mM and then irradiated by blue light emitting diodes ($\lambda_{\text{max}} = 470 \text{ nm}$), and the light intensity was $100 \mu\text{mol m}^{-2} \text{ s}^{-1}$. As the time of PhrB to be fully reduced is 100 min indicated in the results parts, we measured the spectrum at 100 min and found that there was still the semi-reduced spectrum, and then I further irradiated for another 60 min, and semi-reduced spectrum did not change. So I took this semi-reduced PhrB for crystallization assay. The primary screen plate is from Greiner (CrystalQuick™ 3 square wells, flat bottom), and the crystallization buffer kit is JBScreen Classic (Jena Bioscience).

PhrB-I51W mutant crystals were obtained using the hanging drop vapor diffusion method at 289 K in darkness with the crystallization condition consisting of a 1:1 mixture of protein (5 mg/ml in 12.5 mM Tris-HCl, 1.25 mM EDTA, 2.5 % (w/v) glycerol, 75 mM sodium chloride, pH 7.8) and the reservoir solution of 5 % polyethylene glycol 400 and 100 mM 2-(N-morpholino) ethanesulfonic acid, pH 6.5. The crystals of the typical size of $(50 \times 50 \times 100) \mu\text{m}^3$ were harvested and cryo-protected in the mother liquor containing 20 % glycerol or 100 % trimethylamine *N*-oxide (Mueller-Dieckmann *et al.*, 2011).

The PhrB-Y424F mutant was crystallized under the similar condition as PhrB-WT, *i.e.* 4 μl of protein (4-6 mg/ml in 12.5 mM Tris-HCl, 1.25 mM EDTA, 2.5 % (w/v)

glycerol, 75 mM sodium chloride, pH 7.8) mixed with an equal volume of reservoir solution (5 % (w/v) polyethylene glycol 400, 100 mM 2-(N-morpholino) ethanesulfonic acid, pH 6.0) and equilibrated against 1 ml of reservoir solution by the sitting drop vapor diffusion method at 289 K in darkness. Yellow tabular crystals appeared within 3 days and grew to $\sim (20 \times 20 \times 70) \mu\text{m}^3$ at 7 days. The crystals were flash frozen in liquid nitrogen after a stepwise soaking in 15 %, 20 % and 30 % of glycerol for around 1 min or directly with 100 % trimethylamine *N*-oxide.

6.2 Crystal structure determination

The crystal structure analysis was solved by cooperation with other laboratory mentioned in our published paper (Zhang *et al.*, 2017). The main processes are described as following. X-ray diffraction data of PhrB-I51W was collected at the LS-CAT 21-IDG beam station, Advanced Photon Source of Argonne National Laboratory. The diffraction images were indexed, integrated and scaled using *HKL2000*. The crystal structure was determined by molecular replacement (PHASER) (McCoy *et al.*, 2007) using the wild-type PhrB-WT structure (PDB entry 4DJA as the initial search model. The crystal structure was refined at resolution 2.15 Å (Adams *et al.*, 2010).

PhrB-Y424F diffraction data collection and protein structure analytic method are described in the paper (Zhang *et al.*, 2017).

References

- Adams, P.D., Afonine, P.V., Bunkoczi, G., Chen, V.B., Davis, I.W., Echols, N., Headd, J.J., Hung, L.W., Kapral, G.J., Grosse-Kunstleve, R.W., McCoy, A.J., Moriarty, N.W., Oeffner, R., Read, R.J., Richardson, D.C., Richardson, J.S., Terwilliger, T.C., and Zwart, P.H. (2010). PHENIX: a comprehensive Python-based system for macromolecular structure solution. *Acta Crystallogr D Biol Crystallogr* **66**, 213-221.
- Ahmad, M., and Cashmore, A.R. (1993). HY4 gene of *A. thaliana* encodes a protein with characteristics of a blue-light photoreceptor. *Nature* **366**, 162-166.
- Batista, L.F., Kaina, B., Meneghini, R., and Menck, C.F. (2009). How DNA lesions are turned into powerful killing structures: insights from UV-induced apoptosis. *Mutat Res* **681**, 197-208.
- Bayram, Ö., Biesemann, C., Krappmann, S., Galland, P., and Braus, G.H. (2008). More Than a Repair Enzyme: *Aspergillus nidulans* Photolyase-like CryA Is a Regulator of Sexual Development. *Mol Biol Cell* **19**, 3254-3262.
- Benkert, P., Biasini, M., and Schwede, T. (2011). Toward the estimation of the absolute quality of individual protein structure models. *Bioinformatics* **27**, 343-350.
- Bertoni, M., Kiefer, F., Biasini, M., Bordoli, L., and Schwede, T. (2017). Modeling protein quaternary structure of homo- and hetero-oligomers beyond binary interactions by homology. *Sci Rep* **7**, 10480.
- Bienert, S., Waterhouse, A., de Beer, Tjaart A.P., Tauriello, G., Studer, G., Bordoli, L., and Schwede, T. (2017). The SWISS-MODEL Repository—new features and functionality. *Nucleic Acids Res* **45**, D313-D319.
- Blais, J., Douki, T., Vigny, P., and Cadet, J. (1994). Fluorescence quantum yield determination of pyrimidine (6-4) pyrimidone photoadducts. *Photochem Photobiol* **59**, 402-404.
- Braberg, H., Webb, B.M., Tjioe, E., Pieper, U., Sali, A., and Madhusudhan, M.S. (2012). SALIGN: a web server for alignment of multiple protein sequences and structures. *Bioinformatics* **28**, 2072-2073.
- Brem, R., Guven, M., and Karran, P. (2017). Oxidatively-generated damage to DNA and proteins mediated by photosensitized UVA. *Free Radic Biol Med* **107**, 101-109.
- Cadet, J., Sage, E., and Douki, T. (2005). Ultraviolet radiation-mediated damage to cellular DNA. *Mutat Res* **571**, 3-17.
- Costa, R.M., Chigancas, V., Galhardo Rda, S., Carvalho, H., and Menck, C.F. (2003). The eukaryotic nucleotide excision repair pathway. *Biochimie* **85**, 1083-1099.
- Crooks, G.E., Hon, G., Chandonia, J.M., and Brenner, S.E. (2004). WebLogo: a sequence logo generator. *Genome Res* **14**, 1188-1190.
- Dulbecco, R. (1949). Reactivation of ultra-violet-inactivated bacteriophage by visible light. *Nature* **163**, 949.
- Eker, A.P., Kooiman, P., Hessels, J.K., and Yasui, A. (1990). DNA photoreactivating enzyme from the cyanobacterium *Anacystis nidulans*. *J Biol Chem* **265**, 8009-8015.

- Essen, L.O., and Klar, T. (2006). Light-driven DNA repair by photolyases. *Cell Mol Life Sci* **63**, 1266-1277.
- Fischer, M., Haase, I., Feicht, R., Richter, G., Gerhardt, S., Changeux, J.P., Huber, R., and Bacher, A. (2002). Biosynthesis of riboflavin: 6,7-dimethyl-8-ribityllumazine synthase of *Schizosaccharomyces pombe*. *Eur J Biochem* **269**, 519-526.
- Fujihashi, M., Numoto, N., Kobayashi, Y., Mizushima, A., Tsujimura, M., Nakamura, A., Kawarabayashi, Y., and Miki, K. (2007). Crystal structure of archaeal photolyase from *Sulfolobus tokodaii* with two FAD molecules: implication of a novel light-harvesting cofactor. *J Mol Biol* **365**, 903-910.
- Fuss, J.O., and Cooper, P.K. (2006). DNA repair: dynamic defenders against cancer and aging. *PLoS Biol* **4**, e203.
- Geisselbrecht, Y., Fruhwirth, S., Schroeder, C., Pierik, A.J., Klug, G., and Essen, L.O. (2012). CryB from *Rhodobacter sphaeroides*: a unique class of cryptochromes with new cofactors. *EMBO Rep* **13**, 223-229.
- Glas, A.F., Maul, M.J., Cryle, M., Barends, T.R., Schneider, S., Kaya, E., Schlichting, I., and Carell, T. (2009a). The archaeal cofactor F0 is a light-harvesting antenna chromophore in eukaryotes. *Proc Natl Acad Sci U S A* **106**, 11540-11545.
- Glas, A.F., Schneider, S., Maul, M.J., Hennecke, U., and Carell, T. (2009b). Crystal structure of the T(6-4)C lesion in complex with a (6-4) DNA photolyase and repair of UV-induced (6-4) and Dewar photolesions. *Chemistry (Easton)* **15**, 10387-10396.
- Graf, D., Wesslowski, J., Ma, H., Scheerer, P., Krauss, N., Oberpichler, I., Zhang, F., and Lamparter, T. (2015). Key amino acids in the bacterial (6-4) photolyase PhrB from *Agrobacterium fabrum*. *PLoS One* **10**, e0140955.
- Green, J., Bennett, B., Jordan, P., Ralph, E.T., Thomson, A.J., and Guest, J.R. (1996). Reconstitution of the [4Fe-4S] cluster in FNR and demonstration of the aerobic-anaerobic transcription switch *in vitro*. *Biochem J* **316** (Pt 3), 887-892.
- Harm, H., and Rupert, C.S. (1976). Analysis of photoenzymatic repair of UV lesions in DNA by single light flashes. XI. Light-induced activation of the yeast photoreactivating enzyme. *Mutation Research/Fundamental and Molecular Mechanisms of Mutagenesis* **34**, 75-92.
- Heelis, P.F., and Sancar, A. (1986). Photochemical properties of *Escherichia coli* DNA photolyase: a flash photolysis study. *Biochemistry* **25**, 8163-8166.
- Heil, K., Pearson, D., and Carell, T. (2011). Chemical investigation of light induced DNA bipyrimidine damage and repair. *Chem Soc Rev* **40**, 4271-4278.
- Hendrischk, A.K., Fruhwirth, S.W., Moldt, J., Pokorny, R., Metz, S., Kaiser, G., Jager, A., Batschauer, A., and Klug, G. (2009). A cryptochrome-like protein is involved in the regulation of photosynthesis genes in *Rhodobacter sphaeroides*. *Mol Microbiol* **74**, 990-1003.
- Hoeijmakers, J.H. (2001). Genome maintenance mechanisms for preventing cancer. *Nature* **411**, 366-374.
- Holub, D., Ma, H., Krau, Lamparter, T., Elstner, M., and Gillet, N. (2018). Functional role of an unusual tyrosine residue in the electron transfer chain of a prokaryotic (6-4) photolyase. *Chemical Science* **9**, 1259-1272.

- Hsu, D.S., Zhao, X., Zhao, S., Kazantsev, A., Wang, R.P., Todo, T., Wei, Y.F., and Sancar, A. (1996).** Putative human blue-light photoreceptors hCRY1 and hCRY2 are flavoproteins. *Biochemistry* **35**, 13871-13877.
- Huang, F. (2003).** Efficient incorporation of CoA, NAD and FAD into RNA by *in vitro* transcription. *Nucleic Acids Res* **31**, e8.
- Huang, J.C., Svoboda, D.L., Reardon, J.T., and Sancar, A. (1992).** Human nucleotide excision nuclease removes thymine dimers from DNA by incising the 22nd phosphodiester bond 5' and the 6th phosphodiester bond 3' to the photodimer. *Proc Natl Acad Sci U S A* **89**, 3664-3668.
- Ignatz, E., Geisselbrecht, Y., Kiontke, S., and Essen, L.O. (2018).** Nicotinamide adenine dinucleotides arrest photoreduction of class II DNA photolyases in FADH⁻ State. *Photochem Photobiol* **94**, 81-87.
- Johnson, J.L., Hamm-Alvarez, S., Payne, G., Sancar, G.B., Rajagopalan, K.V., and Sancar, A. (1988).** Identification of the second chromophore of *Escherichia coli* and yeast DNA photolyases as 5,10-methenyltetrahydrofolate. *Proc Natl Acad Sci U S A* **85**, 2046-2050.
- Kanavy, H.E., and Gerstenblith, M.R. (2011).** Ultraviolet radiation and melanoma. *Semin Cutan Med Surg* **30**, 222-228.
- Kao, Y.T., Saxena, C., He, T.F., Guo, L., Wang, L., Sancar, A., and Zhong, D. (2008).** Ultrafast dynamics of flavins in five redox states. *J Am Chem Soc* **130**, 13132-13139.
- Kelner, A. (1949).** Effect of visible light on the recovery of *Streptomyces Griseus* conidia from ultra-violet irradiation injury. *Proc Natl Acad Sci U S A* **35**, 73-79.
- Kim, S.T., Malhotra, K., Smith, C.A., Taylor, J.S., and Sancar, A. (1994).** Characterization of (6-4) photoproduct DNA photolyase. *J Biol Chem* **269**, 8535-8540.
- Klar, T., Kaiser, G., Hennecke, U., Carell, T., Batschauer, A., and Essen, L.O. (2006).** Natural and non-natural antenna chromophores in the DNA photolyase from *Thermus thermophilus*. *Chembiochem* **7**, 1798-1806.
- Korol, A.V., and Solov'yov, A.V. (2017).** Dynamics of systems on the nanoscale. *The European Physical Journal D* **71**, 339.
- Kort, R., Komori, H., Adachi, S., Miki, K., and Eker, A. (2004).** DNA apophotolyase from *Anacystis nidulans*: 1.8 Å structure, 8-HDF reconstitution and X-ray-induced FAD reduction. *Acta Crystallogr D Biol Crystallogr* **60**, 1205-1213.
- Lehmann, A.R. (1995).** Nucleotide excision repair and the link with transcription. *Trends Biochem Sci* **20**, 402-405.
- Li, J., Liu, Z., Tan, C., Guo, X., Wang, L., Sancar, A., and Zhong, D. (2010).** Dynamics and mechanism of repair of ultraviolet-induced (6-4) photoproduct by photolyase. *Nature* **466**, 887-890.
- Lin, J.J., and Sancar, A. (1992).** (A)BC excinuclease: the *Escherichia coli* nucleotide excision repair enzyme. *Mol Microbiol* **6**, 2219-2224.
- Lindahl, T., and Wood, R.D. (1999).** Quality control by DNA repair. *Science* **286**, 1897-1905.
- Liu, H., Zhong, D., and Lin, C. (2010).** Searching for a photocycle of the cryptochrome photoreceptors. *Curr Opin Plant Biol* **13**, 578-586.

- Liu, Z., Tan, C., Guo, X., Kao, Y.T., Li, J., Wang, L., Sancar, A., and Zhong, D. (2011).** Dynamics and mechanism of cyclobutane pyrimidine dimer repair by DNA photolyase. *Proc Natl Acad Sci U S A* **108**, 14831-14836.
- Ma, H., Zhang, F., Ignatz, E., Suehnel, M., Xue, P., Scheerer, P., Essen, L.O., Krauß, N., and Lamparter, T. (2017).** Divalent cations increase DNA repair activities of bacterial (6-4) photolyases. *Photochem Photobiol* **93**, 323-330.
- Maul, M.J., Barends, T.R., Glas, A.F., Cryle, M.J., Domratcheva, T., Schneider, S., Schlichting, I., and Carell, T. (2008).** Crystal structure and mechanism of a DNA (6-4) photolyase. *Angew Chem Int Ed Engl* **47**, 10076-10080.
- McCoy, A.J., Grosse-Kunstleve, R.W., Adams, P.D., Winn, M.D., Storoni, L.C., and Read, R.J. (2007).** Phaser crystallographic software. *J Appl Crystallogr* **40**, 658-674.
- Mees, A., Klar, T., Gnau, P., Hennecke, U., Eker, A.P., Carell, T., and Essen, L.O. (2004).** Crystal structure of a photolyase bound to a CPD-like DNA lesion after in situ repair. *Science* **306**, 1789-1793.
- Meistrich, M.L., and Lamola, A.A. (1972).** Triplet-state sensitization of thymine photodimerization in bacteriophage T4. *J Mol Biol* **66**, 83-95.
- Morita, R., Nakane, S., Shimada, A., Inoue, M., Iino, H., Wakamatsu, T., Fukui, K., Nakagawa, N., Masui, R., and Kuramitsu, S. (2010).** Molecular mechanisms of the whole DNA repair system: a comparison of bacterial and eukaryotic systems. *J Nucleic Acids* **2010**, 179594.
- Mouret, S., Baudouin, C., Charveron, M., Favier, A., Cadet, J., and Douki, T. (2006).** Cyclobutane pyrimidine dimers are predominant DNA lesions in whole human skin exposed to UVA radiation. *Proc Natl Acad Sci U S A* **103**, 13765-13770.
- Mueller-Dieckmann, C., Kauffmann, B., and Weiss, M.S. (2011).** Trimethylamine N-oxide as a versatile cryoprotective agent in macromolecular crystallography. *Journal of Applied Crystallography* **44**, 433-436.
- Muller, M., and Carell, T. (2009).** Structural biology of DNA photolyases and cryptochromes. *Curr Opin Struct Biol* **19**, 277-285.
- Nicholls, R.A., Fischer, M., McNicholas, S., and Murshudov, G.N. (2014).** Conformation-independent structural comparison of macromolecules with ProSMART. *Acta Crystallographica Section D-Biological Crystallography* **70**, 2487-2499.
- Nicolas, G., C., P.M., and Torsten, S. (2009).** Automated comparative protein structure modeling with SWISS-MODEL and Swiss-PdbViewer: A historical perspective. *ELECTROPHORESIS* **30**, S162-S173.
- O., R.R., and L., H.J. (1969).** Photochemical studies of thymine in ice. *Photochem Photobiol* **10**, 131-137.
- Oberpichler, I., Pierik, A.J., Wesslowski, J., Pokorny, R., Rosen, R., Vugman, M., Zhang, F., Neubauer, O., Ron, E.Z., Batschauer, A., and Lamparter, T. (2011).** A photolyase-like protein from *Agrobacterium tumefaciens* with an iron-sulfur cluster. *PLoS One* **6**, e26775.
- Okafuji, A., Biskup, T., Hitomi, K., Getzoff, E.D., Kaiser, G., Batschauer, A., Bacher, A., Hidema, J., Teranishi, M., Yamamoto, K., Schleicher, E., and Weber, S. (2010).** Light-

induced activation of class II cyclobutane pyrimidine dimer photolyases. *DNA Repair (Amst)* **9**, 495-505.

Park, H.W., Kim, S.T., Sancar, A., and Deisenhofer, J. (1995). Crystal structure of DNA photolyase from *Escherichia coli*. *Science* **268**, 1866-1872.

Payne, G., Heelis, P.F., Rohrs, B.R., and Sancar, A. (1987). The active form of *Escherichia coli* DNA photolyase contains a fully reduced flavin and not a flavin radical, both *in vivo* and *in vitro*. *Biochemistry* **26**, 7121-7127.

Pfeifer, G.P., You, Y.H., and Besaratinia, A. (2005). Mutations induced by ultraviolet light. *Mutat Res* **571**, 19-31.

Pokorny, R., Klar, T., Hennecke, U., Carell, T., Batschauer, A., and Essen, L.O. (2008). Recognition and repair of UV lesions in loop structures of duplex DNA by DASH-type cryptochrome. *Proc Natl Acad Sci U S A* **105**, 21023-21027.

Rocap, G., Larimer, F.W., Lamerdin, J., Malfatti, S., Chain, P., Ahlgren, N.A., Arellano, A., Coleman, M., Hauser, L., Hess, W.R., Johnson, Z.I., Land, M., Lindell, D., Post, A.F., Regala, W., Shah, M., Shaw, S.L., Steglich, C., Sullivan, M.B., Ting, C.S., Tolonen, A., Webb, E.A., Zinser, E.R., and Chisholm, S.W. (2003). Genome divergence in two *Prochlorococcus* ecotypes reflects oceanic niche differentiation. *Nature* **424**, 1042.

Rupert, C.S. (1962). Photoenzymatic repair of ultraviolet damage in DNA. II. Formation of an enzyme-substrate complex. *J Gen Physiol* **45**, 725-741.

Sancar, A. (1994). Mechanisms of DNA excision repair. *Science* **266**, 1954-1956.

Sancar, A. (2003). Structure and function of DNA photolyase and cryptochrome blue-light photoreceptors. *Chem Rev* **103**, 2203-2237.

Sancar, A. (2016). Mechanisms of DNA repair by photolyase and excision nuclease (nobel lecture). *Angew Chem Int Ed Engl* **55**, 8502-8527.

Sancar, G.B. (2000). Enzymatic photoreactivation: 50 years and counting. *Mutat Res* **451**, 25-37.

Sancar, G.B., and Sancar, A. (2006). Purification and characterization of DNA photolyases. *Methods Enzymol* **408**, 121-156.

Sancar, G.B., Smith, F.W., Reid, R., Payne, G., Levy, M., and Sancar, A. (1987). Action mechanism of *Escherichia coli* DNA photolyase. I. Formation of the enzyme-substrate complex. *J Biol Chem* **262**, 478-485.

Scheerer, P., Zhang, F., Kalms, J., von Stetten, D., Krauss, N., Oberpichler, I., and Lamparter, T. (2015). The class III cyclobutane pyrimidine dimer photolyase structure reveals a new antenna chromophore binding site and alternative photoreduction pathways. *J Biol Chem* **290**, 11504-11514.

Schleicher, E., Hessling, B., Illarionova, V., Bacher, A., Weber, S., Richter, G., and Gerwert, K. (2005). Light-induced reactions of *Escherichia coli* DNA photolyase monitored by Fourier transform infrared spectroscopy. *FEBS J* **272**, 1855-1866.

Selby, C.P., and Sancar, A. (2012). The second chromophore in *Drosophila* photolyase/cryptochrome family photoreceptors. *Biochemistry* **51**, 167-171.

Setlow, R.B., and Carrier, W.L. (1966). Pyrimidine dimers in ultraviolet-irradiated DNA's. *J Mol Biol* **17**, 237-254.

- Shannon, R.t. (1976).** Revised effective ionic radii and systematic studies of interatomic distances in halides and chalcogenides. *Acta Crystallographica Section A: Crystal Physics, Diffraction, Theoretical and General Crystallography* **32**, 751-767.
- Stuchebrukhov, A. (2011).** Watching DNA repair in real time. *Proc Natl Acad Sci U S A* **108**, 19445-19446.
- Studier, F.W. (2005).** Protein production by auto-induction in high density shaking cultures. *Protein Expr Purif* **41**, 207-234.
- Tagua, V.G., Pausch, M., Eckel, M., Gutierrez, G., Miralles-Duran, A., Sanz, C., Eslava, A.P., Pokorny, R., Corrochano, L.M., and Batschauer, A. (2015).** Fungal cryptochrome with DNA repair activity reveals an early stage in cryptochrome evolution. *Proc Natl Acad Sci U S A*.
- Tamura, K., Dudley, J., Nei, M., and Kumar, S. (2007).** MEGA4: Molecular Evolutionary Genetics Analysis (MEGA) software version 4.0. *Mol Biol Evol* **24**, 1596-1599.
- Taylor, J.S. (1994).** Unraveling the Molecular Pathway from Sunlight to Skin Cancer. *Acc Chem Res* **27**, 76-82.
- Tilman Lamparter, Fan Zhang, Dominik Graf, Janine Wesslowski, Inga Oberpichler, Volker Schünemann, Norbert Krauß, and Scheerer, P. (2014).** A Prokaryotic (6-4) Photolyase with a DMRL Chromophore and an Iron-Sulfur Cluster. *Encyclopedia of Inorganic and Bioinorganic Chemistry*.
- Todo, T. (1999).** Functional diversity of the DNA photolyase/blue light receptor family. *Mutat Res* **434**, 89-97.
- Todo, T., Takemori, H., Ryo, H., Ihara, M., Matsunaga, T., Nikaido, O., Sato, K., and Nomura, T. (1993).** A new photoreactivating enzyme that specifically repairs ultraviolet light-induced (6-4)photoproducts. *Nature* **361**, 371-374.
- Ueda, T., Kato, A., Kuramitsu, S., Terasawa, H., and Shimada, I. (2005).** Identification and characterization of a second chromophore of DNA photolyase from *Thermus thermophilus* HB27. *J Biol Chem* **280**, 36237-36243.
- Usman, A., Brazard, J., Martin, M.M., Plaza, P., Heijde, M., Zabulon, G., and Bowler, C. (2009).** Spectroscopic characterization of a (6-4) photolyase from the green alga *Ostreococcus tauri*. *Journal of photochemistry and photobiology B, Biology* **96**, 38-48.
- von Zadow, A., Ignatz, E., Pokorny, R., Essen, L.O., and Klug, G. (2016).** *Rhodobacter sphaeroides* CryB is a bacterial cryptochrome with (6-4) photolyase activity. *FEBS J* **283**, 4291-4309.
- Wacker, M., and Holick, M.F. (2013).** Sunlight and Vitamin D: A global perspective for health. *Dermatoendocrinol* **5**, 51-108.
- Waterhouse, A., Bertoni, M., Bienert, S., Studer, G., Tauriello, G., Gumienny, R., Heer, F.T., de Beer, T.A P., Rempfer, C., Bordoli, L., Lepore, R., and Schwede, T. (2018).** SWISS-MODEL: homology modelling of protein structures and complexes. *Nucleic Acids Res*, gky427-gky427.
- Weber, S. (2005).** Light-driven enzymatic catalysis of DNA repair: a review of recent biophysical studies on photolyase. *Biochim Biophys Acta* **1707**, 1-23.
- Whitby, L.G. (1953).** A new method for preparing flavin-adenine dinucleotide. *Biochem J* **54**, 437-442.

- Yamamoto, J., Plaza, P., and Brettel, K. (2017).** Repair of (6-4) lesions in DNA by (6-4) photolyase: 20 years of quest for the photoreaction mechanism. *Photochem Photobiol* **93**, 51-66.
- Zhang, F., Ma, H., Bowatte, K., Kwiatkowski, D., Mittmann, E., Qasem, H., Krauss, N., Zeng, X., Ren, Z., Scheerer, P., Yang, X., and Lamparter, T. (2017).** Crystal structures of bacterial (6-4) photolyase mutants with impaired DNA repair activity. *Photochem Photobiol* **93**, 304-314.
- Zhang, F., Scheerer, P., Oberpichler, I., Lamparter, T., and Krauss, N. (2013).** Crystal structure of a prokaryotic (6-4) photolyase with an Fe-S cluster and a 6,7-dimethyl-8-ribityllumazine antenna chromophore. *Proc Natl Acad Sci U S A* **110**, 7217-7222.
- Zhang, G., Morais, M.C., Dai, J., Zhang, W., Dunaway-Mariano, D., and Allen, K.N. (2004).** Investigation of metal ion binding in phosphonoacetaldehyde hydrolase identifies sequence markers for metal-activated enzymes of the HAD enzyme superfamily. *Biochemistry* **43**, 4990-4997.
- Zhang, Q., Chen, D., Lin, J., Liao, R., Tong, W., Xu, Z., and Liu, W. (2011).** Characterization of NocL involved in thiopeptide nocathiacin I biosynthesis: a [4Fe-4S] cluster and the catalysis of a radical S-adenosylmethionine enzyme. *J Biol Chem* **286**, 21287-21294.

Appendix

Codon optimized gene sequence of Proma-PL

ATGAACCAAATTAGCATTATCTTCCCGAACCAACTGTTCCGTGAGAGCAGCCTGCTG
AAACTGAGCTGCGAAATCCTGATTATTGAGGACAGCCTGTTCTTTGGTAACGATAAG
TTCCAGAAAAGCATCAACCACAAGAACAACACTGATTTTTTACAAGGCGAGCATGTTG
GCGTACAAGAAATATCTGCAAAACAGCGGTTTCAAGGTGATCTACATTGAGAACAA
AAACAACCTGAGCACC GTTGAATACCTGAGCAAATATCTGCAGGGCAAGTATCAAA
AAGTGAACATCATTAACCCGCACGACTTCCTGATCATGAAGCGTATTAACCGTTTTGT
TGAGGCCGAACAACCTGAAACTGCAGGTGTTCCAAAGCCCGATGTTTGTACCAACGA
AGATCTGCGTAAGAGCTTCAAAGCAACAGCAAGAAACCGCTGATGGGTGTTTTTA
CGAGAACCAGCGTCGTAGCCAAAACATTCTGCTGAACCCGGATGGCAGCCCGCAGG
GTGGCAAGTGGAGCTTCGATGAACTGAACCGTAAGAAACTGCCGAAAAACATCAAC
ATTCCGGAGATCCCGAAGTTCAGAAAAACCAATTTGTGATTCACGCGGAAAAGATC
ATTAGCAACCTGCAAATCGAGTTTATTGGTGAAAGCAACTACTTCATCTATCCGACC
ACTTTGAGGAAGCGGACAGCTGGCTGCACGACTTCTTTGAAGATCGTTTCAGCCTG
TTTGGCGACTACGAGGATGCGATCAGCAAGGAAAAAGTTTTCTGTGGCACAGCCTG
CTGAGCCCGCTGCTGAACAGCGGTCTGCTGACCGCGAAAGAGGTGATCGATAAAGC
GCTGACCTATGGCGAAAAGAACAAGTTCGATTAACAGCCTGGAGGGTTTCATCCG
TCAGATTGTGGGCTGGCGTGAGTTTATCTGCCTGGTTTACGAAAAATATGGTACCCA
AATGCGTACCACCAACTTCTGGAAC TTTGACAACAAGCCGATGCCGGAGTGCTTCTA
CAAAGGTAGCACCGGCATCGACCCGGTGGATATCGTTATCAACAACATCATCAAGTA
CGTTACTGCCACCACATTGAGCGTCTGATGATCATTGGCAACTTTATGCTGCTGTGC
CGTATCCACCCGGATCACGTGTACAAGTGGTTCATGGAAATGTTTCATCGACAGCTAC
GATTGGGTGATGGTTCCGAACGTTTATGGCATGAGCCAGTTCAGCGACGGTGGCATC
TTTAGCACCAAGCCGTACATCAGCAGCAGCAACTATGTGAAGAAAATGAGCGATTAC
AAAAGCGGTCCGTGGTGCAGCATCTGGGATGGCCTGTTCTGGAAGTTCATCAAGGAT
AACGAAACCTACTTCCGTAAGCAGTATCGTCTGGCGATGCTGACCCGTAACCTGGAC
AAAATGAGCGACGAAAAACTGAACGGTCATCTGCGTATCGCGGAAGAATTTATTAG
CAACCTGTATTAA

Acknowledgement

I would like to express my sincere gratitude to Prof. Dr. Tilman Lamparter for accepting me as his doctoral student four years ago, as well as for his continuous support during each step of my research which helped me to accomplish my goals. Especially when I encountered setbacks on experiment, with his supervision and encouragement, I could continuously improve my skills on research and finally complete it successfully.

I thank Ernst Heene for technical assistance and thank Azubi Jonas Müller for helping my experiment and thank to Norbert Krauß, Xiaojing Yang, Lars Oliver Essen, Natacha Gillet, and Daniel Holub for pleasant cooperation. Especially thanks to Norbert Krauß who has gave me very good suggestions on my experiments. I also show my special thanks to master and bachelor students for participating in my work.

I would like to thank all the coauthor of the publications for their work on the text and figures that used in this thesis and for their great advices which help me complete this thesis.

I also thank Thomas Carell and Lars Oliver Essen for the gift of recombinant plasmid pGEX6p1-OtCPF1 and CryB, separately. My work was financially supported by the China Scholarship Council (CSC), I am very grateful to CSC.

I am grateful to my parents for giving me spiritual supports with their unconditional love. I am especially grateful to my husband Xiaobao for letting my non-working time relaxed and happy.